Computational solutions in genomic pathology of non-Hodgkin Lymphomas

Mendeville, Matias Sebastiaan

2023

DOI (link to publisher)
10.5463/thesis.102

document version
Publisher's PDF, also known as Version of record

Computational solutions in genomic pathology of non-Hodgkin lymphomas

Matías Sebastiaan Mendeville

The research described in this thesis was carried out at the department of Pathology at the Amsterdam UMC, location VUmc. The project leading to this thesis was financially supported by grants of the Dutch Cancer Society (KWF 2012-5711, KWF 2013-6269 and KWF 2015-7925) and the Lunenburg Lymphoma Biomarker Consortium.

Financial support for printing of this thesis was kindly provided and supported by Cancer Center Amsterdam, Amsterdam UMC, location VUmc, department of Pathology and VU University Amsterdam.

ISBN:	978-94-6458-981-8
DOI:	10.5463/thesis.102
Cover design:	© Rafaella Wang | www.rafaellawang.nl
Lay-out:	Publiss | www.publiss.nl
Printing:	Ridderprint | www.ridderprint.nl

VRIJE UNIVERSITEIT

COMPUTATIONAL SOLUTIONS IN GENOMIC PATHOLOGY OF NON-HODGKIN LYMPHOMAS

ACADEMISCH PROEFSCHRIFT

ter verkrijging van de graad Doctor aan
de Vrije Universiteit Amsterdam,
op gezag van de rector magnificus
prof.dr. J.J.G. Geurts,
in het openbaar te verdedigen
ten overstaan van de promotiecommissie
van de Faculteit der Geneeskunde
op dinsdag 11 april 2023 om 13.45 uur
in een bijeenkomst van de universiteit,
De Boelelaan 1105

door

Matías Sebastiaan Mendeville

geboren te Amsterdam

promotoren:	prof.dr. D. de Jong prof.dr. B. Ylstra
promotiecommissie:	prof.dr. J. Cloos prof.dr. B. Chapuy prof.dr. L. Van ‘t Veer dr. M.E.D. Chamuleau prof.dr.ir. E. Cuppen dr. O. Krijgsman

Table of contents

Chapter 1

General Introduction

General Introduction

Translational cancer genomics

Concepts on cancer are increasingly complex. While some 30 years ago, cancer could be presented as a "genetic disease", the most recent update on "Hallmarks of Cancer" include the 10 central hallmarks that describe various primarily genetically driven features and primary immunological/microenvironment-driven features. On top of these, entirely novel "enabling characteristics" that are neither directly genetic nor immunological/stromal-related are now introduced (Hanahan 2022). These include differentiation-regulation, non-mutational epigenetic re-programming, microbiomes and a role for senescent cells. Largely, these new concepts underpin the highly complex nature of oncogenesis. It will require much time and research until such insights find their way into clinical practice and impact on patient management. It is timely, however, to move the knowledge on tumor genomics into this phase to apply the aberrant genomic landscape to inform patient management on different levels, including diagnosis, prognosis, treatment stratification, choice of therapy and disease monitoring. The implementation and integration of genomics into routine clinical practice is called translational cancer genomics, which is the scope of this thesis and its application is explored in B-cell non-Hodgkin lymphomas (B-NHL).

Characterization of the genomic tumor landscape by next-generation sequencing

Genome alterations in cancers can be classified in 3 main groups i) *Point mutations* include substitutions, insertions or deletions of one or more DNA nucleotides. ii) *Chromosomal copy number aberrations* (CNAs) encompass loss or gain of entire chromosomes or chromosomal segments. iii) *Structural variants* (SVs) are aberrantly rearranged structures of one or multiple chromosomes. Together these constitute the genomic tumor landscape. To retrieve a comprehensive inventory of the genomic landscape of tumor tissues, next-generation sequencing (NGS) is the current method of choice (Goodwin, McPherson, and McCombie 2016). NGS allows detailed characterization of DNA through massive parallel sequencing, resulting in gigabases of generated nucleotide sequences per instrument run. Below, the various wet- and dry-lab prerequisites for clinical applications of NGS are briefly outlined.

The starting point is DNA of sufficient quality. Since diagnostic biopsy samples are routinely fixed in buffered formalin and embedded in paraffin (FFPE), this material is the logical and inevitable source of tumor DNA. Only occasionally, part of diagnostic tumor samples

may be fresh-frozen (FF) or processed to viable cell suspensions and biobanked as such. The rich annotation with clinical follow-up data of FFPE-based biobanks make these an invaluable resource to study cancer in retrospective studies, including clinical trials as well as in daily practice (Blow 2007). A major drawback of FFPE tissue as input material is suboptimal DNA quality and quantity, as opposed to FF tissue processing. Formalin fixation causes fragmentation and crosslinking of DNA, which causes artefacts on the nucleotide level (Do and Dobrovic 2015). These changes interfere with the detection of true mutations versus artifacts. Moreover, other factors related to FFPE tissue processing can further compromise the extraction-yield of intact DNA molecules, including fixation delay, variable formalin fixation methods and archival storage time (Hedegaard et al. 2014). Over the past years, we and others have therefore invested in optimizing laboratory techniques to overcome these challenges so that FFPE material can be used as a source of DNA for NGS to ultimately describe the genomic landscape of cancers.

Computational approaches and challenges for somatic variant identification

In parallel with the developments for NGS of tumor tissues, the requirements for dedicated genomics data processing and interpretation have evolved, which is the field of bioinformatics. With much of developments happening within the open-source domain, a large amount of bioinformatic tools and pipelines to analyze and interpret cancer NGS data is available. It is the specialist role of the bioinformatician to guarantee reliable information in clinical translational cancer genomics. Irrespective of the NGS-application (whole genome sequencing, whole exome sequencing or targeted panel sequencing) the challenges focus on 1) distinction between true mutation and artefact, 2) distinction between somatic and germline mutations, and 3) distinction between driver and passenger mutations. This is especially challenging in a clinical setting, since the DNA is more often than not derived from FFPE tissue, and where patient matched-normal sample is frequently not available as a reference. In the first phase of this PhD trajectory that have led to this thesis, these have been the major challenges to solve before meaningful studies could be performed that are described in the various chapters.

B-cell non-Hodgkin lymphoma

B-cell non-Hodgkin lymphomas (B-NHL) form a diverse group of neoplasms with respect to cell of origin (various B-cell developmental stages), oncogenesis and clinical features. This group of hematologic malignancies usually develop in the lymph nodes and other secondary lymphoid organs, where they form solid tumor masses or present as a leukemia. The 5th edition of the World Health Organization classification of

lymphoid neoplasms recognizes more than 30 B-NHLs entities, which differ in terms of morphology, immunophenotype and genetics (Alaggio et al. 2022). The clinical behavior of these different lymphoma entities ranges from very indolent to highly aggressive. This difference in clinical outcome is exemplified in the 2 most frequently diagnosed types of lymphomas, diffuse large B-cell lymphoma (DLBCL) and follicular lymphoma (FL), which are the main focus of this thesis.

Diffuse large B-cell lymphoma, not otherwise specified (DLBCL NOS, hereafter DLBCL) is the most frequent lymphoma entity in adults, which is characterized by an extensive biological and clinical heterogeneity. The clinical outcome of DLBCL ranges from 5-year survival of almost 90% to a mere 30%. Also, the clinical presentation is highly variable (e.g., nodal/extranodal, specific sites). The cellular morphology differs enormously between cases as does the immunophenotype. Age at diagnosis, stage, performance status, number of extranodal sites and LDH levels, together as the so-called International Prognostic Index (IPI), form the strongest prognostic biomarkers (Shipp and Harrington 1993). IPI provides little if any biological information however. In view of the remarkably large heterogeneity in so many aspects, one might expect this to be reflected in distinct molecular classes that are dominated by very distinct genetic alterations. Recognizing such alterations has proven to be more difficult than anticipated. Since 2018, NGS-based studies have initiated a new phase in DLBCL classification. The main clinical challenges in DLBCL are to reliably predict patient outcome at diagnosis and following therapy, and to find targetable features. Both lines of information can contribute to personalized treatment of DLBCL patients. To which extent genomic profiling may contribute to these pertinent questions has been the starting point for studies on DLBCL described in this thesis.

Follicular lymphoma (FL), the second most frequent lymphoma entity, is an indolent disease with the majority of patients (~80%) showing long survival, with a median overall survival of more than 10 years (Tan et al. 2013). FL is characterized by frequent relapses with variable remission durations, but these do not necessarily impact on overall survival. However, approximately 20% of FL patients have a poor outcome and die within the first few years after diagnosis, largely due to histological transformation or refractory disease (Casulo et al. 2015). Similarly to DLBCL, the primary prognostic tool is based on clinical factors, captured in the Follicular Lymphoma International Prognostic Index (FLIPI; Solal-Céligny et al. 2004). However, the FLIPI cannot adequately predict whether or when individual patients will progress to the point where treatment is required, which shows that the biological and clinical behavior of FL is likely determined by a more complex interaction between tumor genetics, microenvironment and patient characteristics. Immunophenotypically, FL

is characterized by a distinct phenotype related to germinal center B-cells (CD10, BCL6, AID and others). The characteristic initiating genetic alteration is the t(14;18) translocation involving the IGH and BCL2 genes, that results in overexpression of the anti-apoptotic BCL2 protein (de Jong 2005). The translocation can be found in over 90% of the cases. The fact that this translocation is also observed in healthy individuals, supports the notion that multiple genetic alterations are required for the development of FL (Limpens et al. 1995). In the last decade, large-scale NGS-based studies have elucidated much of the genetic landscape of FL, but their prognostic impact remained unclear (Pasqualucci et al. 2014; Okosun et al. 2014). Besides genetic alterations, the tumor microenvironment (TME) has been shown to play a complementary important role in FL through the crosstalk between malignant B cells and non-malignant immune and stromal cells (Dave et al. 2004; Glas et al. 2005). The need for improved prognostic models, that involve genetic and TME factors, outline the background of the studies on FL described in this thesis.

Primary HHV8-negative effusion-based lymphoma is a rare and particularly indolently behaving B-NHL included in this thesis. As a consequence of its rarity, little is known about its tumor genomic landscape. Insight in the genomic features that drive this tumor entity may give first clues towards the biology of this indolent B-NHL entity and give clues towards the heterogenic behavior of FL and DLBCL.

Aims of this Thesis

To improve personalized management of DLBCL and FL, upfront risk-stratification with identification of specific high-risk and low-risk patients is critical. Improved and reliable tools for patient stratification provide information to avoid overtreatment of low-risk patients and to prioritize alternative, possibly more effective approaches in high-risk patients. The required translational genomic studies form the scope of this thesis, which is approached through the following two aims:

1. To develop a comprehensive assay for simultaneous screening of all three types of genomic alterations using a limited amount of input DNA derived from FFPE biopsy samples without the need of matched normal control DNA, optimized to be implemented in clinical practice for lymphoma diagnostics.
2. To improve our understanding of the biological basis of clinical heterogeneity of B-NHL and thereby enable improved risk stratification for DLBCL and FL patients. We intend to achieve this by applying the assays developed under aim 1, to large, selected patient cohorts of DLBCL and FL.

References

1. Alaggio, Rita, Catalina Amador, Ioannis Anagnostopoulos, Ayoma D. Attygalle, Iguaracyra Barreto de Oliveira Araujo, Emilio Berti, Govind Bhagat, et al. 2022. "The 5th Edition of the World Health Organization Classification of Haematolymphoid Tumours: Lymphoid Neoplasms." *Leukemia* 36 (7). https://doi.org/10.1038/S41375-022-01620-2.
2. Blow, Nathan. 2007. "Tissue Preparation: Tissue Issues." *Nature* 448 (7156): 959–63. https://doi.org/10.1038/448959a.
3. Casulo, Carla, Michelle Byrtek, Keith L. Dawson, Xiaolei Zhou, Charles M. Farber, Christopher R. Flowers, John D. Hainsworth, et al. 2015. "Early Relapse of Follicular Lymphoma after Rituximab plus Cyclophosphamide, Doxorubicin, Vincristine, and Prednisone Defines Patients at High Risk for Death: An Analysis from the National LymphoCare Study." *Journal of Clinical Oncology* 33 (23): 2516–22. https://doi.org/10.1200/JCO.2014.59.7534.
4. Dave, Sandeep S., George Wright, Bruce Tan, Andreas Rosenwald, Randy D. Gascoyne, Wing C. Chan, Richard I. Fisher, et al. 2004. "Prediction of Survival in Follicular Lymphoma Based on Molecular Features of Tumor-Infiltrating Immune Cells." *The New England Journal of Medicine* 351 (21): 2159–69. https://doi.org/10.1056/NEJMOA041869.
5. Do, Hongdo, and Alexander Dobrovic. 2015. "Sequence Artifacts in DNA from Formalin-Fixed Tissues: Causes and Strategies for Minimization." *Clinical Chemistry* 61 (1): 64–71. https://doi.org/10.1373/CLINCHEM.2014.223040.
6. Glas, Annuska M., Marie José Kersten, Leonie J M J Delahaye, Anke T. Witteveen, Robby E. Kibbelaar, Arno Velds, Lodewyk F A Wessels, et al. 2005. "Gene Expression Profiling in Follicular Lymphoma to Assess Clinical Aggressiveness and to Guide the Choice of Treatment." *Blood* 105 (1): 301–7. https://doi.org/10.1182/blood-2004-06-2298.
7. Goodwin, Sara, John D. McPherson, and W. Richard McCombie. 2016. "Coming of Age: Ten Years of next-Generation Sequencing Technologies." *Nature Reviews Genetics* 17 (6): 333–51. https://doi.org/10.1038/nrg.2016.49.
8. Hanahan, Douglas. 2022. "Hallmarks of Cancer: New Dimensions." *Cancer Discovery* 12 (1): 31–46. https://doi.org/10.1158/2159-8290.CD-21-1059.
9. Hedegaard, Jakob, Kasper Thorsen, Mette Katrine Lund, Anne Mette K Hein, Stephen Jacques Hamilton-Dutoit, S??ren Vang, Iver Nordentoft, et al. 2014. "Next-Generation Sequencing of RNA and DNA Isolated from Paired Fresh-Frozen and Formalin-Fixed Paraffin-Embedded Samples of Human Cancer and Normal Tissue." *PLoS ONE* 9 (5). https://doi.org/10.1371/journal.pone.0098187.
10. Jong, Daphne de. 2005. "Molecular Pathogenesis of Follicular Lymphoma: A Cross Talk of Genetic and Immunologic Factors." *Journal of Clinical Oncology : Official Journal of the American Society of Clinical Oncology* 23 (26): 6358–63. https://doi.org/10.1200/JCO.2005.26.856.
11. Limpens, Jacqueline, Robert Stad, Carla Vos, Clementine De Vlaam, Daphne De Jong, Gert Jan B. Van Ommen, Ed Schuuring, and Philip M. Kluin. 1995. "Lymphoma-Associated Translocation t(14;18) in Blood B Cells of Normal Individuals." *Blood* 85 (9): 2528–36. https://doi.org/10.1182/BLOOD.V85.9.2528.BLOODJOURNAL8592528.
12. Okosun, Jessica, Csaba Bödör, Jun Wang, Shamzah Araf, Cheng-Yuan Yang, Chenyi Pan, Sören Boller, et al. 2014. "Integrated Genomic Analysis Identifies Recurrent Mutations and Evolution Patterns Driving the Initiation and Progression of Follicular Lymphoma." *Nature Genetics* 46 (2): 176–81. https://doi.org/10.1038/ng.2856.

13. Pasqualucci, Laura, Hossein Khiabanian, Marco Fangazio, Mansi Vasishtha, Monica Messina, AntonyB Holmes, Peter Ouillette, et al. 2014. "Genetics of Follicular Lymphoma Transformation." *Cell Reports* 6 (1): 130–40. https://doi.org/10.1016/j.celrep.2013.12.027.

14. Shipp, Margaret A, and D P Harrington. 1993. "A Predictive Model for Aggressive Non-Hodgkin's Lymphoma." *The New England Journal of Medicine* 329 (14): 987–94. https://doi.org/10.1056/NEJM199309303291402.

15. Solal-Céligny, Philippe, Pascal Roy, Philippe Colombat, Josephine White, Jim O. Armitage, Reyes Arranz-Saez, Wing Y. Au, et al. 2004. "Follicular Lymphoma International Prognostic Index." *Blood* 104 (5): 1258–65. https://doi.org/10.1182/BLOOD-2003-12-4434.

16. Tan, Daryl, Sandra J. Horning, Richard T. Hoppe, Ronald Levy, Saul A. Rosenberg, Bronislava M. Sigal, Roger A. Warnke, et al. 2013. "Improvements in Observed and Relative Survival in Follicular Grade 1-2 Lymphoma during 4 Decades: The Stanford University Experience." *Blood* 122 (6): 981–87. https://doi.org/10.1182/BLOOD-2013-03-491514.

Chapter 2

The path towards consensus genome classification of diffuse large B-cell lymphoma for use in clinical practice

Matias Mendeville, Margaretha G. M. Roemer, G. Tjitske Los-de Vries, Martine E.D. Chamuleau, Daphne de Jong, Bauke Ylstra

Frontiers in Oncology, 2022;12:970063.

Abstract

Diffuse large B-cell lymphoma (DLBCL) is a widely heterogeneous disease in presentation, treatment response and outcome that results from a broad biological heterogeneity. Various stratification approaches have been proposed over time but failed to sufficiently capture the heterogeneous biology and behavior of the disease in a clinically relevant manner. The most recent DNA-based genomic subtyping studies are a major step forward by offering a level of refinement that could serve as a basis for exploration of personalized and targeted treatment for the years to come. To enable consistent trial designs and allow meaningful comparisons between studies, harmonization of the currently available knowledge into a single genomic classification widely applicable in daily practice is pivotal. In this review, we investigate potential avenues for harmonization of the presently available genomic subtypes of DLBCL inspired by consensus molecular classifications achieved for other malignancies. Finally, suggestions for laboratory techniques and infrastructure required for successful clinical implementation are described.

Introduction

Molecular diagnostics of cancer has entered a new era, propelled by advances in omics- and bioinformatic technologies that provide a new layer of characteristics for tumor classification. In general, current state-of-the-art diagnostic pathology categorizes tumors using phenotypic macro- and microscopic and immunohistochemical (IHC) characteristics, combined with molecular assays for single or limited numbers of markers like PCR, and fluorescent in situ hybridization (FISH). Analyses of highly complex omics data by bioinformatic technologies have identified molecular patterns and pathways that underly biologically distinct, and thereby newly recognized categories. Vice versa, accepted diagnostics distinct categories may proof to be molecularly so closely related they may even be combined into a single entity.

Diffuse large B-cell lymphoma (DLBCL), the most prevalent type of non-Hodgkin lymphoma and the focus of this review, is characterized by a complex, heterogeneous tumor biology that is reflected in clinical heterogeneity (1). This is evident from a wide outcome spectrum with cure for 60% of patients treated with standard immune-chemotherapy (R-CHOP) and disease progression for the other 40% of which the far majority eventually succumbs due to relapsing and/or refractory disease (2, 3). Since 2000, omics information started to contribute layers of comprehensive biological information to the diagnosis of DLBCL (4). At that time, RNA expression profiling by means of microarray analysis followed by unsupervised clustering revealed a relatively simple dichotomous distinction based on cell-of-origin (COO) (5). For universal application in daily clinical practice, this distinction was translated into various algorithms that relied on classic immunohistochemistry (IHC) assay data rather than complex RNA analytics. This undoubtedly aided to have DLBCL COO classification to be included in the updated 4th edition of the World Health Organization (WHO) Classification for Hematolymphoid Malignancies in 2016 (6). Nonetheless, it was never widely applied outside clinical trials, largely since the clinical implications ultimately proved to be limited (7–9). Almost 20 years after the RNA-based COO classification concept, several independent studies proposed DNA-based subtyping by next-generation sequencing (NGS) as an alternative means to capture the biological heterogeneity of DLBCL and to supersede or complement COO classification (10– 13). The different DNA-subtyping studies bear significant similarities, but also differ in some a priori concepts, applied technologies, bioinformatical approaches and ultimately in part in recognized genomic subtypes (14, 15). These differences preclude uniform classification, which is a quintessential step towards clinical implementation and essential to perform meaningful clinical trials (16–18).

Molecular classifications of DLBCL

Classifications based on RNA-expression

The more than 20-year-old RNA-based COO classification recognizes 2 major molecularly distinct classes considered to reflect different stages of B-cell differentiation; activated B-cell (ABC) and germinal center B-cell (GCB) while a small group of patients remains 'unclassified'. Both in the primary discovery studies and various subsequent validation studies, patients with a GCB-type DLBCL consistently showed a better prognosis under guideline therapy than patients with an ABC-type DLBCL (4). The differential clinical outcomes coupled with distinctive underlying biology served as a justification for differential treatment. In the years that followed it became clear however that the complex and heterogeneous biology of DLBCL was not fully captured by this simple dichotomous classification (5). In particular, phase 2 and phase 3 clinical trials that either used COO as an inclusion parameter, or were post-hoc analyzed based on COO class, failed to demonstrate differential improvement of outcome for patients receiving experimental, targeted treatment alternatives (7, 8, 19).

This does however not imply that RNA-based information would not provide essential information to dissect DLBCL biology, as specific host-immune response signatures could already be identified in the early 2000s (20). Most recently, deconvolution algorithms using known cell type specific RNA signatures to computationally infer cellular components from bulk RNA data have allowed to further dissect information on tumor features as well as non-malignant tumor immune microenvironment (TME) features. Thereby, the original GCB class was further divided into three to four differentiation phases (germinal center, dark zone, precursor memory B-cell, light zone) and ABC into two phases (pre-plasmablast, plasmablast/ plasmacell). Hence, TME analysis from RNA expression data provided complementary signatures that could further and largely independently describe DLBCL biology in a clinically meaningful manner (21).

DLBCL defining DNA-alterations and subtyping approaches

The first larger DNA-based next-generation sequencing (NGS) studies for DLBCL that were undertaken revealed a spectrum of mutations, numerical chromosomal copy number aberrations (CNAs) and translocations that were largely characteristic for either of the RNA expression-based COO classes (22–27). For example, mutations in the chromatin modifying genes *CREBBP*, *KMT2D* and *EZH2*, were described as characteristic of GCB-type DLBCL and chromosome 18q gain and *MYD88* mutations characteristic of ABC-type DLBCL. Apart from these few COO-characteristic DNA alterations, the majority was

shown to be only limitedly overrepresented in either class, explanatory for the extensive genetic heterogeneity of DLBCL.

In 2018, research groups from the National Cancer Institute (NCI) and the Dana Farber Cancer Institute (DFCI) independently and practically simultaneously proposed DNA-based subtyping approaches based on whole exome sequencing (WES) (1, 10, 11). The NCI group made a first step towards harmonization of the two approaches by, like DFCI, also including CNAs to their classification which resulted in the LymphGen algorithm (12). The DFCI- and NCI studies included retrospectively collected patient cohorts and identified 5- and 7 genomic subtypes, respectively. Encouraging is that despite the different cohorts and bioinformatical approaches, both defining features and the resulting subtypes are largely overlapping (Figure 1 and Box 1). Other groups, with other cohorts using overlapping bioinformatical approaches have been able to reproduce these subtypes by and large (13, 31–33), including unpublished results by the authors of this review. This all provides confidence that a DNA-based characterization of DLBCL has the potential to disentangle the biological heterogeneity that underlies DLBCL's clinical heterogeneity.

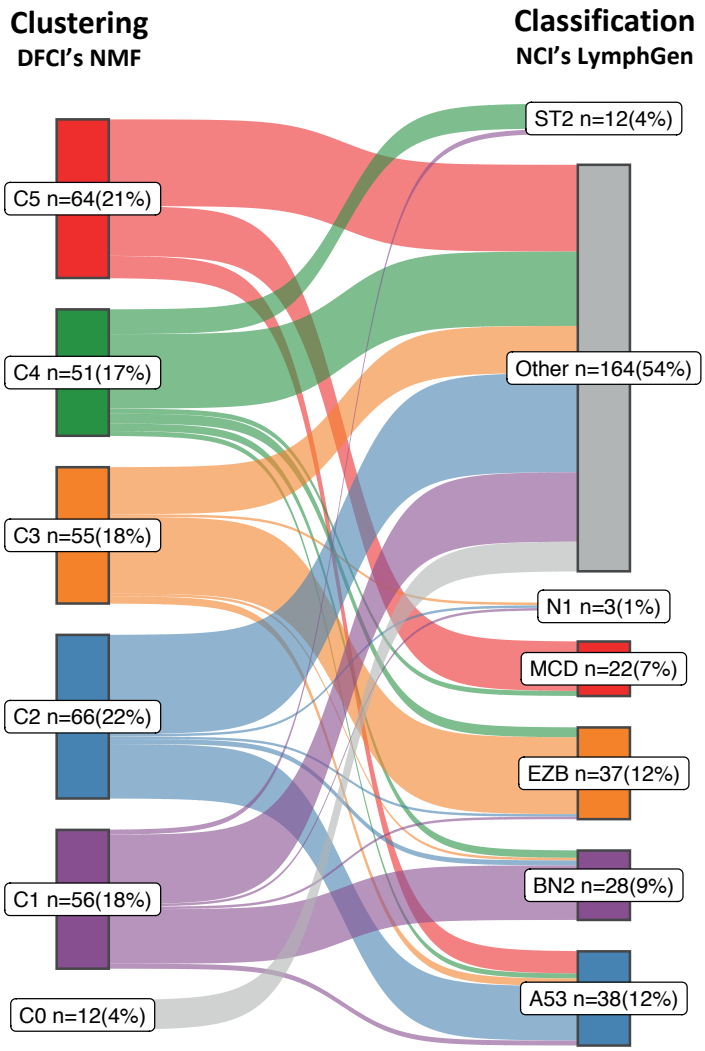

Figure 1. Sankey diagram comparing the two DLBCL subtypes. A Sankey diagram was constructed to illustrate how the LymphGen (12) and NMF (10) subtyping systems compare, as described in Box 1. Therefore the NGS data of 304 diffuse large B-cell lymphoma (DLBCL) cases published by the Dana Farber Cancer Institute (DFCI) (10) was used as input. Left stage: Clustering by means of non-negative matrix factorization (NMF). Right stage: Classification by means of LymphGen algorithm. Flows between the subtypes resemble DLBCL cases and are labelled according to their molecular counterpart; C1/BN2, purple; C2/A53, blue; C3/EZB, orange; C4/ST2, green; C5/MCD, red; samples not assigned to a cluster (NMF, C0) or unclassified (LymphGen, Other) are in gray. Each subtype with numbers of samples (n) and percentage of total (=304).

Box 1 Comparison of the LymphGen and NMF subtyping systems.

The correspondence between the NCI's LymphGen and DFCI's NMF subtypes is 75% based on the 63.1% of patients classified by the LymphGen algorithm (12). If also the LymphGen unclassified samples are considered, the overall agreement between the two subtyping systems is around 50%. Approaches: Both studies performed comprehensive genomic profiling to detect somatic mutations, CNAs and translocations. Because of the lack of matched normal tissue for most samples, both studies applied custom computational pre-processing techniques to eliminate sequencing artifacts and distinguish somatic and germline variations. The DFCI group performed WES on a series of tissue biopsies of 304 patients with primary DLBCL. Samples were from 4 different trials and cohorts, of which 55% were derived from FFPE tissue, and 44% had matched-normal tissue availability (10). The NCI group performed WES on a series of fresh-frozen DLBCL tissue biopsies of 574 patients for which 96.5% were primary DLBCL tissues and the other 3.5% from relapsed or refractory, without matched-normal tissue (12). Below is a short summary of the most defining features which the NCI and DFCI proposed subtypes have in common. For a more comprehensive overview on details of their differences and commonalities we refer to a recent review by Crombie et al. (28).

i. The C1 subtype recognized by DFCIs NMF algorithm finds its analogue in the BN2 subtype recognized by NCIs LymphGen algorithm. Combined, the two algorithms determined 21 defining genetic alterations, of which eight overlap. Overlapping genes include BCL6 translocations, alterations in NOTCH2 signalling genes and mutations targeting the NF-kB pathway. Furthermore, the C1/BN2 subtype is enriched for, but not restricted to ABC-type, and shows a favorable outcome. The C1/BN2 alterations form a genetic basis of immune evasion corresponding to mutations seen in marginal zone lymphoma. Non-overlapping genes include mutations of B2M, FAS, HLA-B and translocations of PD-1 ligands.

ii. The NMF-C2 subtype is analogues to the LymphGen-A53 subtype. Both have characteristic TP53 inactivation, and a high degree of genome instability as reflected by the prominence of genome-wide CNAs. This subtype is not significantly enriched for either of the two COO types, which underpins that the original COO dichotomy was indeed an oversimplification of DLBCL biology. Overall survival of this C2/A53 subtype under R-CHOP treatment is unfavorable. A notable difference between the two subtypes is the high number of discordant subtype-defining features (36 from 41), including driver alterations such as chromosomal deletion of the CDKN2A locus (9p.21).

iii. The NMF-C3 subtype is analogues to the LymphGen-EZB subtype, with a relatively high concordance of subtype-defining alterations (10 out of 18); including translocations of BCL2, and mutations in chromatin modifying genes. Discordant features include amplification of the REL locus (2p16.1) and mutations of FAS. The C3/EZB subtype represents classic GCB-type DLBCLs, and the genetic features are to a large extent alike follicular lymphoma (FL), which suggest that these DLBCLs represent transformed FL (29). Clinically, C3/EZB subtype tumors are considered of most high risk within the GCB-type of DLBCLs. Notably, also the RNA-based DHITSig is enriched in this subtype and used to further subdivide EZB.

iv. The NMF-C4 subtype is analogous to the LymphGen-ST2 subtype. C4/ST2 subtype defining alterations affect BCR/PI3K signalling, the JAK/STAT pathway, and histone genes. Most of these DLBCLs belong to the GCB-type with favorable outcome. Few alterations linked to this subtype are concordant between the two classification systems (6 out of 24). The less defined nature of this subtype is further underpinned by a recent study suggesting that this subtype may be further subdivided into two subtypes with divergent biology: a TET2/SGK1 and a SOCS1/SGK1 subtype (13).

v. The NMF-C5 subtype is analogues to the LymphGen-MCD subtype. Nine of the 24 characteristic alterations overlap which include mutations in genes associated with extranodal involvement (MYD88, CD79B, TBL1XR1). This C5/MCD subtype is highly enriched for ABC-type DLBCLs and is the subtype with the least favorable survival under R-CHOP treatment. Discordant alterations include other markers of immune evasion (mutations of HLA-B and translocations of PD-1 ligands) and copy number gains of chromosomal arms 3q and 18q.

vi. Finally, the LymphGen classification describes the N1 subtype which is characterized by NOTCH1 mutations. This subtype occurs in less than 2% of DLBCLs Figure 1 and has the worst survival among the LymphGen subtypes. This subtype is not recognized by the NMF algorithm with the DFCI cohort. Also, when we extend the DFCI cohort with another 500 DLBCLs treated with R-CHOP, the NMF algorithm still does not recognize this class (authors unpublished results).

The bioinformatic approaches of the current DNA-based subtyping systems for DLBCL

The DFCI group used unsupervised clustering combined with alteration-centric features (Box 2). Driver alterations were discriminated from passengers, thereby reducing the genetic dataset to 158 features. Non-negative matrix factorization (NMF), an unsupervised clustering algorithm that detects patterns of co-occurring features and assigns a subtype to each included tumor, was used. The number of clusters to be identified was predefined between 4 and 10, which is actually an arbitrary choice. The NMF algorithm identified the optimal stability of clusters to be represented by 5 DLBCL groups of similar sizes, which the authors labelled as C1 to C5.

The NCI group used semi-supervised clustering combined with gene-centric features (Box 2). The prior knowledge given were four predefined classes, each composed of 1 or 2 specific DNA "seed" alterations: MCD (seed is co-mutation of *CD79B* and *MYD88L265P*), BN2 (seed is *NOTCH2* mutation or *BCL6* translocation), N1 (seed is *NOTCH1* mutation) and EZB (seed is *EZH2* mutation or *BCL2* translocation). Finally, the algorithm selected the additional genomic features that had the strongest association with the four classes through an iterative approach. All patient samples were included for classification with this 4-class algorithm, yet of the entire cohort, only 46% of cases could be assigned (11). In the remaining 54% of cases in the NCI cohort recurrent alterations of *TP53* (25%), *TET2* (10%) and *SGK1* (6.9%) were identified. This prompted the NCI group to refine and extend the four classes with two additional classes: A53 (seed is mutation and/or CNA of *TP53*) and ST2 (seed is mutations of *SGK1* and *TET2*), resulting in six seed classes (12). Subsequently, a Bayesian predictor model titled "LymphGen" was developed, which calculates for each individual tumor the subtype probabilities for each of the six classes based on its genetic alterations. Tumors designated as "core" tumors were defined as being attributed to one class with a probability score of >90%. Consequently, the Bayesian predictor allows tumors to be assigned to multiple classes. Those with a probability score greater than 90% for more than one class are the so called "genetically composite" tumors. Tumors with a probability score of 50%-90% for one single class were termed "extended" class members. Tumors with few subtype-specific genetic alterations were left unclassified. Thereby, the then 6-class LymphGen algorithm assigned 63.1% of cases of the NCI cohort (12). Later, the RNA expression-based *MYC* double-hit signature (DHITSig), previously developed by others (34), was added as a surrogate for *MYC* translocation status to split the EZB class in *MYC* positive and *MYC* negative cases.

Box 2 Genome feature definition and subtyping algorithms.

The two proposed DNA-based subtyping systems differ in their bioinformatic approaches for i) genomic feature definition, and ii) subtype identification (10, 12):

i. To define genomic features a gene-centric approach can be applied that combines all DNA alterations that impact the same gene into 1 feature, independent of whether they are a mutation, translocation or CNA. For example, a point-mutation of CDKN2A and a deletion of the CDKN2A-locus 9p.21 would be recognized as 1 feature. Alternatively, an alteration-centric approach regards each DNA alteration type separately, independent of their location in the genome. In the example of CDKN2A, the mutation and 9p.21 deletion are regarded as two separate features.

ii. Also machine learning algorithms for patient subtyping can generally be divided in 2 main approaches, supervised or unsupervised (30). The supervised approach uses predefined classes to construct a classification rule from the features. An unsupervised approach leaves it to the algorithm to identify a number of subtypes that are composed of feature characteristics prioritized by the algorithm. Semi-supervised learning would be where some prior knowledge on classes and or features is given.

Critical evaluation of the current subtyping approaches for DLBCL

Despite the different choices in feature identification and machine learning algorithms (Box 2), the NCI and DFCI groups recognize a similar and extensive underlying biological heterogeneity of DLBCL. Some subtypes are already more similar than others. For example LymphGens MCD/NMF C5, LymphGen A53/NMF C2 and LymphGen EZB/NMF C3 are already relatively consistently defined. An important difference is that the LymphGen algorithm does only assign 63.1% of patients to any of their predefined subtypes, whereas the DFCIs NMF algorithm defines a number of subtypes to which 100% of the samples in the cohort are assigned. The N1 subtype is the rarest subtype and is only recognized by the NCI with the *NOTCH1* mutation seed given to the LymphGen algorithm (Box 1).

A small fraction of DLBCL patients (<2%) carry *NOTCH1* mutations which infers potential specific sensitivity to Ibrutinib, a Bruton's tyrosine kinase (BTK) inhibitor. Due to its low frequency, the N1 subtype is not recognized using unsupervised techniques in relatively small series. The size of the currently studied cohorts has been too small, hence underpowered, to detect such rare genomic subtypes by unsupervised analysis. Unknown small genomic subtypes can only get recognized once the sample size is sufficiently large, as exemplified by Curtis et al. for breast cancer (35). Rare subtypes like N1 may be characterized by very specific biological characteristics that make them uniquely targetable with specific potent inhibitors and thereby highly relevant to be recognized. As an example from another cancer entity, in about 1% of metastatic colorectal cancers the *ERBB2* oncogene on chromosome 17q is amplified, which can be effectively targeted by trastuzumab and neratinib and results in high response rates in these tumors (36–38). Likewise, 4-5% of non-small-cell lung cancers have a translocation of the *ALK* gene, which can be effectively targeted by the ALK inhibitor crizotinib (39).

Not recognized by either NCI or DFCI are the actual high- grade B-cell lymphoma (HGBCL), B-cell lymphomas with MYC translocation together with either BCL2 and/or BCL6 translocation (double hit/triple hit). Unsupervised NMF clustering theoretically might be able to recognize this group as a subtype but, like the N1 subtype, it may have remained undetected as a result of the limited number of MYC-translocation positive DLBCLs in the DFCI dataset. The DHITSig signature used by the NCI is a surrogate marker to recognize a MYC subtype and troublesome for various reasons. First it is not DNA alteration derived and requires a different assay, namely RNA expression analysis. Second, the name of this signature is deceiving since it implies a genetic context of HGBCL, whereas only 64% of DHITSig-positive GCB- type DLBCLs actually carry a MYC translocation and 52% are actual double hit/triple hit DLBCLs (34). Third, also other lymphoma classes besides HGBCL double hit/triple hit such as Burkitt lymphoma score positive for DHITSig. This RNA DHIT signature is thus not specific for either *MYC* translocation or HGBCL (40, 41).

Besides the choice of subtyping algorithms, the NCI gene-centric versus DFCI alteration-centric choices for genetic features deserve attention (Box 2). The easiest solved are the focal chromosomal CNAs, aberrations smaller than 3Mb (42) which only encompass one or few genes, and can therefore be combined in a gene-centric fashion (43). The choice between alteration- or gene- centric is not obvious for the larger-scale chromosomal CNAs since they harbor hundreds of genes. Rather than rationalizing a choice between a gene-or alteration-centric approach, the machine learning algorithms can be offered data processed in either manner and side-by-side evaluated for best subtyping performance. Although the unsupervised clustering choice is an elegant data-driven approach to identify subtypes (17, 44, 45), in the end a classifier, like LymphGen, will need to be built to diagnose individual patients in daily clinical practice, which dictates another step towards harmonization.

Towards a unifying classification for DLBCL; Lessons learned from other tumor types

Two steps towards clinical implementation of a DNA-based classification of DLBCL

The currently proposed DNA-based subtypes will be the basis for a unified biological classification that may require a two-step strategy (28). Step 1 would involve harmonization of the current DNA-subtyping systems into a single unified classification, Step 2 would be the development of a reproducible and widely applicable molecular diagnostic assay;

certified, as well as cost- and time-effective to enable clinical implementation. This exposes various challenges, from the choice of laboratory technique, subtype-defining DNA alteration features and interpretation to classification algorithms and bioinformatic procedures.

A universally accepted classification is a prerequisite to improve patient management

Harmonization into a single classification is a first requirement for implementation in diagnostic routine.

Objective, reproducible, and conclusive subtype definition for each patient sample, combined with a detailed understanding of the tumor biology of each defined DNA-class, will enable to explore clinical consequences of such classification, preferably in clinical trials (46). For various organ-specific malignancies molecular classifications for tumor families have now been standardized and integrated in the 5th edition series of the WHO Classifications and are starting to be implemented in the diagnostic workflow for those settings that have access to the technology (47–49). The road towards this level of applicability has been achieved with several research groups proposing their individual molecular classification as a starting point, at different moments in time and with different laboratory and bioinformatical techniques, as is exemplified by the classification of breast cancer, central nervous system (CNS) tumors and colorectal cancer (48, 49).

Lessons learned from classifications that are universally agreed upon for other solid malignancies

Probably breast cancer classification is one of the most successful early examples. An RNA-based classification for breast cancer found its way already into the 4th edition of the WHO Classifications of Breast Tumours in 2012, which was further expanded upon in 5th edition (47). it recognizes 5 molecular classes; each with different prognosis but also different treatment recommendations. The existing close transatlantic collaborations undoubtedly facilitated consensus formation, characterized as “organic” allowing different biological and bioinformatical perspectives to converge (46, 50, 51). Once a consensus classification was established and reproducible assays were developed, exploration of personalized and targeted treatment approaches could be effectively explored to identify bespoke treatment modalities, amongst others in the multi-armed I-SPY clinical trials (52).

From the point of view of development of a molecular-based consensus classification, the present WHO classification for CNS tumors is an impressive result of intensive collaboration leading to a highly refined molecular classification. In 2014 a group of neuro- oncological pathologists, physically converged in 2014 in Haarlem (NLD) and prepared a clinically relevant histo-molecular diagnostic consensus classification, whilst reducing interobserver variability (53), which soon was implemented in the 4th edition of the WHO Classification of CNS Tumors (54). Subsequently, a largely novel approach was taken by means of genome-wide DNA methylation analysis where the large spectrum of CNS tumors were recognized by methylation profiles combined with a form of dimension reduction called t-distributed stochastic neighbor embedding (t- SNE) (55). The t-SNE methylation test alone allows for diagnoses of the large majority of CNS tumors, not seldomly more detailed and/or reliable compared to the histo-molecular diagnosis, resulting in redefinition of these entities. The collaborative effort with inclusion of samples and intellectual input from many research groups across the world as well as extensive discussions in the Consortium to Inform Molecular and Practical Approaches to CNS Tumor Taxonomy (cIMPACT-NOW) (56) has helped a broad acceptance and indeed this molecular classification is now also included in the 5th edition of the WHO Classification of Central Nervous System Tumours (48, 48).

To harmonize colorectal cancer (CRC) classification, the Colorectal Cancer Subtyping Consortium (CRCSC) was formed to integrate six independently published RNA-based classifications (49). As opposed to the CNS assembly consensus, a predefined mathematical harmonization path was taken with the aim to resolve inconsistencies between the various CRC classification systems. This approach culminated in four consensus molecular subtypes (CMSs) (49) to which each CRC sample adheres to a higher (core samples) or lesser (non-core) extend. Since the context in CRC classification is so very similar to the current status in DLBCL, we here provide a summary of this CMS approach where three generic methodological steps were involved (Box 3).

The process to come to a single, harmonized molecular classification for DLBCL may likely be the one taken for the development of colorectal cancer CMS. For DLBCL also, a similar issue in the underlying biology result in single class (core) tumors, unclassified samples and genetically composite tumors (12, 57). What should alleviate the consensus process is that for DLBCL two, rather than the six for colorectal cancer, existing DNA-classifications as a starting point while still various independent published and unpublished (authors of this review) datasets are available.

Box 3 Summary of the data-driven bioinformatic path to the four consensus molecular subtypes for colorectal cancer.

Three generic methodological steps are involved in the path taken for consensus classification of colorectal cancer.

i. Independent expert team subtyping prediction on normalized raw data sets: Eighteen RNA-based CRC gene expression data sets, derived from different continents and research groups were assembled from public resources (Gene Expression Omnibus and The Cancer Genome Atlas). The data sets were compiled from various genome-wide expression analysis techniques (arrays and RNA-sequencing), different sample types (formalin-fixed paraffin embedded and fresh- frozen tissue materials) and different study designs (retrospective and prospective series, including clinical trials). The first bioinformatics step concerned central pre-processing and normalization aimed to obtain expression profiles for each of the patients of the 18 gene-expression datasets, independent of cohort or technique. Next, each of the six initial participating research teams applied their original classification algorithm to each of the 18 data sets. Thus, resulting in six classifications, with a total of 27 different subtypes for all 3,962 patients.

ii. Network analysis for consensus subtype identification: Using the six classification systems of the 3,962 patients, a network-based approach was applied to study the association between all the 27 subtypes. To detect robust clusters of recurrent molecular subtypes, an unsupervised Markov clustering approach was performed, resulting in the identification of four consensus molecular subtypes (CMSs). Of the 3962 samples, 3104 (78%) were identified as highly representative of a particular subtype and labelled as core consensus samples and the remaining n=858 as non-consensus samples. The core consensus samples were used to train the novel CMS classifier in the subsequent step.

iii. CMS classifier construction and application: To allow classifications of individual cases, which is mandatory for diagnostic routine, a classification algorithm is required. Since the data sets were created using different RNA gene expression profiling techniques across the different studies, not all genes were included in all data sets. The CRCSC first converted all 18 separate data sets into a single data set. The genes that were commonly profiled by all separate data sets were selected to allow aggregation of all 18 data sets into a single data matrix. To construct the CMS classifier, the single data matrix, CMS classes and consensus sample set were used. The consensus samples were randomly split using two-third as training and one-third as validation set, and a random forest classifier was generated to calculate a prediction value for subtype assignment for each sample, by means of bootstrapping with 500 iterations. Application of the CMS classifier on the validation set demonstrated an overall accuracy of 90%. The CMS classifier was robust enough to allow assignment of 40% of the non-consensus samples, while the rest showed heterogeneous patterns of CMS subtypes and contained biological information of more than one class.

From DLBCL genome classification to clinical implementation

DNA alterations required for DLBCL genome classification

Any consensus classification for DLBCL will include a combination of mutations and structural chromosomal variations (CNAs and translocations) (Box 1). Therefore, inclusion of this information into a single genome subtyping assay would be highly attractive. Various common laboratory and bioinformatics applications are available for mutation and CNA detection by NGS. Also NGS-based translocation detection is starting to become a cost-effective alternative for routinely used Fluorescent in situ hybridization (FISH) to determine translocations. (Figure 2). FISH benefits from a choice of worldwide commercially available probes and assays but is labor-intensive with a certain level of technical variability and subjectivity in interpretation.

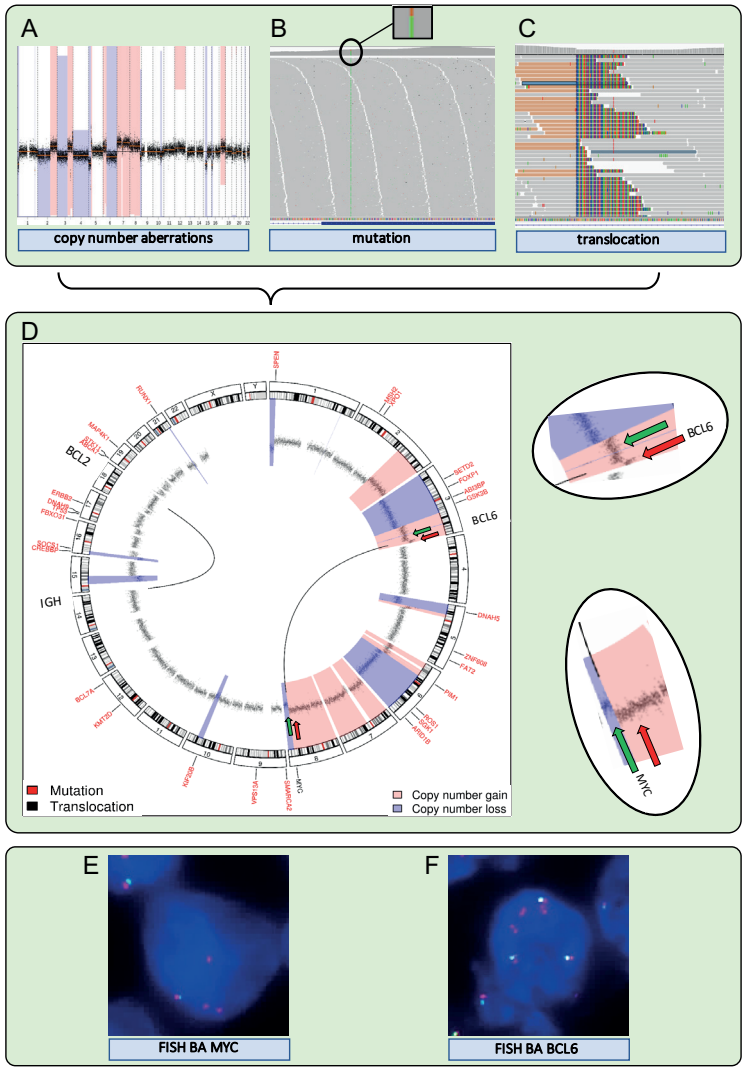

Figure 2. A single NGS assay to detect somatic mutations and structural variations, including translocations and CNAs, from DNA extracted from FFPE tissue. (A–C) Visualization of the detection by NGS of CNAs, mutations, and translocations for a DLBCL sample. (A) Genome-wide chromosomal CNAs. x-axis shows chromosomes 1 to 22, from left to right, y-axis shows copy number gains (light red) and copy number losses (blue). (B) Screenshot of high coverage (200X) NGS sequence reads aligned to the reference genome highlighting a somatic mutation in KMT2D. (C) Screenshot of high coverage (200X) NGS sequence reads aligned to the reference genome highlighting a translocation breakpoint in MYC. (D) A circular representation of the genome depicting mutations (genes denoted in small red letters), translocations (genes denoted with large black letters connected by black lines) and CNAs (inner circle: black dots are measurement bins and called losses are colored in blue and gains in light red). Green and red arrows point to the position of break apart (BA) FISH probes that were used as a control for the translocations detected by NGS. (E) FISH BA MYC. (F) FISH BA BCL6. Integrated NGS analysis explains aberrant FISH pattern: a loss (green arrow) and a gain (red arrow) at the MYC locus coincide with a single (green arrow) and double gain (red arrow) at the translocation partner BCL6 locus.

Thereby, NGS outperforms FISH in several ways: it avoids interobserver variability, it can be performed with small and histologically compromised materials, and it is able to identify exact translocation breakpoints on nucleotide level. An additional advantage of some of the NGS approaches is that unknown translocation partners may be identified, that may be of clinical relevance for the biological and clinical interpretation of DLBCL patients with a *MYC* translocation (40). Various combinations of NGS and bioinformatics platforms have been successfully developed in this direction (58–61).

Assays for clinical implementation

World-wide clinical implementation of any diagnostic routine requires relatively simple assays that are applicable to routine diagnostic tissue material, such as formalin-fixed paraffin embedded (FFPE) specimens. The elaborate laboratory- and informatics infrastructure needed for current NGS or array analysis may only be available in selected settings of large medical centers or commercial providers as exemplified for CNS tumors. Favorable aspects of commercial involvement are the wide availability, extensive standardization, quality control and rapid turnover time due to high case volumes. Downsides are amongst others worldwide availability, financial dependency and commercial goals, market dominance of individual commercial providers, lack of technical transparency and development, lack of flexibility to include most recent research developments and generally lack of integrated interpretation with other pathology parameters. Another option to bring a genome subtyping assay to implementation in daily practice is to "reduce" complex molecular information to simpler and widely applicable techniques. The DLBCL-COO classification alternative is a good example; genome-wide molecular classification with elaborate bioinformatics was translated into several simple immunohistochemistry (IHC) markers, of which the Hans classification is most widely used (62). All IHC-based COO assays show limited concordance with the gold standard of RNA expression-based assays (63). This prompted the development of a digital gene expression assay based on 20 key genes that can be applied on FFPE material (64). This Lymph2Cx assay, restricted to equipment from the company Nanostring (Seattle, USA), showed high concordance with the original RNA expression- based COO classification with a 2% error rate in COO assignment (65). These characteristics, together with a short turnaround time of less than 36 hours, allowed for rapid molecular characterization of patients, making this assay a suitable middle-ground alternative for employment in research and clinical trials (19). Similar assays have been commercialized by others (66). In view of the expected high-dimensional nature of a consensus molecular classifier for DLBCL, simple translation to an IHC is not likely. Current NGS techniques are already reliably applicable for FFPE biopsy samples offered by

commercial providers. It may be expected that these companies will readily offer products for consensus molecular DLBCL classification once this would be developed.

Assay and turnaround time

A single genome subtyping assay that detects CNAs, mutations, and translocations in parallel would conceivably be most efficient in terms of labor, cost and tissue material. But is this also efficient in terms of turnaround time? A recent study showed that real-time molecular profiling of RNA-based COO determination of DLBCL is realistic to stratify patients in a timely manner, with a median turnaround time of 8 days (8). This would be a desirable timeframe for DNA-based DLBCL classification, such that based on tumor vulnerabilities, patients can be diverted after 1 or 2 cycles standard R-CHOP treatment, which is a successful approach facilitating rapid trial inclusion (67). A recent feasibility study in the Netherlands, which involves a WGS specialized non-profit organization, was performed to evaluate implementation of WGS into routine diagnostics (68). Meanwhile, they were able to optimize the turnaround time from biopsy to DNA report to 7 working days, demonstrating the potential of clinical implementation of NGS methods for these purposes.

Application in daily clinical practice and promising future developments

Bespoke treatment of DLBCL patients

Once validated, uniform and widely applicable, consensus molecular subtypes of DLBCL will be a sound basis to explore more effective, targeted treatment methods (1). The potential of DNA-based classification for precision medicine of DLBCL has been demonstrated in a recent retrospective analysis of a randomized phase-III trial (69). In this study, patients under 60 with two specific DNA subtypes (LymphGen's MCD and N1) that received R-CHOP with Ibrutinib had significantly better survival (both subtypes 100% 3-year event-free survival) than patients that received R-CHOP alone (42.9% and 50%, respectively), clearly indicating the potential predictive value of the novel genomic subtypes. Next, prospective clinical trials may further explore associations with genomic subtypes and associations with targeted compounds, such as NFkB-inhibitors, PI3K inhibitors, P53-modulators and apoptosis modulators, as well as immunotherapy such as immune checkpoint inhibitors and CAR- T cell therapy. For this purpose, various dedicated next-generation designs are now proposed (70).

It is obvious to further investigate to what extent the integration of the current DNA-based and RNA/ microenvironmental-based subtyping methods for DLBCL would be of

added value. Adding a layer of epigenetic information as for CNS (55) or even germline genetic characteristics might be considered (71). Also liquid biopsy strategies measuring circulating tumor DNA (ctDNA), will provide other lines of opportunities in diagnosis and disease monitoring of DLBCL patients (72–74) Future studies are required to investigate the potential integration of these approaches for the management of DLBCL patients.

Consensus classification serves the DLBCL patient

The step forward to allow evaluation of new treatment modalities based on DLBCL genetics is now impeded by a discordancy between the 2 independently suggested genomic subtyping approaches, which dictates the challenge that lies ahead of us. Based on various other tumor entities we suggest a blueprint for harmonization of the proposed DNA subtypes, which may allow more widespread clinical implementation. Once this hurdle is taken, a diagnostic work up, applicable in a clinically relevant timeframe, will enable the design of next- generation prospective biomarker-based clinical trials. If successful, the precision medicine with targeted therapies that match dependencies of the molecular subtypes of DLBCL may be brought forward.

Author contributions

MM, MR, DJ, and BY contributed to conception and design of the review and wrote the first draft of the manuscript. All authors contributed to manuscript revision, read, and approved the submitted version.

Funding

This work was supported by the Dutch Cancer Society grant KWF 2012-5711.

Acknowledgments

The authors like to thank dr. Erik van Dijk for critically reading the manuscript prior to submission and Prof. Dr. Pieter Wesseling for helpful discussions on CNS diagnostics, both affiliated to Amsterdam UMC, Vrije Universiteit Amsterdam, Department of Pathology, Amsterdam, The Netherlands.

Conflict of interest

The authors declare that the research was conducted in the absence of any commercial or financial relationships that could be construed as a potential conflict of interest.

Publisher's note

References

1. Sehn LH, Salles G. Diffuse Large b-cell lymphoma. N Engl J Med (2021) 384 (9):842–58. doi: 10.1056/NEJMra2027612
2. He MY, Kridel R. Treatment resistance in diffuse large b-cell lymphoma. Leukemia (2021) 35(8):2151–65. doi: 10.1038/s41375-021-01285-3
3. Gisselbrecht C, Schmitz N, Mounier N, Singh Gill D, Linch DC, Trneny M, et al. Rituximab maintenance therapy after autologous stem-cell transplantation in patients with relapsed CD20(+) diffuse large b-cell lymphoma: final analysis of the collaborative trial in relapsed aggressive lymphoma. J Clin Oncol (2012) 30 (36):4462–9. doi: 10.1200/JCO.2012.41.9416
4. Alizadeh AA, Eisen MB, Davis RE, Ma CL, Lossos IS, Rosenwald A, et al. Distinct types of diffuse large b-cell lymphoma identified by gene expression profiling. Nature (2000) 403(6769):503–11. doi: 10.1038/35000501
5. Rosenwald A, Wright G, Chan WC, Connors JM, Campo E, Fisher RI, et al. The use of molecular profiling to predict survival after chemotherapy for diffuse large-b-cell lymphoma. N Engl J Med (2002) 346(25):1937–47. doi: 10.1056/ NEJMoa012914
6. Swerdlow SH, Campo E, Pileri SA, Harris NL, Stein H, Siebert R, et al. The 2016 revision of the world health organization classification of lymphoid neoplasms. Blood (2016) 127(20):2375–90. doi: 10.1182/blood-2016-01-643569
7. Younes A, Sehn LH, Johnson P, Zinzani PL, Hong X, Zhu J, et al. Randomized phase III trial of ibrutinib and rituximab plus cyclophosphamide, doxorubicin, vincristine, and prednisone in non–germinal center b-cell diffuse large b-cell lymphoma. J Clin Oncol (2019) 37(15):1285–95. doi: 10.1200/JCO.18.02403
8. Davies A, Cummin TE, Barrans S, Maishman T, Mamot C, Novak U, et al. Gene-expression profiling of bortezomib added to standard chemoimmunotherapy for diffuse large b-cell lymphoma (REMoDL-b): an open-label, randomised, phase 3 trial. Lancet Oncol (2019) 20(5):649–62. doi: 10.1016/S1470-2045(18)30935-5
9. Nowakowski GS, Chiappella A, Gascoyne RD, Scott DW, Zhang Q, Jurczak W, et al. ROBUST: A phase III study of lenalidomide plus r-CHOP versus placebo plus r-CHOP in previously untreated patients with ABC-type diffuse Large b-cell lymphoma. J Clin Oncol Off J Am Soc Clin Oncol (2021) 39(12):1317–28. doi: 10.1200/JCO.20.01366
10. Chapuy B, Stewart C, Dunford A, Kim J, Kamburov A, Redd R, et al. Molecular subtypes of diffuse Large b-cell lymphoma are associated with distinct pathogenic mechanisms and outcomes. Nat Med (2018) 24(5):679–90. doi: 10.1038/s41591-018-0016-8
11. Schmitz R, Wright GW, Huang DW, Johnson CA, Phelan JD, Wang JQ, et al. Genetics and pathogenesis of diffuse Large b-cell lymphoma. N Engl J Med (2018) 378(15):1396–407. doi: 10.1056/NEJMoa1801445
12. Wright GW, Huang DW, Phelan JD, Coulibaly ZA, Roulland S, Young RM, et al. A probabilistic classification tool for genetic subtypes of diffuse Large b cell lymphoma with therapeutic implications. Cancer Cell (2020) 37(4):551–568.e14. doi: 10.1016/j.ccell.2020.03.015
13. Lacy SE, Barrans SL, Beer PA, Painter D, Smith AG, Roman E, et al. Targeted sequencing in DLBCL, molecular subtypes, and outcomes: a haematological malignancy research network report. Blood (2020) 135(20):1759– 71. doi: 10.1182/blood.2019003535
14. Roschewski M, Phelan JD, Wilson WH. Molecular classification and treatment of diffuse Large b-cell lymphoma and primary mediastinal b-cell lymphoma. Cancer J (2020) 26(3):195–205. doi: 10.1097/PPO.0000000000000450

15. Weber T, Schmitz R. Molecular subgroups of diffuse Large b cell lymphoma: Biology and implications for clinical practice. Curr Oncol Rep (2022) 24(1):13–21. doi: 10.1007/s11912-021-01155-2

16. SimonR.Developmentandvalidationoftherapeuticallyrelevantmulti-gene biomarker classifiers. JNCI J Natl Cancer Inst (2005) 97(12):866–7. doi: 10.1093/ jnci/dji168

17. Zhao L, Lee VHF, Ng MK, Yan H, Bijlsma MF. Molecular subtyping of cancer: current status and moving toward clinical applications. Brief Bioinform (2019) 20(2):572–84. doi: 10.1093/bib/bby026

18. Ennishi D, Hsi ED, Steidl C, Scott DW. Toward a new molecular taxonomy of diffuse large B-cell lymphoma. Cancer Discov (2017) 10(9):1267–81. doi: 10.1158/2159-8290.CD-20-0174

19. Nowakowski GS, Chiappella A, Witzig TE, Scott DW, Spina M, Gascoyne RD, et al. Variable global distribution of cell-of-origin from the ROBUST phase III study in diffuse large b-cell lymphoma. Haematologica (2020) 105(2):e72–5. doi: 10.3324/haematol.2019.220475

20. Monti S, Savage KJ, Kutok JL, Feuerhake F, Kurtin P, Mihm M, et al. Molecular profiling of diffuse large b-cell lymphoma identifies robust subtypes including one characterized by host inflammatory response. Blood (2005) 105 (5):1851–61. doi: 10.1182/blood-2004-07-2947

21. Steen CB, Luca BA, Esfahani MS, Azizi A, Sworder BJ, Nabet BY, et al. The landscape of tumor cell states and ecosystems in diffuse large b cell lymphoma. Cancer Cell (2021) 39(10):1422–1437. e10. doi: 10.1016/j.ccell.2021.08.011

22. Morin RD, Mendez-Lago M, Mungall AJ, Goya R, Mungall KL, Corbett RD, et al. Frequent mutation of histone-modifying genes in non-Hodgkin lymphoma. Nature (2011) 476(7360):298–303. doi: 10.1038/nature10351

23. Pasqualucci L, Dominguez-Sola D, Chiarenza A, Fabbri G, Grunn A, Trifonov V, et al. Inactivating mutations of acetyltransferase genes in b-cell lymphoma. Nature (2011) 471(7337):189–95. doi: 10.1038/nature09730

24. Pasqualucci L, Trifonov V, Fabbri G, Ma J, Rossi D, Chiarenza A, et al. Analysis of the coding genome of diffuse large b-cell lymphoma. Nat Genet (2011) 43(9):830–7. doi: 10.1038/ng.892

25. Lohr JG, Stojanov P, Lawrence MS, Auclair D, Chapuy B, Sougnez C, et al. Discovery and prioritization of somatic mutations in diffuse large b-cell lymphoma (DLBCL) by whole-exome sequencing. Proc Natl Acad Sci U S A. (2012) 109 (10):3879–84. doi: 10.1073/pnas.1121343109

26. Zhang J, Grubor V, Love CL, Banerjee A, Richards KL, Mieczkowski PA, et al. Genetic heterogeneity of diffuse large b-cell lymphoma. Proc Natl Acad Sci U S A. (2013) 110(4):1398–403. doi: 10.1073/pnas.1205299110

27. Oudejans JJ, Van Wieringen WN, Smeets SJ, Tijssen M, Vosse SJ, Meijer CJLM, et al. Identification of genes putatively involved in the pathogenesis of diffuse large b-cell lymphomas by integrative genomics. Genes Chromosom Cancer (2009) 48(3):250–60. doi: 10.1002/gcc.20632

28. Crombie JL, Armand P. Diffuse Large b-cell lymphoma's new genomics: The bridge and the chasm. J Clin Oncol (2020) 38(30):3565–74. doi: 10.1200/JCO.20.01501

29. Okosun J, Bödör C, Wang J, Araf S, Yang C-Y, Pan C, et al. Integrated genomic analysis identifies recurrent mutations and evolution patterns driving the initiation and progression of follicular lymphoma. Nat Genet (2014) 46(2):176–81. doi: 10.1038/ng.2856

30. Greener JG, Kandathil SM, Moffat L, Jones DT. A guide to machine learning for biologists. Nat Rev Mol Cell Biol (2021) 23(1):40–55. doi: 10.1038/s41580-021-00407-0

31. Runge HFP, Lacy S, Barrans S, Beer PA, Painter D, Smith A, et al. Application of the LymphGen classification tool to 928 clinically and genetically- characterised cases of diffuse large b cell lymphoma (DLBCL). Br J Haematol (2021) 192(1):216–20. doi: 10.1111/bjh.17132

32. Bolen CR, Klanova M, Trnény M, Sehn LH, He J, Tong J, et al. Prognostic impact of somatic mutations in diffuse large b-cell lymphoma and relationship to cell-of-origin: data from the phase III GOYA study. Haematologica (2020) 105 (9):2298–307. doi: 10.3324/haematol.2019.227892
33. Dubois S, Tesson B, Mareschal S, Viailly PJ, Bohers E, Ruminy P, et al. Refining diffuse large b-cell lymphoma subgroups using integrated analysis of molecular profiles. EBioMedicine (2019) 48:58–69. doi: 10.1016/ j.ebiom.2019.09.034
34. Ennishi D, Jiang A, Boyle M, Collinge B, Grande BM, Ben-Neriah S, et al. Double-hit gene expression signature defines a distinct subgroup of germinal center b-Cell-Like diffuse Large b-cell lymphoma. J Clin Oncol (2019) 37(3):190– 201. doi: 10.1200/JCO.18.01583
35. Curtis C, Shah SP, Chin S-F, Turashvili G, Rueda OM, Dunning MJ, et al. The genomic and transcriptomic architecture of 2,000 breast tumours reveals novel subgroups. Nature (2012) 486(7403):346–52. doi: 10.1038/nature10983
36. Meric-Bernstam F, Hurwitz H, Raghav KPS, McWilliams RR, Fakih M, VanderWalde A, et al. Pertuzumab plus trastuzumab for HER2-amplified metastatic colorectal cancer (MyPathway): an updated report from a multicentre, open-label, phase 2a, multiple basket study. Lancet Oncol (2019) 20(4):518–30. doi: 10.1016/S1470-2045(18)30904-5
37. Hyman DM, Piha-Paul SA, Won H, Rodon J, Saura C, Shapiro GI, et al. HER kinase inhibition in patients with HER2- and HER3-mutant cancers. Nat (2018) 554(7691):189–94. doi: 10.1038/ nature25475
38. Haan JCJC, Labots M, Rausch C, Koopman M, Tol J, Mekenkamp LJMLJM, et al. Genomic landscape of metastatic colorectal cancer. Nat Commun (2014) 5:5457. doi: 10.1038/ncomms6457
39. Chia PL, Mitchell P, Dobrovic A, John T. Prevalence and natural history of ALK positive non-small-cell lung cancer and the clinical impact of targeted therapy with ALK inhibitors. Clin Epidemiol (2014) 6:423. doi: 10.2147/CLEP.S69718
40. Rosenwald A, Bens S, Advani R, Barrans S, Copie-Bergman C, Elsensohn MH, et al. Prognostic significance of MYC rearrangement and translocation partner in diffuse Large b-cell lymphoma: A study by the lunenburg lymphoma biomarker consortium. J Clin Oncol (2019) 37(35):3359–68. doi: 10.1200/JCO.19.00743
41. Sha C, Barrans S, Cucco F, Bentley MA, Care MA, Cummin T, et al. Molecular high-grade b-cell lymphoma: Defining a poor-risk group that requires different approaches to therapy. J Clin Oncol (2018) 37(3):202–12. doi: 10.1200/ JCO.18.01314
42. Krijgsman O, Carvalho B, Meijer GA, Steenbergen RDM, Ylstra B. Focal chromosomal copy number aberrations in cancer-needles in a genome haystack. Biochim Biophys Acta - Mol Cell Res (2014) 1843(11):2698–704. doi: 10.1016/j.bbamcr.2014.08.001
43. Santarius T, Shipley J, Brewer D, Stratton MR, Cooper CS. A census of amplified and overexpressed human cancer genes. Nat Rev Cancer (2010) 10(1):59– 64. doi: 10.1038/nrc2771
44. Brunet JP, Tamayo P, Golub TR, Mesirov JP. Metagenes and molecular pattern discovery using matrix factorization. Proc Natl Acad Sci U S A. (2004) 101 (12):4164–9. doi: 10.1073/ pnas.0308531101
45. Tamayo P, Scanfeld D, Ebert BL, Gillette MA, Roberts CWM, Mesirov JP, et al. Metagene projection for cross-platform, cross-species characterization of global transcriptional states. Proc Natl Acad Sci U S A. (2007) 104(14):5959–64. doi: 10.1073/pnas.0701068104
46. Russnes HG, Lingjærde OC, Børresen-Dale A-L, Caldas C. Breast cancer molecular stratification: From intrinsic subtypes to integrative clusters. Am J Pathol (2017) 187(10):2152–62. doi: 10.1016/j.ajpath.2017.04.022

47. Tan PH, Ellis I, Allison K, Brogi E, Fox SB, Lakhani S, et al. The 2019 world health organization classification of tumours of the breast. Histopathology (2020) 77(2):181–5. doi: 10.1111/his.14091

48. Louis DN, Perry A, Wesseling P, Brat DJ, Creel A, Figarella-Branger D, et al. The 2021 WHO classification of tumors of the central nervous system: a summary. Neuro Oncol (2021) 23(8):1231–51. doi: 10.1093/neuonc/noab106

49. Guinney J, Dienstmann R, Wang X, de Reynies A, Schlicker A, Soneson C, et al. The consensus molecular subtypes of colorectal cancer. Nat Med (2015) 21 (11):1350–6. doi: 10.1038/nm.3967

50. Perou CM, Sørile T, Eisen MB, Van De Rijn M, Jeffrey SS, Ress CA, et al. Molecular portraits of human breast tumours. Nature (2000) 406(6797):747–52. doi: 10.1038/35021093

51. Sørlie T, Perou CM, Tibshirani R, Aas T, Geisler S, Johnsen H, et al. Gene expression patterns of breast carcinomas distinguish tumor subclasses with clinical implications. Proc Natl Acad Sci U S A. (2001) 98(19):10869–74. doi: 10.1073/ pnas.191367098

52. Chien AJ, Tripathy D, Albain KS, Symmans WF, Rugo HS, Melisko ME, et al. MK-2206 and standard neoadjuvant chemotherapy improves response in patients with human epidermal growth factor receptor 2–positive and/or hormone receptor–negative breast cancers in the I-SPY 2 trial. J Clin Oncol (2020) 38 (10):1059–69. doi: 10.1200/JCO.19.01027

53. Louis DN, Perry A, Burger P, Ellison DW, Reifenberger G, von Deimling A, et al. International society of neuropathology-haarlem consensus guidelines for nervous system tumor classification and grading. Brain Pathol (2014) 24(5):429– 35. doi: 10.1111/bpa.12171

54. Louis DN, Ohgaki H, Wiestler OD. World health organization histological classification of tumours of the central nervous system. 4th edition. France: International Agency for Research on Cancer (2016).

55. Capper D, Jones DTW, Sill M, Hovestadt V, Schrimpf D, Sturm D, et al. DNA Methylation-based classification of central nervous system tumours. Nature (2018) 555:469. doi: 10.1038/nature26000

56. Louis DN, Aldape K, Brat DJ, Capper D, Ellison DW, Hawkins C, et al. Announcing cIMPACT-NOW: the consortium to inform molecular and practical approaches to CNS tumor taxonomy. Acta Neuropathol (2017) 133(1):1–3. doi: 10.1007/s00401-016-1646-x

57. Mendeville M, Janssen J, Kim Y, van Dijk E, de Jong D, Ylstra B., et al. A bioinformatics perspective on molecular classification of diffuse large b-cell lymphoma. Leukemia (2022) 36(9):2177–9. doi: 10.1038/s41375-022-01670-6

58. Allahyar A, Pieterse M, Swennenhuis J, Los-de Vries GT, Yilmaz M, Leguit R, et al. Robust detection of translocations in lymphoma FFPE samples using targeted locus capture-based sequencing. Nat Commun (2021) 12(1):3361. doi: 10.1038/S41467-021-23695-8

59. Mendeville M, Roemer MGM, Van Den Hout MFCM, Los-de Vries GT, Bladergroen R, Stathi P, et al. Aggressive genomic features in clinically indolent primary HHV8-negative effusion-based lymphoma. Blood (2019) 133(4):377–80. doi: 10.1182/blood-2017-12-822171

60. Yellapantula V, Hultcrantz M, Rustad EH, Wasserman E, Londono D, Cimera R, et al. Comprehensive detection of recurring genomic abnormalities: a targeted sequencing approach for multiple myeloma. Blood Cancer J (2019) 9 (12):101. doi: 10.1038/S41408-019-0264-Y

61. He J, Abdel-Wahab O, Nahas MK, Wang K, Rampal RK, Intlekofer AM, et al. Integrated genomic DNA/RNA profiling of hematologic malignancies in the clinical setting. Blood (2016) 127(24):3004–15. doi: 10.1182/blood-2015-08- 664649

62. Hans CP, Weisenburger DD, Greiner TC, Gascoyne RD, Delabie J, Ott G, et al. Confirmation of the molecular classification of diffuse large b-cell lymphoma by immunohistochemistry using a tissue microarray. Blood (2004) 103(1):275–82. doi: 10.1182/blood-2003-05-1545

63. Abdulla M, Hollander P, Pandzic T, Mansouri L, Ednersson SB, Andersson PO, et al. Cell-of-origin determined by both gene expression profiling and immunohistochemistry is the strongest predictor of survival in patients with diffuse large b-cell lymphoma. Am J Hematol (2020) 95(1):57–67. doi: 10.1002/ajh.25666

64. Scott DW, Wright GW, Williams PM, Lih C-J, Walsh W, Jaffe ES, et al. Determining cell-of-origin subtypes of diffuse large b-cell lymphoma using gene expression in formalin-fixed paraffin-embedded tissue. Blood (2014) 123(8):1214–7. doi: 10.1182/blood-2013-11-536433

65. Nowakowski GS, Feldman T, Rimsza LM, Westin JR, Witzig TE, Zinzani PL, et al. Integrating precision medicine through evaluation of cell of origin in treatment planning for diffuse large b-cell lymphoma. Blood Cancer J (2019) 9 (6):48. doi: 10.1038/s41408-019-0208-6

66. Ahmed S, Glover P, Taylor J, Sha C, Care MA, Tooze R, et al. Comparative analysis of gene expression platforms for cell-of-origin classification of diffuse large b-cell lymphoma shows high concordance. Br J Haematol (2021) 192(3):599–604. doi: 10.1111/bjh.17246

67. Chamuleau MED, Burggraaff C, Nijland M, Bakunina K, Mous R, Lugtenburg PJ, et al. Treatment of patients with MYC rearrangement positive large b-cell lymphoma with r-CHOP plus lenalidomide: results of a multicenter HOVON phase II trial. Haematologica (2019) 105(12 SE-Articles):2805–12. doi: 10.3324/haematol.2019.238162

68. Samsom KG, Bosch LJW, Schipper LJ, Roepman P, de Bruijn E, Hoes LR, et al. Study protocol: Whole genome sequencing implementation in standard diagnostics for every cancer patient (WIDE). BMC Med Genomics (2020) 13 (1):169. doi: 10.1186/s12920-020-00814-w

69. Wilson WH, Wright GW, Huang DW, Hodkinson B, Balasubramanian S, Fan Y, et al. Effect of ibrutinib with r-CHOP chemotherapy in genetic subtypes of DLBCL. Cancer Cell (2021) 39(12):1643–1653.e3. doi: 10.1016/j.ccell.2021. 10.006

70. Woodcock J, LaVange LM. Master protocols to study multiple therapies, multiple diseases, or both. N Engl J Med (2017) 377(1):62–70. doi: 10.1056/ NEJMra1510062

71. Leeksma OC, De Miranda NF, Veelken H. Germline mutations predisposing to diffuse large b-cell lymphoma. Blood Cancer J (2017) 7(2):e532– 2. doi: 10.1038/bcj.2017.15

72. Keller L, Belloum Y, Wikman H, Pantel K. Clinical relevance of blßood-based ctDNA analysis: mutation detection and beyond. Br J Cancer (2020) 124(2):345–58. doi: 10.1038/s41416-020-01047-5

73. Beagan JJ, Drees EEE, Stathi P, Eijk PP, Meulenbroeks L, Kessler F, et al. PCR-free shallow whole genome sequencing for chromosomal copy number detection from plasma of cancer patients is an efficient alternative to the conventional PCR-based approach. J Mol Diagn (2021) 23(11):1553–63. doi: 10.1016/j.jmoldx.2021.08.008

74. Kurtz DM, Green MR, Bratman SV, Scherer F, Liu CL, Kunder CA, et al. Noninvasive monitoring of diffuse large b-cell lymphoma by immunoglobulin high-throughput sequencing. Blood (2015) 125(24):3679–87. doi: 10.1182/blood- 2015-03-635169

Chapter 3

A bioinformatics perspective on molecular classification of diffuse large B-cell lymphoma

Matias Mendeville, Jurriaan Janssen, Yongsoo Kim, Erik van Dijk,
Daphne de Jong, Bauke Ylstra

Leukemia, 2022; 36(9): 2177-2179

Introduction

The wide range in presentation, treatment response and outcome of diffuse large B-cell lymphoma (DLBCL) reflects a large underlying biological heterogeneity(1). Various molecular DNA-, RNA- and protein based subtyping approaches have been proposed over time, but failed to sufficiently capture its biological heterogeneity in a clinically sufficient manner, precluding major clinical consequences(2–5). The most recent DNA-based subtyping studies as independently proposed by the Dana Farber Cancer Institute (DFCI) and the National Cancer Institute (NCI) are a major step forward(6,7). These subtypes are based on DNA-mutation, genome-wide copy number aberration (CNAs), and translocation information. Despite different bioinformatic approaches, the resulting 5- to 7 subtypes largely recognize similar DLCBL pathogenicities and starts to offer a clinically impactful refinement at a level sufficient to serve as a basis for exploration of personalized and targeted treatment in the coming years. Its clinical potential already paid off with the recent finding that benefit from the BTK inhibitor ibrutinib plus R-CHOP is highly specifically associated with two of the genetic subtypes(8). To enable consistent trial designs and meaningful comparisons between studies, we consider it pivotal to harmonize the currently available DNA-subtyping knowledge into a single classification, preferably widely applicable in diagnostic routine. In this perspective we investigate harmonization opportunities and suggest potential avenues from a bioinformatics point of view.

Bioinformatics approaches for the current DNA-based DLBCL subtyping

The DFCI and NCI DLBCL subtyping studies are both based on whole exome sequencing data but differ essentially in *a priori* concepts and bioinformatic strategies. In brief, the DFCI group used unsupervised clustering combined with alteration-centric features. Driver alterations were discriminated from passengers, reducing the genetic dataset to 158 features. Next, unsupervised clustering by means of non-negative matrix factorization (NMF) identified patterns of co-occurring features to define clusters and assign each included patient sample. The NMF algorithm uncovered the optimal stability of subtype clusters to be represented by 5 groups of similar sizes, which the authors labelled as C1 to C5. The NCI group used semi-supervised clustering combined with gene-centered features. Prior knowledge was used to define four classes with 1 or 2 DNA 'seed' features, the *a priori* assumption. The algorithm subsequently selected additional features with the strongest association to those seeds unsupervised by iteration. All patient samples were included for this 4-class algorithm, but only 46% of cases could be assigned(9).

Recurrent alterations in unassigned cases prompted an extension with two classes. The 'seed' features for one of these additional classes were '*TP53* inactivation' and 'high CNA load', in analogy with DFCIs C2 subtype with p53 mutation and deletion (17p) as its top features and a multiplicity of CNAs. This was a first step towards harmonization. The resulting Bayesian-based probability score, named Lymphgen classifier, assigned 63% of cases(7). Despite the very different designs, most subtypes are remarkably similar with similar underlying biology(1,7), though some are more similar than others and some only are recognized by one of the algorithms.

Critical evaluation of the current subtyping systems

Prior to applying their subtyping algorithms, the DFCI and NCI groups used different ways to convert the detected DNA-alterations into features. DFCIs alteration-centric approach regards each DNA alteration type separately be it mutation, translocation, or CNA. Hence, a point-mutation of *CDKN2A*, a deletion at the *CDKN2A*-locus 9p.21 or the entire chromosome 9 arm would each be regarded as separate features. NCIs gene-centric approach combines any DNA-alterations that impact the same gene into a single feature. Hence, any alteration detected that affects *CDKN2A*, would be reduced into a single feature. These two different ways of handling biological features leads to discrepancy in their contribution to subtype assignment that determine biological deregulation and clinical impact. For harmonization we argue that focal chromosomal CNAs which only encompass only one or few genes(10) can be readily combined with point-mutations in a gene-centric fashion as these can be assumed to lead to the same overall biological effect(11). The choice is less obvious for large-scale chromosomal CNAs since these harbour hundreds of genes such that biological insights remain elusive(12) and maybe resolved mathematically by calculating an optimal biological characterization of the classes with either feature choice.

Supervised- and unsupervised (machine learning) algorithms may be chosen for subtyping(13). A supervised approach uses predefined classes to construct a classification rule from the features, while in an unsupervised approach, the algorithm identifies patterns and distinct feature characteristics in unlabelled data. A supervised approach precludes recognition of unknown subtypes. Unsupervised clustering is an elegant data-driven approach that can identify unknown subtypes in high-dimensional data(14–16). Yet, due to the high number of features unsupervised clustering requires sufficiently large sample sets to recognize rarer subtypes. Rare subtypes are pivotal to recognize since targeted treatment may be available exemplified by 3-4% of *ALK* translocated lung cancers

or *ERBB2* positive colon cancers that can be targeted with respectively trastuzumab/neratinib or crizotinib(17,18). Likewise, potential specific sensitivity to Ibrutinib of a small fraction of DLBCL patients (<2%) which carry NOTCH1 mutations justifies inclusion as a seed by NCI Lymphgen(8).

Not specifically captured by either of the algorithms are the high-grade B-cell lymphomas (HGBCLs) characterized by prognostic features *MYC*- combined with *BCL2* and/or *BCL6* rearrangement(19). As a solution, NCI Lymphgen introduced a previously published RNA expression-based signature (DHITSig) as a surrogate for *MYC* status as an add-on to the EZB subtype(20). From a diagnostics point of view this would be suboptimal as it requires two separate assays. Also about 35% of all DLBCLs are assigned as DHITSig-pos whereas genuine *MYC* double- or triple-hits only occur in about 5% of all DLBCL patients(20), indicating that DHITSig is not specific. To resolve the actual relation between DNA-subtyping and HGBCL, we argue that unsupervised clustering is the method of choice, whereby the NMF algorithm is attractive given its robustness against the high number of features. However, to enable NMF to recognize a HGBCL cluster the number of patient samples should be enlarged with sufficient MYC positive cases and *BCL2* and *BCL6* features.

Unsupervised NMF clustering assigns each sample to a cluster, whereas the Lymphgen algorithm assigns samples based on probability, and recognizes that not every DLBCL sample contains sufficient subtype characteristics. A simple exercise of 1000 NMF clustering iterations with each time 80% resampling to determine consensus clustering(21) shows that only about 70% of the DFCI patients are consistently assigned to the same cluster (Figure 1). The other 30% do not have (sufficient) specific characteristics to be consistently assigned to one or any subtype, like with the Lymphgen algorithm. We believe that this reflects the heterogeneous and continuous nature of DLBCL, supported by recent studies that included mechanistically different mutation-types and thereby further dissect molecular DLBCL classes(22).

While unsupervised clustering is suitable for class identification, ultimately a classifier trained by a supervised algorithm, like the one used in LymphGen, will be required for diagnosis of individual patients, which dictates another step towards harmonization. For training and validation of such parsimonious classification algorithm it will be pivotal to only include consistently assigned samples to eventually provide a classification that is applicable for any DLBCL sample.

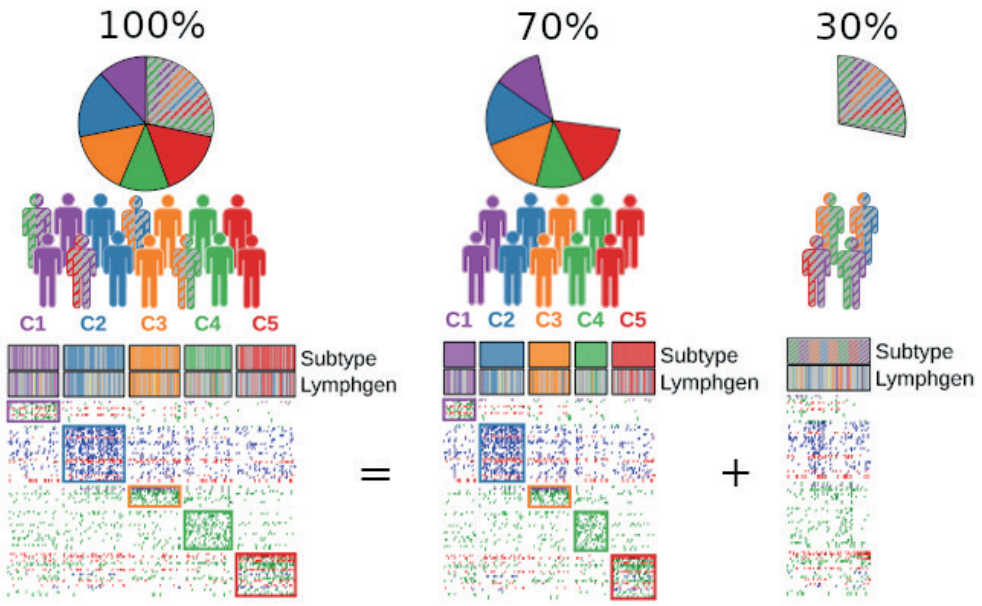

Figure 1. Cluster adherence of DLBCL samples. Cluster adherence was determined using NMF clustering with the 304 DLBCL samples from the DFCI cohort, recapitulating the results from the original study, including 5 subtypes (C1, C2, C3, C4 and C5) and identical subtype assignment for all samples (left panel). Consensus clustering by resampling(21) illustrates the unstable character of NMF clustering, core patients (solid colour, middle panel) and non-core patients (dashed colour, right panel). To make this distinction, a stability score was determined by examining co-occurring sample pairs in the same subtype through 1000 iterations of NMF clustering. The heatmaps show patients by column and genomic features by row. Genomic feature colours in the heatmap indicate mutations (green), copy number losses (blue), copy number gains (red) and translocations (purple). DLBCL samples are clustered by subtype. The subtype bars on top indicate core DLBCL samples (coloured bars) and non-core DLBCL samples (grey and dashed bars). Lymphgen annotation of the DFCI samples were taken from Wright et al(7). Left panel: heatmap of all 304 DLBCL samples from the DFCI cohort. Middle panel: heatmap of the 70% core samples with a high stability score and robust molecular subtypes. Right panel: heatmap of the 30% non-core samples with inconsistent subtype assignment throughout the clustering iterations.

Concluding remarks

Classification for a biologically heterogeneous disease like DLBCL is required for clinical trial inclusion to come to bespoke treatment. To achieve any meaningful classification, there may be well-defined quantitative criteria by which classification schemas can be objectively assessed, but these are inevitably balanced by more subjective choices. We describe here that consensus classification depends on choices concerning the incentive to recognize rare DLBCL subtypes or recognition that not all DLBCLs may have sufficiently specific DNA characteristics to be classified at all. Also, technical choices are to be made such as on the nature and weight of DNA-features, and on mathematics with their pros

and cons. Most important is the choice if a consensus classification and a common classifier algorithm is timely and needed. Thereby, we feel that the added value of the achievements of the DFCI and NCI classifications should be exploited by a consensus approach. Arguably, this would be preferred over first evaluating their clinical impact in clinical trials separately or just starting from scratch on yet another classification.

Other translational research groups in the solid tumour arena have met with similar challenges. Probably breast cancer is one of the most successful early examples of an RNA-based classification that found its way into the WHO Classification(23). Here, international groups converged their biological and bioinformatical approaches through collaboration. Once consensus cell-of-origin classification was achieved and reproducible assays were developed, personalized and targeted treatment could be explored systematically, amongst others in the multiple-armed I-SPY clinical trials(24). Similarly, a consortium was formed to integrate six independently published RNA-based classifications for colorectal cancer by means of a predefined mathematical approach. The resulting four consensus molecular subtypes are now the basis for various international clinical trials(25).

In our opinion, decisive evaluations of new treatment modalities based on genetics in the heterogeneous disease DLBCL is now largely impeded by a discordancy between the main molecular subtyping approaches. Progress towards personalized treatment of DLBCL would require an international consensus approach for which we have suggested various avenues.

Author contributions

JJ, YK and EvD re-analysed the data to draft the figure, edited and approved the final version of the manuscript. MM wrote a first version of the manuscript, edited and approved the final version of the manuscript. DdJ designed the manuscript format and wrote the manuscript. BY initiated writing, designed the manuscript format with figure and wrote the manuscript.

Financial support

This work was supported by the Dutch Cancer Society grant KWF 2015-7925 and KWF 2012-5711.

Competing interests

The authors declare no potential conflicts of interest.

References

1. Sehn LH, Salles G. Diffuse Large B-Cell Lymphoma. N Engl J Med. 2021;384(9):842–58.
2. Alizadeh AA, Eisen MB, Davis RE, Ma CL, Lossos IS, Rosenwald A, et al. Distinct types of diffuse large B-cell lymphoma identified by gene expression profiling. Nature. 2000 Feb 3;403(6769):503–11.
3. Younes A, Sehn LH, Johnson P, Zinzani PL, Hong X, Zhu J, et al. Randomized phase III trial of ibrutinib and rituximab plus cyclophosphamide, doxorubicin, vincristine, and prednisone in non–germinal center B-cell diffuse large B-cell lymphoma. J Clin Oncol. 2019 May 20;37(15):1285–95.
4. Davies A, Cummin TE, Barrans S, Maishman T, Mamot C, Novak U, et al. Gene-expression profiling of bortezomib added to standard chemoimmunotherapy for diffuse large B-cell lymphoma (REMoDL-B): an open-label, randomised, phase 3 trial. Lancet Oncol. 2019 May 1;20(5):649–62.
5. Nowakowski GS, Chiappella A, Gascoyne RD, Scott DW, Zhang Q, Jurczak W, et al. ROBUST: A Phase III Study of Lenalidomide Plus R-CHOP Versus Placebo Plus R-CHOP in Previously Untreated Patients With ABC-Type Diffuse Large B-Cell Lymphoma. J Clin Oncol. 2021 Apr 20;39(12):1317–28.
6. Chapuy B, Stewart C, Dunford A, Kim J, Kamburov A, Redd R, et al. Molecular subtypes of Diffuse Large B-cell Lymphoma are associated with distinct pathogenic mechanisms and outcomes. Nat Med. 2018;24(5):679–90.
7. Wright GW, Huang DW, Phelan JD, Coulibaly ZA, Roulland S, Young RM, et al. A Probabilistic Classification Tool for Genetic Subtypes of Diffuse Large B Cell Lymphoma with Therapeutic Implications. Cancer Cell. 2020;37(4):551-568.e14.
8. Wilson WH, Wright GW, Huang DW, Hodkinson B, Balasubramanian S, Fan Y, et al. Effect of ibrutinib with R-CHOP chemotherapy in genetic subtypes of DLBCL. Cancer Cell. 2021 Dec 13;39(12):1643-1653.e3.
9. Schmitz R, Wright GW, Huang DW, Johnson CA, Phelan JD, Wang JQ, et al. Genetics and Pathogenesis of Diffuse Large B-Cell Lymphoma. N Engl J Med. 2018;378(15):1396–407.
10. Krijgsman O, Carvalho B, Meijer GA, Steenbergen RDM, Ylstra B. Focal chromosomal copy number aberrations in cancer-Needles in a genome haystack. Biochim Biophys Acta - Mol Cell Res. 2014;1843(11):2698–704.
11. Santarius T, Shipley J, Brewer D, Stratton MR, Cooper CS. A census of amplified and overexpressed human cancer genes. Nat Rev Cancer. 2010 Jan;10(1):59–64.
12. Eleveld TF, Bakali C, Eijk PP, Stathi P, Vriend LE, Poddighe PJ, et al. Engineering large-scale chromosomal deletions by CRISPR-Cas9. Nucleic Acids Res. 2021 Dec 2;49(21):12007–16.
13. Greener JG, Kandathil SM, Moffat L, Jones DT. A guide to machine learning for biologists. Nat Rev Mol Cell Biol. 2021 Sep 13;23(1):40–55.
14. Brunet JP, Tamayo P, Golub TR, Mesirov JP. Metagenes and molecular pattern discovery using matrix factorization. Proc Natl Acad Sci U S A. 2004 Mar 23;101(12):4164–9.
15. Tamayo P, Scanfeld D, Ebert BL, Gillette MA, Roberts CWM, Mesirov JP. Metagene projection for cross-platform, cross-species characterization of global transcriptional states. Proc Natl Acad Sci U S A. 2007 Apr 3;104(14):5959–64.
16. Zhao L, Lee VHF, Ng MK, Yan H, Bijlsma MF. Molecular subtyping of cancer: current status and moving toward clinical applications. Brief Bioinform. 2019 Mar 25;20(2):572–84.

17. Meric-Bernstam F, Hurwitz H, Raghav KPS, McWilliams RR, Fakih M, VanderWalde A, et al. Pertuzumab plus trastuzumab for HER2-amplified metastatic colorectal cancer (MyPathway): an updated report from a multicentre, open-label, phase 2a, multiple basket study. Lancet Oncol. 2019 Apr 1;20(4):518–30.
18. Chia PL, Dobrovic A, Dobrovic A, John T. Prevalence and natural history of ALK positive non-small-cell lung cancer and the clinical impact of targeted therapy with ALK inhibitors. Clin Epidemiol. 2014 Nov 20;6:423.
19. Swerdlow SH, Campo E, Pileri SA, Lee Harris N, Stein H, Siebert R, et al. The 2016 revision of the World Health Organization classification of lymphoid neoplasms. Vol. 127, Blood. American Society of Hematology; 2016. p. 2375–90.
20. Rosenwald A, Bens S, Advani R, Barrans S, Copie-Bergman C, Elsensohn M-H, et al. Prognostic Significance of MYC Rearrangement and Translocation Partner in Diffuse Large B-Cell Lymphoma: A Study by the Lunenburg Lymphoma Biomarker Consortium. J Clin Oncol. 2019 Sep 9;JCO1900743.
21. Monti S, Tamayo P, Mesirov J, Golub T. Consensus clustering: A resampling-based method for class discovery and visualization of gene expression microarray data. Mach Learn. 2003 Jul;52(1–2):91–118.
22. Hübschmann D, Kleinheinz K, Wagener R, Bernhart SH, López C, Toprak UH, et al. Mutational mechanisms shaping the coding and noncoding genome of germinal center derived B-cell lymphomas. Leukemia. 2021 May 5;35(7):2002–16.
23. Tan PH, Ellis I, Allison K, Brogi E, Fox SB, Lakhani S, et al. The 2019 World Health Organization classification of tumours of the breast. Histopathology. 2020 Aug 1;77(2):181–5.
24. Chien AJ, Tripathy D, Albain KS, Symmans WF, Rugo HS, Melisko ME, et al. MK-2206 and standard neoadjuvant chemotherapy improves response in patients with human epidermal growth factor receptor 2–positive and/or hormone receptor–negative breast cancers in the I-SPY 2 trial. J Clin Oncol. 2020 Apr 1;38(10):1059–69.
25. Guinney J, Dienstmann R, Wang X, De Reyniès A, Schlicker A, Soneson C, et al. The consensus molecular subtypes of colorectal cancer. Nat Med. 2015 Nov 1;21(11):1350–6.

Chapter 4

Molecular subtyping significantly improves outcome prediction in diffuse large B-cell lymphoma

Matias Mendeville, G. Tjitske Los-de Vries*, Jurriaan Janssen*, Julia Richter, Erik van Dijk, Marcel Nijland, Margaretha G. M. Roemer, Phylicia Stathi, Nathalie J. Hijmering, Reno Bladergroen, Diego A. Pelaz, Arjan Diepstra, Jakoba J. Eertink, Coreline N. Burggraaff, Yongsoo Kim, Pieternella J. Lugtenburg, Anke van den Berg, Alexandar Tzankov, Stefan Dirnhofer, Ulrich Duhrsen, Andreas Huttmann, Wolfram Klapper, Josée M. Zijlstra, Bauke Ylstra*, Daphne de Jong*

*Authors contributed equally

Under review with *Journal of Clinical Oncology*, Oct 2022

Chapter 5

ACE: estimating absolute copy numbers from low-coverage whole-genome sequencing data

Jos B Poell, Matias Mendeville, Daoud Sie, Arjen Brink, Ruud H Brakenhoff, Bauke Ylstra

Bioinformatics, 2019; 35(16): 2847-2849

Abstract

Summary: Chromosomal copy number aberrations can be efficiently detected and quantified using low-coverage whole-genome sequencing, but analysis is hampered by the lack of knowledge on absolute DNA copy numbers and tumor purity. Here, we describe an analytical tool for Absolute Copy number Estimation, ACE, which scales relative copy number signals from chromosomal segments to optimally fit absolute copy numbers, without the need for additional genetic information, such as SNP data. In doing so, ACE derives an estimate of tumor purity as well. ACE facilitates analysis of large numbers of samples, while maintaining the flexibility to customize models and generate output of single samples.

Availability and implementation: ACE is freely available via www.bioconductor.org and at www. github.com/tgac-vumc/ACE.
Supplementary information: Supplementary data are available at Bioinformatics online.

Introduction

Cancer arises through accumulation of genetic and epigenetic changes. The genetic changes encompass small somatic mutations and gross chromosomal alterations, including translocation and copy number aberrations (CNAs). CNAs are a common trait of most cancers (Beroukhim et al., 2010) and are used as biomarkers in prognostic and predictive patient stratification (Macintyre et al., 2016).

Low-coverage whole-genome sequencing (lcWGS, ~0.1X coverage of the genome) is an efficient and cost-effective method to detect CNAs. The data yield relative sequence depth signals at each genomic location, but does not enumerate chromosomal copies. Determining absolute copy numbers would add valuable information on tumor content (cellularity) and intratumoral heterogeneity of the samples. Currently available tools that provide estimates of absolute copy numbers are mostly limited to data generated by SNP arrays (Van Loo et al., 2010), whole exome sequencing or high-coverage WGS (Favero et al., 2015; Riester et al., 2016) or require matched normal samples (Gusnanto et al., 2012; Oesper et al., 2014). ABSOLUTE (Carter et al., 2012) and ichorCNA (Adalsteinsson et al., 2017) provide cellularity and ploidy estimates from lcWGS data, but lack dynamic functionality to visually inspect the absolute copy number estimations and select the best fits. We therefore developed a tool for Absolute Copy number Estimation, ACE, which includes dynamic data visualization. Using simulation data and a published dataset, we demonstrate that its estimates are generally more accurate than other software tools. Additionally, it offers an interactive environment to evaluate the optimal predicted model besides alternative models.

Materials and methods

ACE is an R package. Complete software availability, dependencies and version information is available in the Supplementary Material, via www.bioconductor.org and at www.github.com/tgac-vumc/ ACE.

Segment data are obtained from lcWGS reads through the QDNAseq pipeline, which bins the mapped sequencing reads, corrects for mappabilty and GC-content (Scheinin et al., 2014) and segments the data by incorporating DNAcopy (Venkatraman and Olshen, 2007). For model fitting in ACE, errors per segment are calculated based on the difference between the segment value and the closest value of an integer copy number, as a function of ploidy and cellularity. ACE calculates the error of the fit as the root mean square error (default) or mean absolute error (optional) of all segments. To account for segment length, segment errors are repeated as many times as the number of bins the segment comprises. To balance sensitivity,

specificity and accuracy, ACE features customizable penalty factors for low cellularity and divergent ploidies. See Supplementary Material for formulae and further details.

A fitting procedure is executed over a range of ploidies (Fig. 1A) or one fixed ploidy (Fig. 1B). Ploidy represents the number of copies associated with the median segment value. Error of fits are calculated for each cellularity and the indicated ploidy. Cellularities (and ploidies when variable) are reported when the error of the fit reaches a minimum. Inversely, absolute copy numbers of segments and bins are calculated using the derived cellularity and ploidy (Fig. 1C).

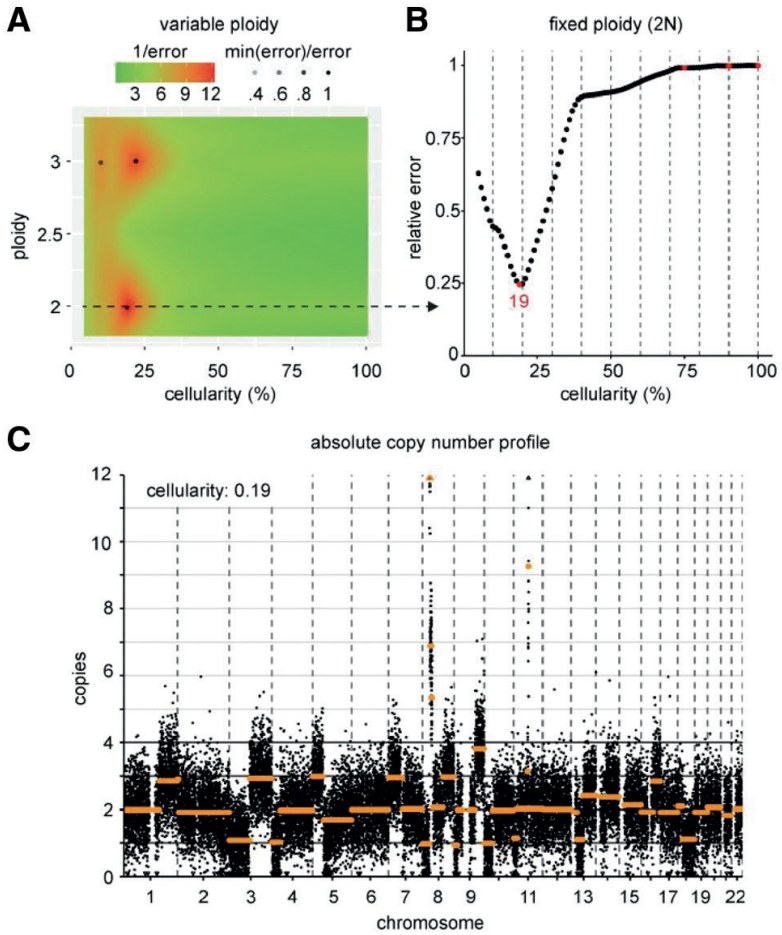

Figure 1. Results of ACE on a permutation sample with 20% of sequencing reads derived from cell line UM-SCC-22A. ACE performs model fitting as a function of both cellularity and ploidy (A) or cellularity at a fixed ploidy (B). In (A), the relative error is color-coded and minima are indicated with a black dot. The cellularity (and ploidy, 2N in this example) corresponding to the top prediction is used to produce an absolute copy number profile with number of copies on the Y-axis and bins ordered by chromosomal location on the X-axis (C)

Results

We applied ACE to lcWGS data of DNA from a near-diploid cell line with many CNAs (UM-SCC-22A), a diploid cell line with few and only single copy CNAs (HCT116), a triploid cell line (HT29) and a tetraploid cell line (MOLT-4), using lcWGS data of DNA from exfoliated oral cells of a healthy individual as negative control. To assess ACE performance at all ranges of tumor cell percentages, we generated in silico admixtures of sequencing reads derived from tumor and normal cells, and analyzed these with varying bin sizes, penalty and error methods (Supplementary Material). We also estimated tumor cell percentage of these admixture permutations using ABSOLUTE and ichorCNA (Table 1). The three methods have comparable accuracies between ~30% and 80% tumor-derived reads (Supplementary Fig. S1). For all three algorithms, we determined the range of tumor DNA percentage at which the algorithm was able to produce an accurate top prediction. Overall, ACE performed very well both at low and high cellularity (Table 1), and showed the largest range of accurate predictions for the triploid and tetraploid cell lines. More details are available in the Supplementary Material.

Table 1. Prediction accuracy of ACE, ABSOLUTE and ichorCNA on simulated data of three cell lines with varying copy number profiles

	UM-SCC-22A	HCT116	HT29	MOLT-4
	(2N)	(2N)	(3N)	(4N)
ACE	12–100	20–100	14–100	15[a]–100
ABSOLUTE	21–100	19–100[b]	28–100	36–100
ichorCNA	10–100	16–81	31–91	26–100

Notes: Numbers indicate the range of tumor DNA percentages at which the specified algorithm estimates the correct tumor cell percentage (less than 25% deviation) in at least 9 out of 10 permutations.

[a]Only 8 out of 10 at 17% and 20% tumor DNA percentage.

[b]Only 8 out of 10 at 95% tumor DNA percentage.

Increasing the penalty factor for low cellularities improves specificity (no false positive estimates) and accuracy of models, but at the cost of decreased sensitivity. To determine the lowest penalty at which ACE is still highly specific, we analyzed all permutation samples without any tumor DNA for false positive fits. A penalty of 0.1 proved sufficient to prevent false positive fits in all healthy control permutations with 10 million sequencing reads (Supplementary Fig. S2) and is thus the optimal penalty for high sensitivity in this dataset, whereas a penalty between 0.25 and 0.5 is better-suited for optimizing accuracy of predictions (Supplementary Fig. S3).

Finally, we analyzed a recently published dataset of 253 ovarian carcinoma samples (Macintyre et al., 2018). Importantly, the samples varied in tumor purity and were selected for their clonal TP53 mutations, of which the frequency was accurately determined. This allowed the authors to estimate tumor purity accurately based on both clonal mutation data and copy number data. We used their tumor purity determination as gold standard and compared it with the estimates corresponding to the best fits of ACE and ABSOLUTE based solely on copy number data (see Supplementary Material for details). The estimates of ACE are in good concordance with the gold standard over the entire range of tumor purity (Fig. 2). The median difference between the gold standard and ACE was 0.07, compared to 0.28 for ABSOLUTE. In relative terms, estimates of ACE deviated from the gold standard by a median factor of 1.15 compared to a median factor of 1.94 for ABSOLUTE. Because of ABSOLUTE's high deviation from the gold standard when considering only its highest ranked model, we also tested at which fit ACE and ABSOLUTE approximate the gold standard model. Generally, ACE arrives at the correct model with fewer fits than ABSOLUTE, illustrating its efficacy in model prioritization (Supplementary Fig. S5).

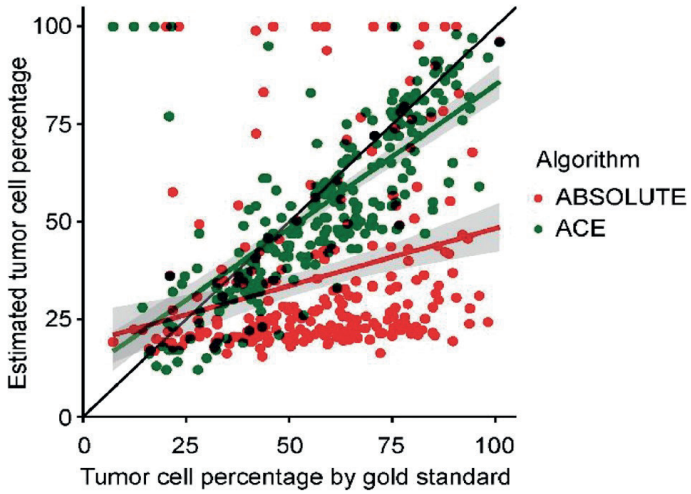

Figure 2. Tumor purity estimates of an ovarian carcinoma dataset. Segmented copy number data from lcWGS was used to derive tumor purity estimates using ABSOLUTE (red) and ACE (green). The results of the algorithms (on the Y-axis) are plotted against a manually curated tumor purity estimate based on both copy number data and high-depth mutation data (X-axis, gold standard)

Discussion

ACE is a comprehensive tool to produce absolute copy number profiles and arrive at estimates of tumor purity and ploidy based on lcWGS data only. ACE's model fitting accuracy performs better than currently available algorithms ABSOLUTE and ichorCNA largely irrespective of tumor purity and ploidy, on both simulated data and an ovarian carcinoma dataset. On the one hand, ACE facilitates analysis of multiple samples directly from mapped reads; on the other hand, it accommodates extensive evaluation of single samples. ACE is therefore a well-suited bioinformatics tool to maximize interpretable outcome of lcWGS experiments.

Acknowledgements

The authors thank Tom Carey, University of Michigan, for cell line UM-SCC- 22A. They also thank Geoff Macintyre and James Brenton, Cancer Research UK Cambridge Institute, for assistance and discussion on analysis of the ovarian carcinoma dataset.

Funding

This work was supported by a Cancer Center Amsterdam institutional grant.
Conflict of Interest: none declared.

References

1. Adalsteinsson,V.A. et al. (2017) Scalable whole-exome sequencing of cell-free DNA reveals high concordance with metastatic tumors. Nat. Commun., 8, 1324.
2. Beroukhim,R. et al. (2010) The landscape of somatic copy-number alteration across human cancers. Nature, 463, 899–905.
3. Carter,S.L. et al. (2012) Absolute quantification of somatic DNA alterations in human cancer. Nat. Biotechnol., 30, 413–421.
4. Favero,F. et al. (2015) Sequenza: allele-specific copy number and mutation profiles from tumor sequencing data. Ann. Oncol., 26, 64–70.
5. Gusnanto,A. et al. (2012) Correcting for cancer genome size and tumour cell content enables better estimation of copy number alterations from next-generation sequence data. Bioinformatics, 28, 40–47.
6. Macintyre,G. et al. (2016) Sequencing structural variants in cancer for precision therapeutics. Trends Genet., 32, 530–542.
7. Macintyre,G. et al. (2018) Copy number signatures and mutational processes in ovarian carcinoma. Nat. Genet., 50, 1262–1270.
8. Oesper,L. et al. (2014) Quantifying tumor heterogeneity in whole-genome and whole-exome sequencing data. Bioinformatics, 30, 3532–3540.
9. Riester,M. et al. (2016) PureCN: copy number calling and SNV classification using targeted short read sequencing. Source Code Biol. Med., 11, 13.
10. Scheinin,I. et al. (2014) DNA copy number analysis of fresh and formalin-fixed specimens by shallow whole-genome sequencing with identification and exclusion of problematic regions in the genome assembly. Genome Res., 24, 2022–2032.
11. Van Loo,P. et al. (2010) Allele-specific copy number analysis of tumors. Proc. Natl. Acad. Sci. USA, 107, 16910–16915.
12. Venkatraman,E.S. and Olshen,A.B. (2007) A faster circular binary segmentation algorithm for the analysis of array CGH data. Bioinformatics, 23, 657–663.

Appendix

Supplementary Methods

DNA isolation

UM-SCC-22A tumor cells were obtained from Dr. T. Carey (University of Michigan, Ann Arbor MI, USA). HCT116, HT29, and MOLT-4 cells were purchased from ATCC (ATCC number CCL-247, HTB-38, CRL-1582). After limited additional expansion *in vitro*, cells were collected in PBS and pelleted. Exfoliated cells from a healthy donor were obtained by brushing the cheek mucosa with an Orgenex brush (Rovers medical devices, Oss, NL) and collecting cells in PBS. Cells were subsequently pelleted. Genomic DNA was isolated from cell pellets using the Purelink genomic DNA isolation kit (Invitrogen, Carlsbad, CA). DNA concentration was measured by fluorometric quantitation (Qubit 3.0, Thermo Fisher Scientific, Carlsbad CA, USA).

Low-coverage WGS

DNA (750 ng in 130 µL TE buffer pH 8.0) was sheared to a median fragment size of 200 base pairs using focused ultrasonication (Covaris S220, Woburn MA, USA). Concentration and fragment size were subsequently determined by electrophoresis (Bioanalyzer 2100, Agilent Genomics, Santa Clara CA, USA). Sequencing libraries were prepared using 250 ng of sheared DNA. Samples were end-repaired and A-tailed following manufacturer's instructions (KAPA HyperPrep, KAPA Biosystems, Cape Town, South Africa). Adapters (SeqCap Adapter Kit A, Roche Nimblegen, Madison WI, USA) were ligated overnight at 16 °C. All samples were subjected to 9 cycles of PCR. Resulting libraries were analyzed on a BioAnalyzer 2100 for quality control and quantification. Libraries were pooled equimolarly in a pool of 24 samples in total and sequenced on a next-generation sequencer (HiSeq 2500 HTS, Illumina, San Diego CA, USA) using a single-read 50 protocol, according to the manufacturer's instructions.

Data preparation for copy number analysis

Sequence reads were aligned to the human genome (hg19) using bwa-mem (Li and Durbin, 2009). Copy number analysis was performed in R using the QDNAseq package version 1.12.0 (Scheinin, et al., 2014). In brief, QDNAseq was used for binning the reads (30, 100, 500, and 1,000 kilobase pairs), filtering bins, correcting for GC-content, and normalization. The segmentation function in QDNAseq requires DNAcopy (Venkatraman and Olshen, 2007). The resulting QDNAseq output was used as input for ACE.

Model fitting procedure

Segment data (signal intensity and number of bins) are obtained from the QDNAseq-object using the R function *rle()*. For any cellularity (sometimes called tumor fraction or tumor purity) between 0.05 and 1 (with increments of 0.01), the expected relative signal is calculated for all integer copy numbers between 1 and 12 as follows:

$$xpected\ signal = standard \cdot \left(\frac{cellularity \cdot copies + 2 \cdot (1 - cellularity)}{cellularity \cdot ploidy + 2 \cdot (1 - cellularity)}\right)$$

In this formula, the standard is the median segment value of all bins, cellularity is the fraction of aberrant cells, copies is the integer copy number, and ploidy is the general ploidy of the aberrant cells. Thus, each potential cellularity has 12 expected signals corresponding with 1-12 absolute copies (0 copies is omitted to prevent unlikely fits with many or large completely deleted segments). Subsequently, each segment is fitted to the closest expected signal. The difference between the segment value and the closest expected signal is the error of the segment. In case of high-level amplification (a segment with more than 12 copies), the segment is assigned the maximum error of 0.5. The 12 copy cut-off is chosen to prevent overfitting at low cellularities and reducing the impact of high-level amplifications, which are generally small in genomic span, and their exact copy number per cell is more likely to be (highly) variable than small gains. We have included an optional parameter to penalize for fits at low cellularity. The segment error is corrected as follows: *error* = *error / cellularity*^{penalty}. The default setting of ACE calculates the error of the fit as the root mean square error (RMSE) of all segments. To account for segment length, segment errors are repeated as many times as the number of bins the segment comprises. Alternatively, when mean absolute error (MAE) is chosen as error method, the error of the fit is the mean of the absolute segment errors (again segment length is accounted for as described above). The result of the procedure is a list of errors of fits at each potential cellularity for a given sample at a given general (tumor) ploidy. ACE reports cellularities at which the error reaches a minimum. In case of variable ploidy as seen in Figure 1A, errors are still calculated using formula (1), but now minima are found in a matrix (columns represent cellularity, rows represent ploidy) instead of a list. Additionally, it is possible to penalize ploidies for how different they are from 2N: *error* = *error* * (1 + |*ploidy* –2|)^{penploidy}, where *penploidy* is a user-set variable. In this manuscript, only the cellularity corresponding with the top prediction (lowest relative error) was used. NOTE: from our benchmarking experiments we noted that predictions of cellularity and ploidy were accurate without considering subclonal states, despite their obvious presence

(for example cell line UM-SCC-22A). It is therefore not included in the core fitting algorithm of ACE.

Scaling bin values and segment values to absolute copies

Relative signal intensities for bins and segments derived from the QDNAseq-object are converted to absolute copies with the formula:

$$copies = 2 - \frac{2}{cellularity} + signal \cdot \frac{cellularity \cdot ploidy + 2 \cdot (1 - cellularity)}{cellularity \cdot standard}$$

Which can be rewritten as:

$$copies = ploidy + (signal - standard) \cdot \frac{cellularity \cdot ploidy + 2 \cdot (1 - cellularity)}{cellularity \cdot standard}$$

This is in principle the same formula as formula (1), but solving for copies instead of (expected) signal.

Software

ACE is an R package. The release version is available via Bioconductor (www.bioconductor.org), and the development version at www.github.com/tgac-vumc/ACE.

The release version can be installed in R using the Bioconductor installer:

BiocManager::install("ACE")

The development version can be installed by downloading the package from GitHub and installing it in R,

install.packages("<filepath_to_ACE_archive>", repos = NULL)

or directly using the devtools package in R.

devtools::install_github("tgac-vumc/ACE")

ACE's dependencies are QDNAseq (Scheinin, et al., 2014), Biobase (Huber, et al., 2015), and ggplot2 (Wickham, 2009). We ran ACE using QDNAseq version 1.12.0, Biobase version 2.30.0, ggplot2 version 2.2.1, and DNAcopy version 1.44.0 (as part of the QDNAseq pipeline).

Benchmarking ACE versus ABSOLUTE and ichorCNA

To assess tumor cell percentage estimates of ACE, we used lcWGS data of healthy control cells (0% tumor, no copy number aberrations), and tumor cell lines (100% tumor), and generated *in silico* admixtures with predetermined tumor percentages of mapped sequencing reads assigned to 1,000 kilobase pair bins. We performed benchmarking on four independent tumor cell lines with different copy number characteristics. UM-SCC-22A (Buchhagen, et al., 1996, near-diploid with numerous copy number aberrations), HCT116 (diploid with only single gains and losses in a small fraction of the genome), HT29 (triploid with numerous copy number aberrations) and MOLT-4 (tetraploid). Because the sequencing reads represent tumor DNA, expected tumor cell percentage had to be converted to correct for the fact that tumor cells may contain more DNA than healthy cells:

$$tumor\ cell\ percentage = \frac{200}{2 + ploidy \cdot \left(\frac{100}{tumor\ DNA\ percentage} - 1\right)}$$

Ploidy in this case represents the DNA content per tumor cell and is calculated by multiplying the general (integer) ploidy with the mean segment value of all bins, divided by the median segment value of all bins. Ten permutations were created for all percentages between 0 and 100 by sampling (with replacement) 10 million reads out of the tumor-derived and normal-derived reads (how much of each depending on the intended percentage). The resulting permutations were converted to a QDNAseqReadCounts-object. For analysis with ichorCNA, WIG-files were created. We verified that binning of reads via QDNAseq and via ichorCNA (which uses HMMcopy) resulted in the same number of reads per bin. The ichorCNA pipeline performs its own normalization, GC-correction, and segmentation. For both ACE and ABSOLUTE, the obtained permutations were subjected to the QDNAseq pipeline to obtain segmented data. Segment data were converted to the correct format for ABSOLUTE. Algorithms were applied using the following parameters:

ACE: penalty = 0.5, method = "MAE", ploidy = 2 in case of UM-SCC-22A and HCT116, ploidy = 3 in case of HT29, and ploidy = 4 in case of MOLT-4. A modified version of the *singlemodel* function was used that starts model fitting at cellularity 0.01 instead of 0.05, so that fitting of ACE on samples with very low cellularity could be examined. We note that we would normally not recommend trying fits at cellularities below 0.05. Cellularity with the lowest relative error was used for analysis.

ABSOLUTE: the following parameters were used in the *runAbsolute* function: sigma.p = 0, max.sigma.h = 0.015, min.ploidy = 0.95, max.ploidy = 10, max.as.seg.count = 1500, max.non.clonal = 0.5, max.neg.genome = 0.05, platform = "SNP_6.0", copy_num_type = "total", primary.disease = "Head and Neck Cancer" (in case of UM-SCC-22A) and primary.disease = "Colorectal" (in case of HCT116 and HT29). Primary disease was left blank for MOLT-4, because its karyotype is atypical for leukemia. ABSOLUTE heavily penalizes non-diploid fits for leukemia. Two parameters were changed from their default (i.e. max.non.clonal and max.neg.genome), which we found improved the estimates in both simulation data and the ovarian cohort. The cellularity of the top prediction with the correct ploidy (rounds to 2 for UM-SCC-22A and HCT116, rounds to 3 for HT29, and rounds to 4 for MOLT-4) was used for analysis. We note that choice of platform has no consequences in this analysis, since we provide ABSOLUTE with the segment information.

ichorCNA: *runIchorCNA* was used with default settings, except that for HT29 ploidy was specified to be 3. Cellularity of the top prediction was used for analysis.

Extended analysis of ACE on simulated data

Additional analyses were performed using ACE to further clarify the impact of bin size and number of reads, and ACE-specific parameters "method" (RMSE versus MAE) and "penalty". Permutations were made as described above for additional read depths (1, 2, 5 and 10 million sampled reads) and bin sizes (100, 500, and 1000 kilobase pairs). For model fitting, a modified version of *singlemodel* was used that starts model fitting at cellularity 0.01 instead of 0.05 as described earlier. Top predictions (cellularities corresponding with the lowest relative error) were calculated with *singlemodel* using varying values for the parameters penalty (0, 0.25, 0.5, and 1) and error method (MAE and RMSE). To address the sensitivity of ACE as a function of the penalty factor, we analyzed all permutations without any tumor-derived reads. For this analysis, we used the default *singlemodel* function with both error methods (MAE and RMSE) and varying penalty factor (between 0 and 1 with increments of 0.01). Following this, bootstrapping was repeated once more with the default *singlemodel* function using penalty = 0.1 on permutations of 10 million reads, 1,000 kilobase pair bin size, at all tumor read percentages of all three cell lines.

Analysis of a cohort of ovarian carcinoma tumors

Segmented copy number data from 253 ovarian carcinoma samples were kindly provided by Brenton and colleagues. Preprocessing of the data and estimation of tumor purity has

previously been described (Macintyre, *et al.*, 2018). Segmented data was used as input for ACE and ABSOLUTE to estimate tumor purity. ACE: the two main modes for model fitting, one using a fixed ploidy and one using variable ploidy, were both assessed. In both cases, the error method used was "RMSE" and the penalty factor was set at 0.5. Additionally, in case of variable ploidy (using ACE's squaremodel function), the following parameters were used: penploidy = 0.5 (this penalty prevents overfitting at high ploidies), ptop = 4.3 (the highest ploidy tested), pbottom = 1.8 (the lowest ploidy tested), prows = 250 (number of rows, each one representing an increment in ploidy between pbottom and ptop). Only the tumor purity estimate of the best fit (lowest error) was used for analysis. Results are shown in Supplementary Figure 4. We used the estimates from the squaremodel function (variable ploidy) in the comparison with ABSOLUTE. ABSOLUTE: non-default parameters were max.non.clonal. = 0.95, max.ploidy = 5, and primary.disease = "Ovarian Cancer". These settings resulted in better estimates than the default settings (not shown). Tumor purity estimate of the top ranked model was used for analysis. The comparison between ACE and ABSOLUTE is shown in Figure 2. An extended analysis considering all produced fits is given in Supplementary figure 5. We note that ichorCNA could not be used to analyze the ovarian cancer data, because we only had preprocessed, segmented data at our disposal.

Supplementary References

1. Buchhagen, D.L., et al. Two regions of homozygosity on chromosome 3p in squamous cell carcinoma of the head and neck: comparison with cytogenetic analysis. *Head Neck* 1996;18(6):529-537.
2. Huber, W., et al. Orchestrating high-throughput genomic analysis with Bioconductor. *Nat Methods* 2015;12(2):115-121.
3. Li, H. and Durbin, R. Fast and accurate short read alignment with Burrows-Wheeler transform. *Bioinformatics* 2009;25(14):1754-1760.
4. Macintyre, G., et al. Copy number signatures and mutational processes in ovarian carcinoma. *Nat Genet* 2018;50(9):1262-1270.
5. Scheinin, I., et al. DNA copy number analysis of fresh and formalin-fixed speci-mens by shallow whole-genome sequencing with identification and exclusion of problematic regions in the genome assembly. *Genome Res* 2014;24(12):2022-2032.
6. Venkatraman, E.S. and Olshen, A.B. A faster circular binary segmentation algo-rithm for the analysis of array CGH data. *Bioinformatics* 2007;23(6):657-663.
7. Wickham, H. ggplot2: Elegant Graphics for Data Analysis. New York: Springer-Verlag; 2009.

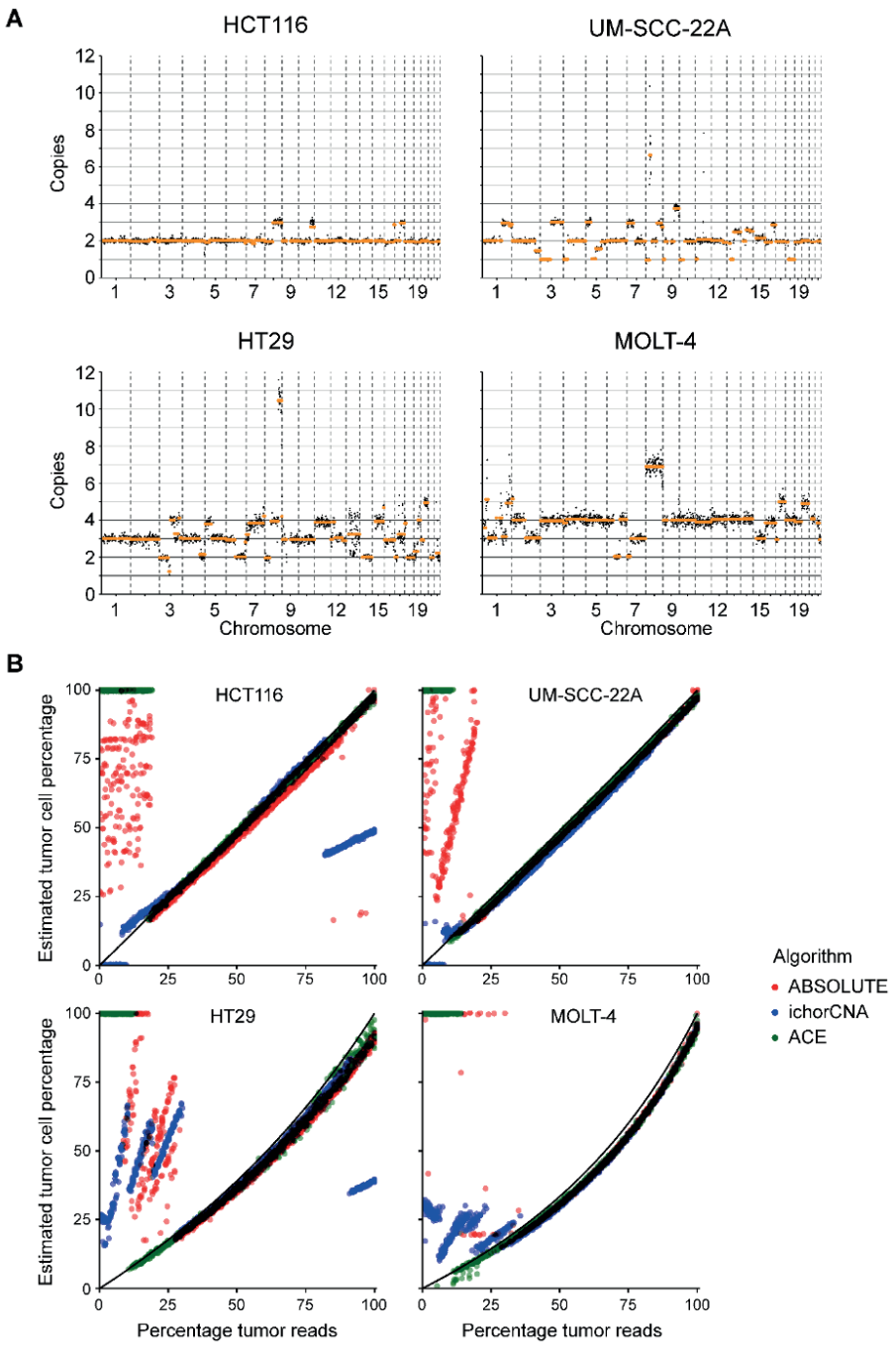

Supplementary figure 1. Benchmarking results of ACE, ABSOLUTE and ichorCNA. (A) Absolute copy number profiles of HCT116, UM-SCC-22A, HT29, and MOLT-4 from the "unsampled" data. Total

Supplementary figure 1. Continued

reads analyzed were $9.2*10^6$, $9.7*10^6$, $10.3*10^6$ and $9.8*10^6$ for the respective cell lines. (B) Accuracy of tumor purity estimates of ACE, ABSOLUTE and ichorCNA. *In silico* admixtures of 10 million reads, with the indicated percentage tumor-derived reads, were analyzed with ABSOLUTE, ichorCNA, and ACE. The estimated tumor cell percentage of the top prediction calculated by the three programs for 10 permutations at all tumor read percentages is shown. Expected tumor cell percentage based on percentage tumor reads and DNA content of the respective cell lines is shown by a black line. Only estimates at the relevant ploidy were considered (2N for HCT116 and UM-SCC-22A, 3N for HT29 and 4N for MOLT-4). Darkened colors are used for overlapping points of different programs, indicating concordant estimates among algorithms. The figure demonstrates that estimates obtained with ABSOLUTE are relatively inaccurate at low tumor cell percentages (note that 4N fits were largely missing for ABSOLUTE in the analysis of MOLT-4 between until tumor DNA percentage reached 35%). In two of four cell lines, ichorCNA produced inaccurate estimates at high tumor cell percentages. In polyploid cell lines HT29 and MOLT-4 only ACE gave accurate estimates in the range of 13-28% tumor-derived reads (see also table 1). For optimal accuracy, ACE model fitting was performed with error method "MAE" and a penalty factor of 0.5 (see also Supplementary figure 3). Parameters and results for optimal sensitivity are covered in Supplementary figure 2.

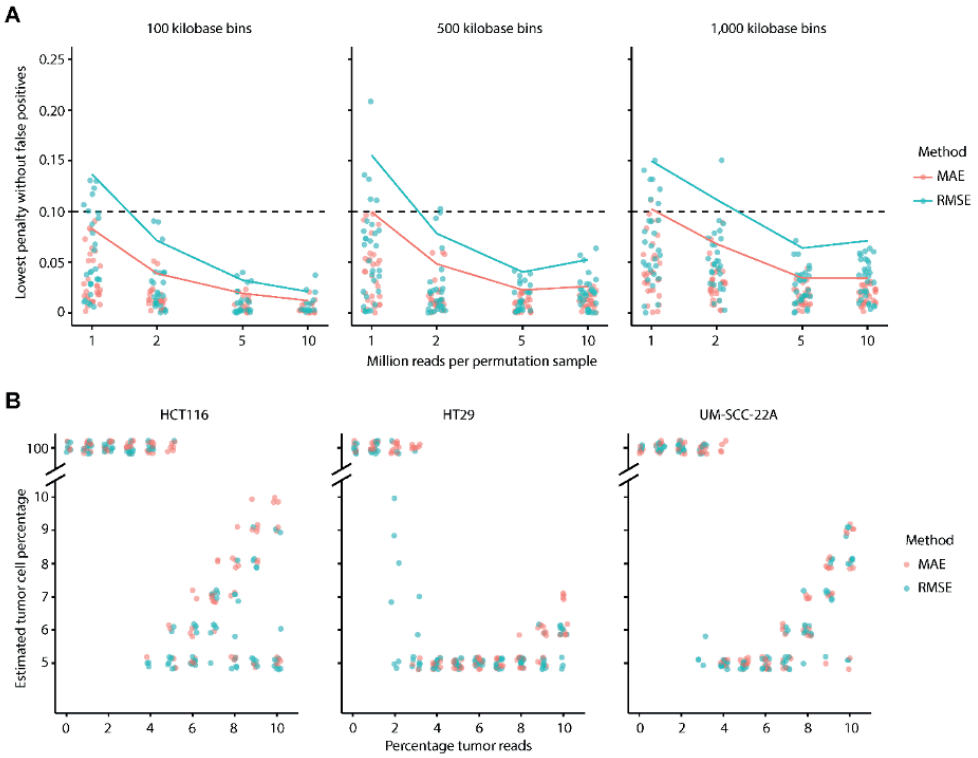

Supplementary figure 2. Optimization of ACE model fitting parameters for high sensitivity. (A) Permutation of only control-derived sequencing reads were tested for false positive tumor estimates using the *singlemodel* function with varying penalty factor and both error methods (MAE and RMSE). Each combination of bin size (different panels) and read depth (X-axis) is represented by 30 permutation samples. The lowest penalty factor at which ACE did not produce a false positive result is plotted. Lines indicate the upper bound of the 95% range of penalty factors. False positive results, based on this normal controls sample, are highly unlikely using a penalty factor of 0.1 (dashed line). We emphasize that this result represents a high quality, fresh, healthy control DNA sample. The penalty factor for optimal sensitivity should be trained using the appropriate control (e.g. FFPE, cell-free DNA). (B) Benchmarking with ACE was repeated at penalty 0.1. Note that an estimate of 1 (100% tumor cell percentage) by ACE generally indicates a negative result, as ACE defaults to 1 instead of 0 to produce "flat" absolute copy number profiles for samples without CNAs. By default, ACE does not estimate lower percentages than 5%. Sensitivity depends on the highest level genomic amplification that is still recognized as a segment by DNAcopy, which is why ACE is more sensitive for HT29 than for HCT116 (copy number profiles in Supplementary figure 1A).

Supplementary figure 3. {is available at Bioinformatics online} Benchmarking of ACE with varying bin size, read depth, error method, and penalty factor for three cell lines. Ten permutations with the indicated amount of sequencing reads (rows) were created for each percentage tumor-derived reads (X-axis). Tumor cell percentage (Y-axis) corresponding to the top prediction were derived from an adapted version of the *singlemodel* function that estimates tumor cell percentages starting from 1%, not 5%. The black line shows expected tumor cell percentage. Columns represent varying penalty factors. Each page contains a combination of cell line and bin size. As expected, an increase in read depth has a positive influence on both accuracy (deviation from the black line) and sensitivity. Generally, a larger bin size improves sensitivity, but may decrease accuracy, depending on the genomic size and abundance of CNAs. Differences depending on error

methods can vary due to subtle difference in the CNAs (compare different bin sizes of HCT116), but become less notable with higher penalties. When top predictions correspond with the expected tumor cell percentage (black line), MAE tends to produce slightly more accurate results. Penalizing for low cellularity (penalty) increases accuracy but at the cost of sensitivity (see also Supplementary figure 2). Note: due to its size, Supplementary figure 3 is provided as a separate file.

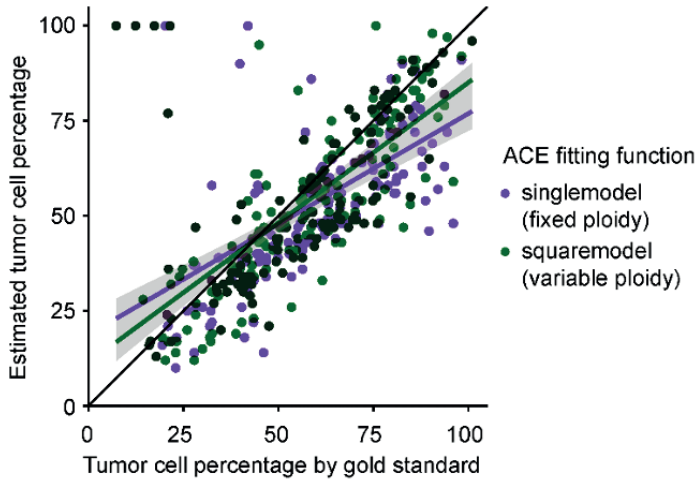

Supplementary figure 4. Performance of ACE's purity estimation using either fixed ploidy or variable ploidy. Tumor purity of 253 ovarian cancer samples was estimated using either ACE's singlemodel function, which uses a fixed ploidy (set to 2 in this instance), or ACE's squaremodel function, which calculates fits over a range of ploidies (from 1.8 to 4.3 in this instance). For both functions, the purity of the top prediction was plotted against the tumor purity reported by Macintyre and colleagues (see also Supplementary methods). The colored lines in the figure represent the linear regression models of the corresponding functions, while the black line represents the ideal line (estimated purity equals gold standard). The figure demonstrates that purity estimates using variable ploidy (green) are overall slightly better than estimates using fixed ploidy (purple), with median absolute differences between the estimate and the gold standard of 0.067 and 0.094 respectively (p-value 0.0062, Wilcoxon rank sum test).

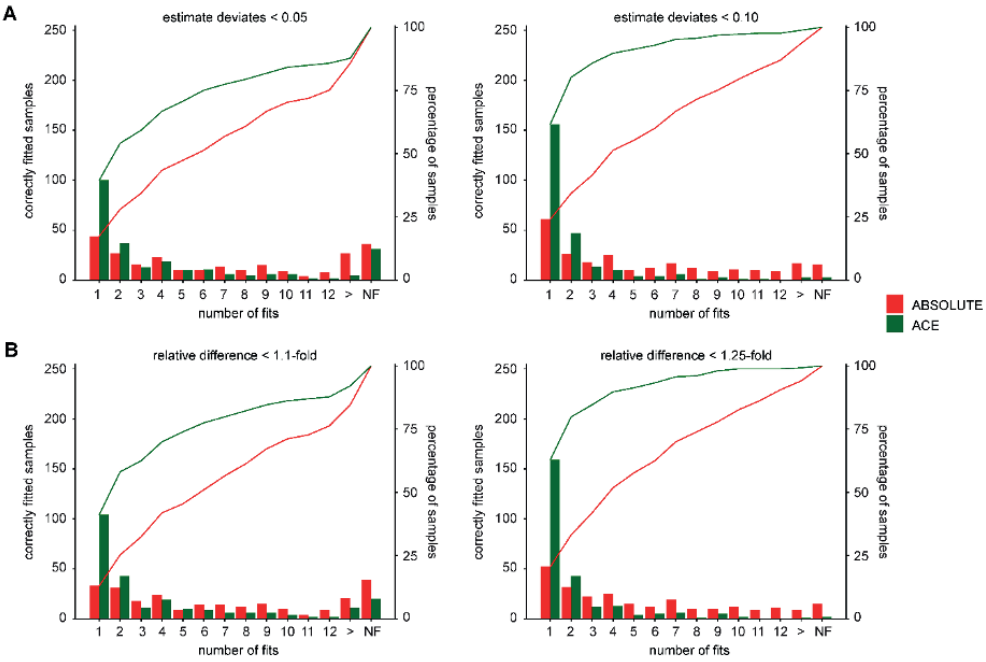

Supplementary Figure 5. Efficacy of model prioritization of ABSOLUTE and ACE on the ovarian carcinoma data set, consisting of 253 samples. The tumor purity of these samples were previously determined by combining copy number data and deep sequencing of clonal *TP53* mutations (Macintyre et al., 2018). These reported tumor purities were used as gold standard to test performance of ACE and ABSOLUTE when applied to copy number data of the ovarian carcinoma data set as described in the supplementary methods. For both ABSOLUTE and ACE, purity estimates of maximally 20 fits were recorded. For each sample, we determined how many fits were reported until the estimated tumor purity came within the indicated range of the gold standard purity determination (**A,** differences smaller than 0.05 or 0.10, or **B**, relative differences smaller than 1.1-fold or 1.25-fold). The bar graph summarizes the number of samples (Y-axis) that arrived at the correct model (within the cutoff displayed at the top of the graph) at the designated number of fits (X-axis). The line graph shows the cumulative number of samples with a correct fit. For example, ACE produced a first estimate deviating less than 0.05 from the gold standard for 100 samples (**A**, left panel, leftmost green bar). Of the remaining samples, 37 approximated the gold standard with the second estimate, yielding a cumulative 137 samples that were correctly estimated within two fits. The "greater than" sign on the X-axis denotes samples for which the correct model appeared at fit 13 to 20. The NF denotes samples for which no correct fit was given within the maximum of 20 fits.

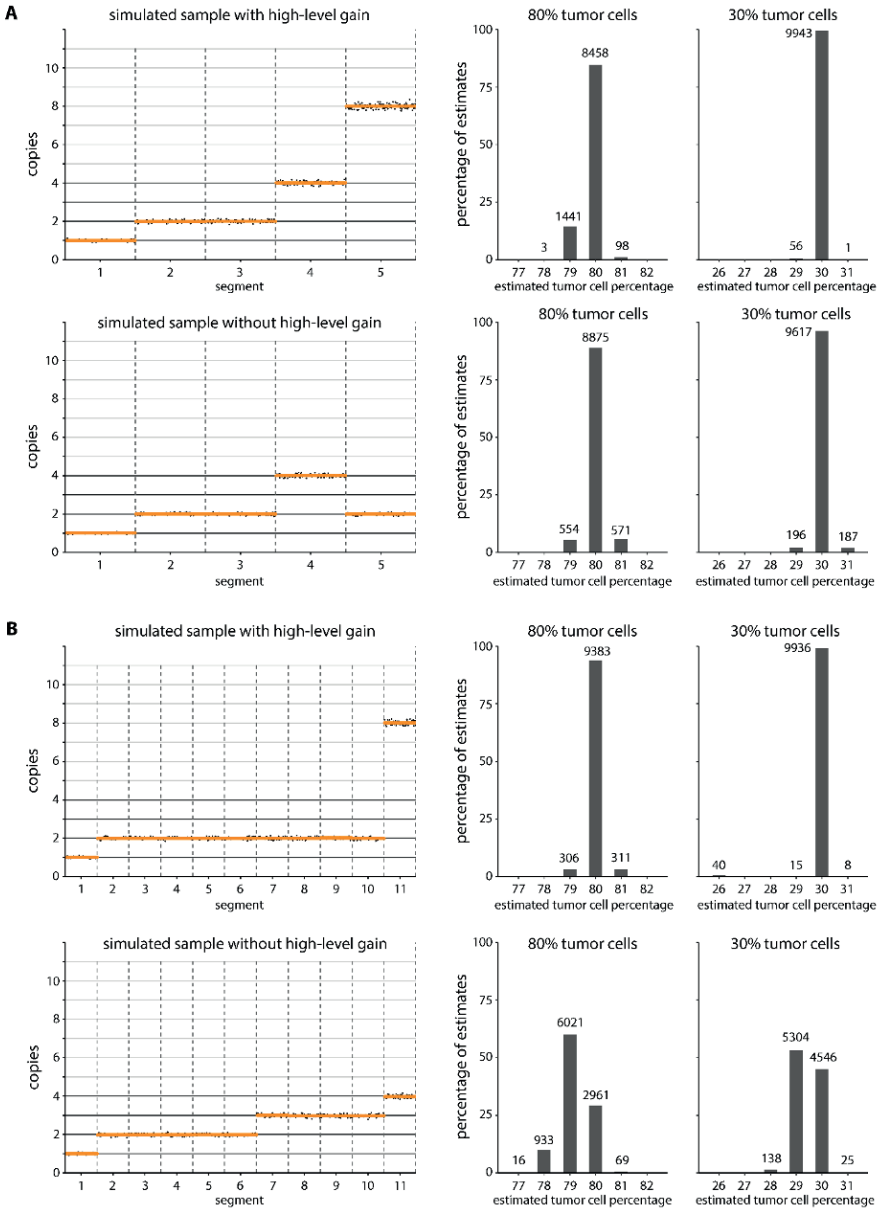

Supplementary figure 6. Effect of high-level gains on ACE's prediction accuracy. Copy number profiles were created by sampling "reads" originating from 500 bins divided over 5 segments (A) or 550 bins divided over 11 segments (B). The probability to sample from a bin was set proportional to the number of intended copies, e.g. 1, 2, 2, 4, 8 for the first variant. In both (A) and (B), a sample with high-level gain (top row) is compared to a similar sample without high-level gain (bottom row). The variants in (A) only differ on a single segment. The variants in (B) were created in such a way that their "tumor content" is equal. For all variants, 10,000 permutations were created using either 80% or 30% tumor cell percentage. Tumor percentage estimates for all permutations were calculated using ACE and plotted in the histograms.

Chapter 6

Prognostic relevance of CD163 and CD8 combined with EZH2 and gain of chromosome 18 in follicular lymphoma: A study by the Lunenburg Lymphoma Biomarker Consortium

Wendy B.C. Stevens*, Matias Mendeville*, Robert Redd, Andrew J. Clear, Reno Bladergroen, Maria Calaminici, Andreas Rosenwald, Eva Hoster, Wolfgang Hiddemann, Philippe Gaulard, Luc Xerri, Gilles Salles, Wolfram Klapper, Michael Pfreundschuh, Andrew Jack, Randy D. Gascoyne, Yasodha Natkunam, Ranjana Advani, Eva Kimby, Birgitta Sander, Laurie H. Sehn, Anton Hagenbeek, John Raemaekers, John Gribben, Marie José Kersten, Bauke Ylstra, Edie Weller, Daphne de Jong

*Authors contributed equally

Haematologica, 2017; 102(8):1413-1423

Abstract

In follicular lymphoma, studies addressing the prognostic value of microenvironment-related immunohistochemical markers and tumor cell-related genetic markers have yielded conflicting results, precluding implementation in practice. Therefore, the Lunenburg Lymphoma Biomarker Consortium performed a validation study evaluating published markers.

To maximize sensitivity, an end-of-spectrum design was applied for 122 uniformly immunochemotherapy-treated follicular lymphoma patients retrieved from international trials and registries; early failure: progression or lymphoma-related death <2 years versus long remission: response duration of >5 years. Immunohistochemical staining for T-cells and macrophages was performed on tissue microarrays from initial biopsies and scored with a validated computer-assisted protocol. Shallow whole-genome and deep targeted sequencing was performed on the same samples.

The 96/122 cases with complete molecular and immunohistochemical data were included in the analysis. *EZH2* wild-type (p=0.006), gain of chromosome 18 (p=0.002), low percentages of CD8+ cells (p=0.011) and CD163+ areas (p=0.038) were associated with early failure. No significant differences in other markers were observed, thereby refuting previous claims of their prognostic significance.

Using an optimized study design, this Lunenburg Lymphoma Biomarker Consortium study substantiates wild-type *EZH2* status, gain of chromosome 18, low percentages of CD8+ cells and CD163+ area as predictors of early failure to immunochemotherapy in follicular lymphoma treated with R-CHOP (like), while refuting the prognostic impact of various other markers.

Introduction

The disease course of follicular lymphoma (FL) is characterized by multiple relapses with variable remission durations, which tend to get shorter after each line of treatment.[1-7] Approximately 15% of patients die within the first few years, largely due to histological transformation or refractory disease. In contrast, the majority of patients show prolonged survival without relapse and a substantial number of patients never even require treatment. Currently, clinical factors captured in the Follicular Lymphoma International Prognostic Index (FLIPI)[8, 9] and the adjusted FLIPI2[10] are the primary prognostic tools utilized to predict disease progression. FLIPI is based on easily available clinical data designed to offer an accurate, yet simple prognostic index. However, the biological behavior of FL is likely determined by a more complex interaction between tumor genetics, -microenvironment and patient characteristics.

Several gene expression-profiling studies have underlined the major influence of characteristics of the non-malignant tumor microenvironment on prognosis in FL.[11, 12] However, evaluation by immunohistochemistry (IHC) of T-cell and macrophage populations for their prognostic translational impact have produced valuable yet conflicting results.[13-25] Contradictory results are likely caused by multiple factors, including variable patient selection, heterogeneity of treatments across cohorts,[25] insufficient statistical power due to underrepresentation of poor-outcome patients, technical issues in IHC staining and inter-observer variability in scoring. Previous IHC based validation studies of microenvironment cell populations by the Lunenburg Lymphoma Biomarker Consortium (LLBC), in both diffuse large B-cell Lymphoma (DLBCL) and FL, have highlighted the poor reproducibility of manual scoring even by experienced pathologists and advocated computer-assisted scoring as being the more reliable technique.[26, 27]

Recently, the mutational spectrum of FL tumor cells and their prognostic value have been reported.[28-30] Most notably, Pastore et al demonstrated the value of combining mutation status with clinical FLIPI and performance status to improve upon the prognostic value of FLIPI alone (45-55%) to 64-72% for M7-FLIPI, with a comparable negative prognostic value.[31]This method may also be valuable for very high-risk FL cohorts, as reported by the same group.[32]

The objective of the present study of the LLBC consortium was to critically asses, in a homogeneously treated patient cohort, whether the previously implicated micro environmental and molecular markers of the tumor have clinically relevant prognostic value. We hypothesized that the micro environmental and molecular markers, would

be most prominent when we compare tissue samples of patients with an extremely poor prognosis (i.e. progression or death within 2 years, a well-established criterion for poor prognosis in FL)[33] with those with a very favorable prognosis (a response to 1st line treatment lasting > 5 years). The LLBC gene panel incorporated the, at that time published, molecular markers which were frequently mutated as well as markers that were rarely mutated such as *FAS* and *MYD88*.[28-30] Since with our study design we hypothesized to reveal prognostic value of also rare mutations.

To avoid interlaboratory technical variations and interpretation, all assays were uniformly processed in a single laboratory and IHC was scored using computer-assisted technology based on a previous LLBC FL validation study,[27] and molecular analysis was performed using established next generation sequencing (NGS) procedures for mutation and copy number analyses.

Methods

Patient selection for an end-of-spectrum design

Tumor specimens of patients with FL, histologic grades 1, 2 and 3A were retrieved from the randomized Lymphoma Study Association (LYSA) FL2000 study,[4, 6] the German low-grade Lymphoma Study Group (GLSG) GLSG2000 study,[3] and the St Bartholomew's Hospital Registry, London. The patients required treatment and the inclusion criteria in the trials were comparable. All patients were treated with rituximab, cyclophosphamide, adriamycin, vincristine and prednisone (R-CHOP) or R-CHOP-like regimens, with or without interferon-alpha (IFN) maintenance for 2 years. Patients were selected for an end-of spectrum design as: (1) early failure (EF), defined as: no remission or progression or lymphoma-related death within 2 years after start of 1st line treatment or, (2) long remission (LR), defined as: a complete or partial remission lasting >5 years after 1st line treatment. Patients that fell in between these criteria were not included in this study. Availability of complete clinical information at diagnosis, follow-up data until relapse, progression or at least 5 years post-treatment if the patient was still in remission and availability of formalin-fixed paraffin embedded (FFPE) diagnostic biopsy samples was a prerequisite for inclusion. Detailed clinical information on demographic parameters, staging procedures, treatment regimens and outcome were collected by the involved data centers (LYSA, GLSG and St Bartholomew's Hospital).

Microenvironment analysis on tissue micro-arrays using immunohisto-chemistry and automated image analysis scoring

Tissue microarrays (TMAs) were constructed centrally according to LLBC validated protocols[27] at the Department of Pathology, Würzburg, Germany, from the biopsy part identified by the pathologist (AR), using duplicate cores of 1 mm diameter. Three µm slides were stained for CD3, CD4, CD8, CD68, CD163, FOXP3, PD1, and P53 (Supplementary Table S1) according to standard procedures at the Bartholomew's Pathology Research Laboratory, London, UK.

A computerized system with automated scanning microscope and computerized image analysis (Ariol SL-8, Leica Microsystems, Wetzlar, Germany) was used for scoring as described in the LLBC validation study.[27] Macrophages and all T-cell populations were scored for the whole core, and in the intrafollicular and interfollicular areas separately, as described by Wahlin et al.[22] Color- and shape class defined positive- and negative nucleated cells, or positive- and negative areas.[16] Cores with less than 50% scorable core surface (non representative areas or tissue artifacts) were excluded and average scores of duplicates were used when available.

Using the Ariol software algorithm CD3, CD4, CD8, PD1, FOXP3 and p53 positive nucleated cells were scored as the percentage of all nucleated cells. For CD68 and CD163 the positive area versus the whole area was scored to accommodate the large size and long cytoplasmic extensions of macrophages as an optimal determination of cell numbers. The typical perifollicular infiltration pattern of FOXP3 was scored manually by three observers[27] and was considered positive if at least two out of the three pathologists (DdJ, AR and MC) identified and counted at least one rim of densely packed positive cells at the periphery of a follicle.[14] All histopathological assessments were done without insight into the patient's clinical data and outcome.

Gene mutation and copy number analysis using next generation sequencing (NGS)

DNA was extracted from FFPE cores with a QIAamp DNA FFPE Tissue Kit (Qiagen, Hilden, Germany) and quantified using a Qubit 2.0 Fluorometer (Thermo Fisher Scientific, Carlsbad CA, USA). Of each patient sample 250ng DNA was sheared on a Covaris S2 (Covaris Inc, Woburn MA, USA), with settings adjusted to DNA from FFPE tissue.[34]NGS libraries were prepared using the KAPA Library Preparation kits (KAPA Biosystems, Wilmington MA, USA). In

short, uniquely 8-bp indexed adapters (Roche Nimblegen, Madison WI, USA.) were ligated to the FFPE-extracted DNA, followed by size selection of fragments in the range of 150 to 400bp.

One aliquot of this library was subjected to shallow whole genome sequencing (WGS) for genome-wide copy number analysis,[34] and another aliquot was subjected to hybrid capture target enrichment (Roche Nimblegen, Madison WI, USA) for mutation analysis. Eight libraries were equimolarly pooled per capture. The hybrid capture panel covers 122 exons (~50.000 base pairs) of 11 frequently mutated genes (*KMT2D*, *CREBBP*, *MEF2B*, *EZH2*, *EP300*, *BCL2*, *FAS*, *TNFRSF14*, *CARD11*, *TNFAIP3* and *MYD88*) in FL-LLBC-NGS target enrichment panel, (Supplementary Table S2). All libraries were sequenced on a HiSeq 2000 (Illumina, San Diego CA, USA), 50bp single-end for shallow WGS and 125bp paired-end for mutation analysis. All sequence lanes were multiplexed with up to 24barcoded sample libraries.

Shallow WGS data was analyzed using the Bioconductor package QDNAseq (v1.5.1).[34] For gene mutation analysis, variant calling was performed by VarScan2 (v2.3.7)[35] using very strict criteria, excluding all germline variants from the Single Nucleotide Polymorphism database (dbSNP build142), any synonymous mutation and intronic mutations with low predicted impact. For prognostic analysis, only non-silent mutations (missense, nonsense, in-frame or frame-shift insertions and deletions) were included.

For detailed laboratory data analysis procedures see supplementary methods section.

Ethical Committee statement

The study and protocols to obtain human archival tissues and patient data were approved by the local ethical committee of the VU University Medical Center, Amsterdam (FWA00017598) for all collaborating centers and comply with the Code for Proper Secondary Use of Human Tissue in the Netherlands (http://www.fmwv.nl).

Statistics

Uni- and multivariate analyses were used to evaluate the distribution of the biomarkers for the two cohorts. For microenvironment analysis, biomarkers were included in the analysis using the scoring categories as defined above and the average of the biomarker score from two cores was used in the analysis. For mutation analysis, the genes were included in the analysis as mutated or wild-type. To correct for multiple comparisons, the Benjamini-Hochberg method was used, and p-values less than 0.05 were considered significant. Patient characteristics were summarized with descriptive statistics. Fisher's exact test was used to test for association between pairs of categorical

variables, and univariate and multivariable logistic regression was used for the binary outcome of cohort. Odds ratios (OR) and 95% confidence intervals (CI) were reported, The Wilcoxon rank-sum test was used to assess a location shift in the distribution of continuous variables between two groups. In a secondary analysis, optimal cut points for eight continuous markers were determined using recursive partitioning models a binary outcome. To evaluate agreement among the three pathologists for the FOXP3 patterns the free marginal Kappa statistics of Brennan and Prediger are reported with a bootstrap confidence interval.[36, 37] Analyses were performed using SAS Software version 9.3 (SAS Institute Inc, Cary, NC; 2005) and R version 3.3.0 (R Core Team, Vienna, Austria; 2016).[38]

Results

Patient selection and immunohistochemical biomarker assessment

A total of 122 patients fulfilled the selection criteria and had biopsy material available that met the input requirements for both immunohistochemistry (IHC) and gene mutation analysis (EF, n=49 and LR, n=73). In 105 cases a complete set of IHC markers was available (Supplementary Table S3). For NGS analysis, DNA of sufficient quality and with sufficient NGS read depth could be retrieved for 111 cases, resulting in the complete molecular data for gene mutation analysis and copy number profiles.

For 96 of the 122 cases (79%) both IHC and molecular data could be generated that met our quality criteria and was included for downstream analysis. Table 1 shows the clinical characteristics of the 96 patients (Supplementary Table S4 provides the characteristics for all 122 patients, with marginal statistical differences for prognostic subgroup representation). FLIPI high-risk category was overrepresented in the EF cohort (p=0.009), underpinning the validity of the selection criteria for this end-of-spectrum design.

Impact of microenvironment T-cell and macrophage cell populations by cohort

The distribution of IHC markers per end-of-spectrum prognostic subgroup analyzed in the whole core is shown in Figure 1 and Supplementary Table S5 (Supplementary Table S6 shows the distribution of IHC markers of the 105 cases). Statistically significant differences were found in the median percentage of CD8+ nucleated cells (median EF vs LR is 7.9% vs. 8.6%, p=0.011) and CD163+ macrophages area (median EF vs. LR is 3.6% vs. 5.2%, p=0.038). In logistic regression analyses, the estimated OR for CD8+ cells are 3.9 (95% CI: [1.5-12.1], p=0.01) for a decrease of 10% CD8+ cells. For CD163+ area the odds are 2.0 (95% CI: [1.1- 4.4], p=0.04) for a decrease of 10% CD163+ area (Supplementary Table S7).

Table 1. Clinical characteristics of patients with all immunohistochemical and molecular markers available.

	Total	Early failure	Long remission
	n = 96	n = 39	n = 57
Group			
Barts	8 (8%)	6 (15%)	2 (4%)
GLSG	80 (83%)	29 (74%)	51 (89%)
LYSA	8 (8%)	4 (10%)	4 (7%)
Age at diagnosis			
Median (range)	58 (27-75)	61 (27-75)	58 (32-69)
< 60	50 (52%)	18 (46%)	32 (56%)
Sex			
Female	47 (49%)	17 (44%)	30 (53%)
Grade			
Grade 1, 2	75 (78%)	28 (72%)	47 (82%)
Grade 3A	6 (6%)	3 (8%)	3 (5%)
Missing	15 (16%)	8 (21%)	7 (12%)
Stage			
Stage I-II	2 24%)	1 (3%)	1 (2%)
Stage III-IV	94 (87%)	38 (97%)	55 (96%)
Missing	1 (1%)	0	1 (2%)
B-symptoms			
Absent	59 (61%)	23 (59%)	36 (63%)
Present	35 (36%)	16 (41%)	19 (33%)
Missing	2 (2%)	0	2 (4%)
ECOG PS			
0	32 (33%)	13 (33%)	19 (33%)
1	58 (60%)	21 (54%)	37 (65%)
2	2 (2%)	2 (5%)	0 (0%)
3	1 (1%)	1 (3%)	0 (0%)
Missing	3 (2%)	2 (5%)	1 (2%)
FLIPI risk categories			
Low	10 (10%)	1 (3%)	9 (16%)
Intermediate	35 (36%)	11 (28%)	24 (42%)
High	46 (48%)	26 (67%)	20 (36%)
Missing	5 (5%)	1 (3%)	4 (7%)
First line therapy			
R-CHOP	87 (91%)	34 (87%)	53 (93%)
R-CHVP-I	9 (9%)	5 (13%)	4 (7%)

Abbreviations: Barts: Bartholomew's Hospital Registry London, GLSG: German low-grade Lymphoma Study Group, LYSA: the Lymphoma Study Association, ECOG: Eastern Cooperative Oncology Group, PS: performance score, FLIPI: follicular lymphoma international prognostic index. R-CHOP: rituximab, cyclophosphamide, adriamycin, vincristine and prednisone R-CHVP-I: rituximab, cyclophosphamide, adriamycin, etoposide, prednisolone and interferon-alpha2a

Adjusting for other IHC markers without the FLIPI score in a multivariable model, only the CD8+ T-cells retained significance (OR=4.5, 95% CI: [1.1-21.2] p=0.04), but with the FLIPI score included it does no longer reach significance. No significant differences were found for the other markers (CD3, CD4, CD68, CD163, PD1, FOXP3 and p53) between the two cohorts (Supplementary Table S7).

Since CD163 was binary scored as positive or negative, a high overall score for the two prognostic subgroups might be caused by a higher cell density and/or by larger individual cells. Visual assessment by two pathologists (DdJ, MC) was performed and confirmed that the higher percentage of positive areas was due to higher cell density.

A secondary analysis using recursive partitioning was performed to evaluate markers that could separate the two prognostic subgroups and to determine the optimal cut points for the identified markers for the whole core. The optimal cut points were 12.6% and 6.3% for CD8+ and CD163+, respectively. The percentage of patients with low levels of both CD8+ T-cells and CD163+ area (defined as lower than the optimal cut points) is 79% (95% CI 64 – 91%) vs. 39% (95% CI 16 -52%) for EF (n=39) vs. LR (n=57) ($p<0.001$). Similarly, results were obtained if the upper quartiles are used instead of the optimal cut points (12.2% (n=39) vs 8.4% (n=57) for EF (79% (95% CI: 64 – 91%)) vs LR (46% (95% CI: 32 – 59%)), p = 0.001).

Impact of spatial distribution and perifollicular pattern of FOXP3 by prognostic subgroup

The spatial distribution of T-cell populations and macrophages has been claimed to be of greater influence on prognosis than the overall numbers of infiltrating cells and therefore intra- and interfollicular populations were assessed separately.[14-17, 19, 22, 39] However, in this series, we could not validate this claim for most T-cell or macrophage classes. Except in the univariate analysis of the interfollicular population, CD8+ cells and CD163+ area are significant, CD8+ cells with an OR 3.6 (95% CI: [1.2-6.4], p=0.03) and CD163+ area 1.9 (95% CI: [1.1-3.6], p=0.03). Only CD8+ interfollicular populations have a minor influence in multivariate analysis without the FLIPI score included (OR3.7, 95% CI [1.2-15.5], $p<0.01$) (Supplementary Tables S8 and S9).

The perifollicular pattern of FOXP3+ T-cells was scored manually by three pathologists (DdJ, AR, BS). Agreement between pathologists reached similar levels as in the validation study (Brennan-Predigar estimate of 0.78 and 0.83 for cores 1 and 2 in this study versus 0.85 for validation study). [29] The perifollicular pattern did not differ significantly (p=0.46) between the two prognostic subgroups, 10/39 (26%) EF subgroup and 11/57 (19%) LR subgroup (Supplementary Table S10).

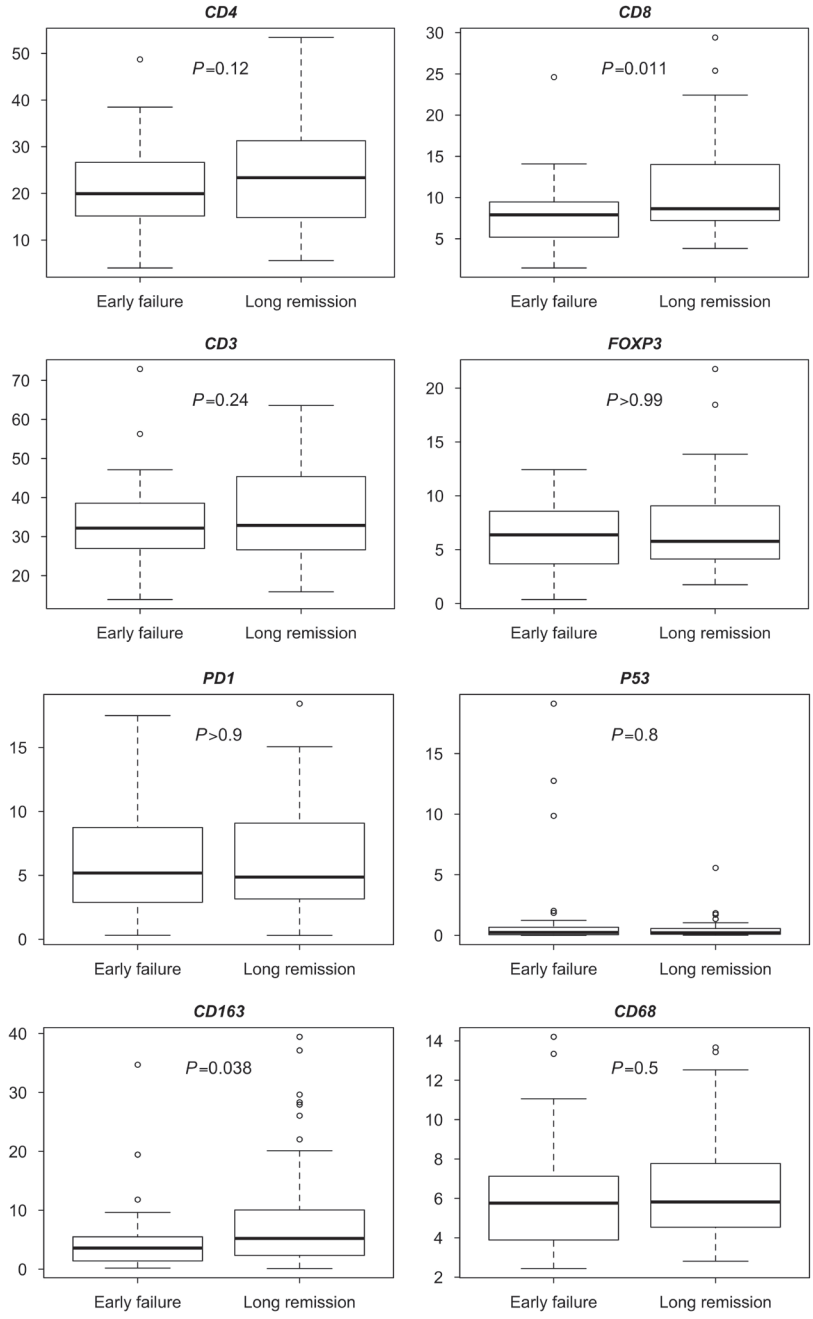

Figure 1. Boxplots per immunohistochemical marker. For CD4, CD8, CD3, FOXP3, PD1 and P53 is it the percentage of positive nucleated cells of all nucleated cells, and for CD163 and CD68 is it the percentage of positive cell area of the total cell area. Early failure n=39, long remission n=57

Frequency distribution of chromosomal copy numbers and gene mutations in FL

Shallow WGS resulted in high quality genome-wide copy-number aberration (CNA) plots for all cases. The most common aberrations, detected in at least 10% of patients, included complete or partial gains of chromosomes 1q, 2, 7, 8, 12 and 18 and losses of 1p, 6q and 10q (Figure 2 and Supplementary Table S11). The landscape of CNAs shows notable enrichment of FL-related genes, including focal losses of *TNFRSF14* (1p36.32), *TNFAIP3*(6p23.3) and FAS and *PTEN* (10q23.31) and focal gains that harbour FL-related oncogenes, like *BCL11A* and *REL*(2p16.1).

Genes included in the LLBC-NGS target enrichment panel showed non-synonymous mutations in at least 2 FL cases (Figure 3 and Supplementary Table S12). *BCL2,* a known target for aberrant somatic hypermutation (aSHM) in FL, was most frequently mutated (88/96, 92%) with 0 to 78 mutations per case. Chromatin modifying genes *KMT2D* (71%) and *CREBBP* (67%) were mutated with high frequency and epigenetic modifiers *EZH2 (18%), MEF2B (10%), EP300 (7%)* at lower rates with non-silent mutations in 1-4 of these chromatin modifying genes in 90% of FL patients, consistent with the critical role of epigenetic deregulation in the majority of FL. No patterns of co-occurrence or mutual exclusivity were observed. Non-silent mutations were found in *TNFRSF14* (30%), *TNFAIP3* (7%), *CARD11* (8%), *FAS* (2%) and *MYD88* (2%) (Table 2, Supplementary Table S13 shows the distribution of mutations of the 111 cases).

Impact of chromosomal copy numbers and gene mutations by prognostic subgroup

The distribution of CNAs and gene mutations by prognostic subgroup are shown in Figure 2 and 3. Statistically significant differences after multiple testing correction were only found for gain of chromosomal region 18p11.32-q21.33 (gain EF vs LR 49% vs 12%, $p<0.001$), with an estimated OR in logistic regression analysis of 0.15 (95% CI: [0.05-0.44]) and for *EZH2* mutation status (unmutated EF vs LR 90% vs 72%, $p<0.001$) (Table 2). The odds ratio for unmutated *EZH2* is 14.53 (95% CI:[2.06-635.92]). No significant impact was found for various markers, previously implicated as (borderline) prognostic such as *CREBBP* (OR 0.55, 95% CI [0.20-1.45], p=0.6), *EP300* (OR 1.77, 95% CI [0.27-19.52], $p>0.99$), *CARD11* (OR 1.15, 95% CI [0.21-7.89], $p>0.99$) and *MEF2B* (OR 1.03, 95% CI [0.22-5.33], $p>0.99$).

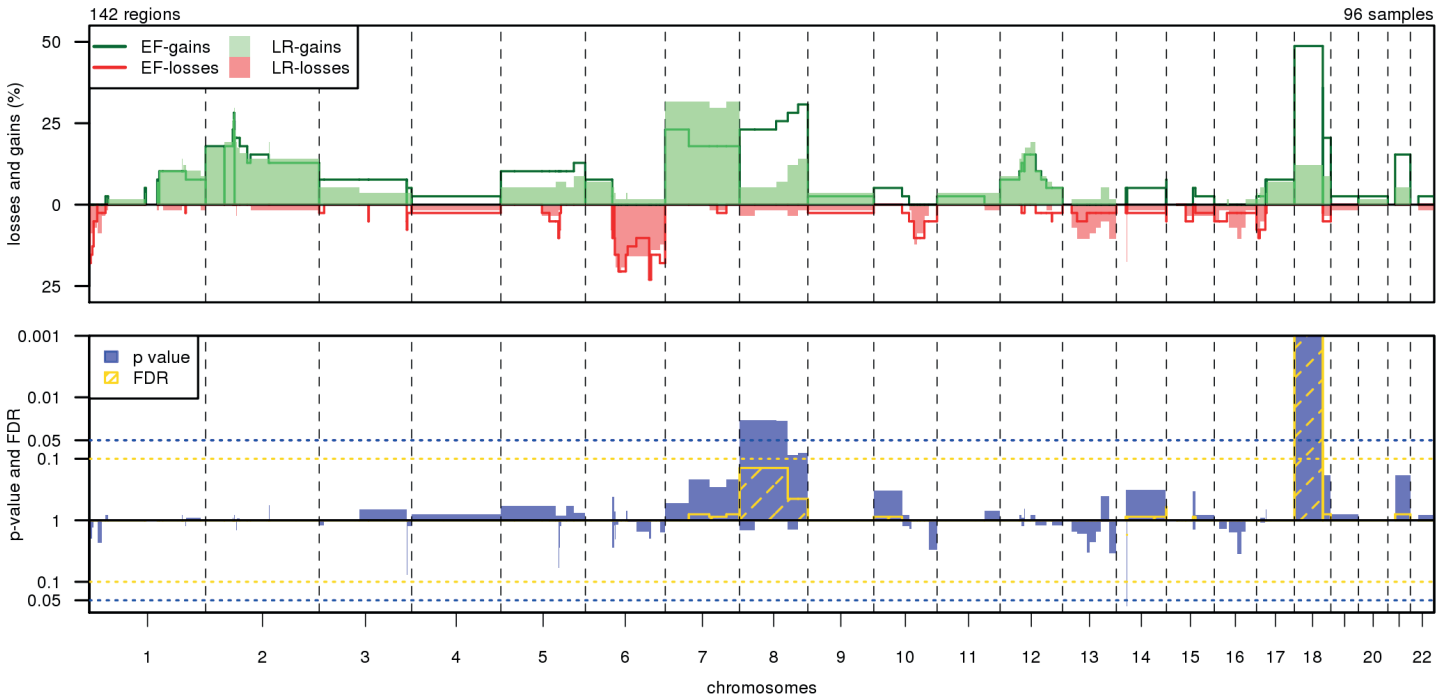

Figure 2. Distribution and significance of copy number gains and losses by subgroup. Top panel: Percentages of gains (top; green) and losses (bottom; red) in early failure (EF, n=39) and long remission (LR, n=57) per chromosomal region. X-axis: chromosomal regions, ordered by genomic coordinates of chromosomes 1 to 22. y-axis: percentage of cases showing CNAs. Vertical-dotted lines: boundaries between chromosomes. Bottom panel: significance of differences in frequencies of gains (top) and losses (bottom) between cohorts. X-axis: chromosomal regions, ordered by genomic coordinates of chromosomes 1 to 22.y-axis: P-value (blue) and false discovery rate (FDR; yellow). Horizontal-dotted lines show the threshold of significance for P (0.05) and FDR (0.1), based on a Wilcoxon rank-sum test with 10 000 permutations.

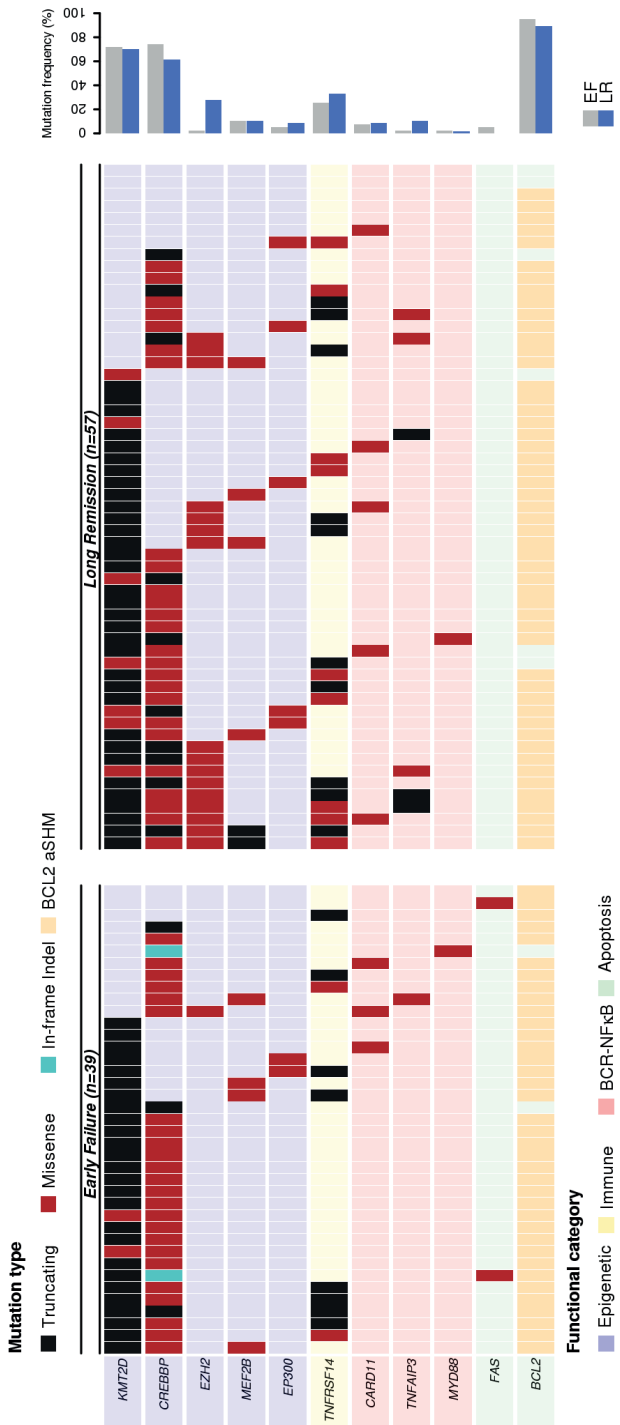

Figure 3. Distribution of mutations in 11 genes by subgroup. Each column represents an individual case. Genes are clustered based on functional category and mutations are color-coded based on effect prediction. Mutation frequencies for each gene by cohort are shown in the bar graph on the right.

Table 2. Distribution of gene mutation status by cohort (n=96)

	Total n=96 (%)	Early failure n=39 (%)	Long remission n=57 (%)	OR [95% CI]	*p (unadjusted)*	*p (adjusted)*
BCL2						
Mutated	88 (92)	37 (95)	51 (89)	0.46 [0.04 - 2.78]	*0,47*	*0,9*
Unmutated	8 (8)	2 (5)	6 (11)			
KMT2D						
Mutated	68 (71)	28 (72)	40 (70)	0.93 [0.34 - 2.47]	*> 0.99*	*> 0.99*
Unmutated	28 (29)	11 (28)	17 (30)			
CREBBP						
Mutated	64 (67)	29 (74)	35 (61)	0.55 [0.20 - 1.45]	*0,27*	*0,6*
Unmutated	32 (33)	10 (26)	22 (39)			
TNFRSF14						
Mutated	29 (30)	10 (26)	19 (33)	1.44 [0.54 - 4.04]	*0,5*	*0,9*
Unmutated	67 (70)	29 (74)	38 (67)			
MEF2B						
Mutated	10 (10)	4 (10)	6 (11)	1.03 [0.22 - 5.33]	*> 0.99*	*> 0.99*
Unmutated	86 (90)	35 (90)	51 (89)			
EZH2						
Mutated	17 (18)	1 (3)	16 (28)	14.53 [2.06 - 635.92]	*< 0.001*	*0,006*
Unmutated	79 (82)	38 (97)	41 (72)			
TNFAIP3						
Mutated	7 (7)	1 (3)	6 (11)	4.41 [0.50 - 210.74]	*0,23*	*0,6*
Unmutated	89 (93)	38 (97)	51 (89)			
EP300						
Mutated	7 (7)	2 (5)	5 (9)	1.77 [0.27 - 19.52]	*0,7*	*> 0.99*
Unmutated	89 (93)	37 (95)	52 (91)			
CARD11						
Mutated	8 (8)	3 (8)	5 (9)	1.15 [0.21 - 7.89]	*> 0.99*	*> 0.99*
Unmutated	88 (92)	36 (92)	52 (91)			
FAS						
Mutated	2 (2)	2 (5)	0 (0)	0.00 [0.00 - 3.62]	*0,16*	*0,6*
Unmutated	94 (98)	37 (95)	57 (100)			
MYD88						
Mutated	2 (2)	1 (3)	1 (2)	0.68 [0.01 - 54.63]	*> 0.99*	*> 0.99*
Unmutated	94 (98)	38 (97)	56 (98)			

Integrated modelling of immunohistochemical and molecular analysis of the prognostic subgroups

Correlation analysis was performed for molecular- and IHC markers, showing significant correlation between mutated *CREBBP* status and higher level infiltrates of PD1 positive T-cells ($p<0.005$), but not with CD4 and CD8 positive T-cells (Figure 4A). *TNFRSF14* mutation status showed significant correlation with lower CD4 and CD8 positive T-cell infiltrates (p=0.037 and p=0.030) (Figure 4B). Microenvironmental populations were not significantly differentially distributed for other molecular markers, including *EZH2* (data not shown).

In a multivariable model combining the four markers, CD8, CD163, gain chromosome 18 and *EZH2* mutation, that are statically significant in the univariate analysis, only the gain of chromosome 18 (OR 0.27 (95% CI: [0.09,0.79], p=0.019)) and *EZH2* (OR 13.76 (95% CI: [2.53,264.94], p=0.017)) retain significant. After incorporating the FLIPI score into the model, gain of chromosome 18 (p=0.018) and *EZH2* (p=0.036) (Table 3) retain significance.

Table 3. Odds ratio (OR) (95% CI) for a 10% change in the immunohistochemical markers and absent or present molecular markers in univariate analysis, and multivariate analysis without and with the FLIPI.

	Univariate		Multivariable without FLIPI		Multivariable with FLIPI	
	OR (95% CI)	P	OR (95% CI)	P	OR (95% CI)	P
%CD8	3.86 (1.48, 12.13)	0.01	3.15 (1.03, 11.87)	*0.064*	2.58 (0.83, 10.02)	*0.13*
%CD163	2.01 (1.11, 4.37)	*0.04*	1.54 (0.75, 3.83)	*0.29*	1.43 (0.69, 3.52)	*0.38*
CHR 18	0.15 (0.05, 0.39)	<0.001	0.27 (0.09, 0.79)	0.019	0.24 (0.07, 0.75)	0.018
EZH2	14.83 (2.82, 274.07)	0.011	13.76 (2.35, 264.94)	0.017	9.99 (1.69, 192.73)	0.036
FLIPI high	0.28 (0.11, 0.66)	0.005			0.36 (0.12, 0.98)	0.048

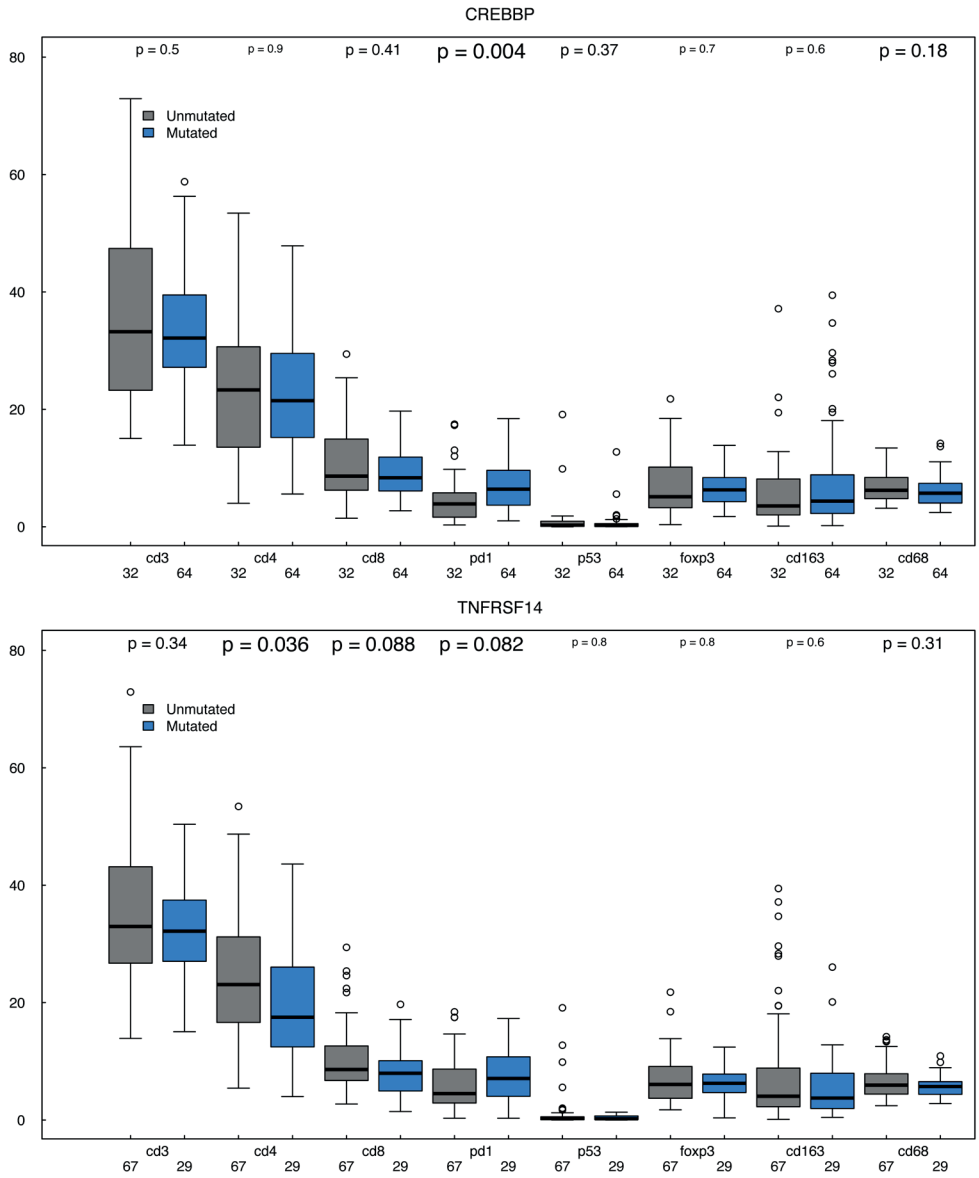

Figure 4. Correlation molecular markers and IHC markers. A: CREBBP, B: TNFRSF14. Blue bars are mutated, grey bars are wild-type. On the X-axis the number of cases per IHC marker, on the Y-axis the percentages of positive cells or area.

Discussion

This LLBC study is as far as we know the first to comprehensively explore the combined prognostic impact of microenvironment T-cell and macrophage infiltration and tumor genetics of FL patients with extremely poor outcome (EF) versus those with a prolonged remission (LR). We show poor outcome to be characterized by a lower number of CD8+ T-cells, a smaller CD163+ macrophage area (indicative of fewer macrophages), wild-type *EZH2* and a copy number gain of chromosome 18. These observations in part confirm previous studies. The gain of chromosome 18, despite its statistically strong prognostic value, was not previously reported. Equally important, cellular densities of various other cell populations, such as PD1+ T follicular helper (T_{FH}) cells and FOXP3+ T regulatory (Treg) cells, previously claimed to predict clinical outcome, were not confirmed in our study.[16, 22, 24, 39-41]

This study was specifically designed to verify the impact of previously published IHC and molecular markers in FL in the rituximab-chemotherapy era. Therefore, we implemented a dedicated study design to reduce noise such that all cases were retrieved from clinical trials and registries which guaranteed complete clinical information at presentation and detailed treatment information. This allowed us to make a homogeneously treated patient selection, with subgroups at the extreme ends of the prognostic spectrum, the EF and the LR subgroups. By balancing inclusion of the rare EF subgroup, we maximize the sensitivity to observe clinically relevant differences in the microenvironment and mutations, while allowing an overall relatively small patient cohort. To reduce inter-observer variability, the validated quantitative computerized IHC scoring method of the TMA was implemented, which was previously shown to be more reproducible than any semi-quantitative method.[27]

For microenvironment populations, our results of CD163+ area validate those of Kridel et al, showing that a higher CD163+ pixel count or CD163+ area are independent predictors of prolonged progression free survival (PFS) in patients treated with R-CHOP (p=0.011-0.030), while the CD68+ macrophages population did not have a significant impact by pixel count or area.[42] Previous reports provided conflicting data for CD68+ macrophages, suggesting correlation with either adverse[17, 39, 43, 44] or favorable outcome[45].Differences in scoring methods and variations in treatment characteristics may explain these discrepancies.

This LLBC study also showed that a lower percentage of CD8+ cytotoxic T- cells, in the whole TMA core and interfollicular areas were associated with EF after treatment with

rituximab-chemotherapy. This confirms findings in several series using computerized scoring or flow cytometry of cell suspensions, both in the rituximab-era and pre-rituximab-era.[15, 22, 46]However, inconsistent results were obtained in studies using manual scoring, [14, 18, 47]corroborating the need for a reliable scoring method of CD8+ T-cells.

None of the other T-cell markers, including CD3, CD4, PD1 and FOXP3 demonstrated a significant prognostic impact. Debates are mostly on PD1+ cells, FOXP3+ cells and perifollicular patterns of FOXP3 positive T-cells with conflicting results published. However, positive prognostic value of PD1+ cells was seen in studies in which only some of the patients received rituximab,[16, 22] whereas in studies in which the majority of patients were treated with rituximab-chemotherapy, no or a negative effect was reported.[39, 41]

Frequencies of mutations and distribution of alterations in hotspots and functional domains of the tested genes are largely in line with those previously reported.[28, 31, 48-50] Almost all FLs are reported to have mutations in one or more histone-modifying genes such as *KMT2D* (reported as 76-89%), *CREBBP* (reported as 33-68%), *MEF2B* (reported as 15%), *EP300* (reported as 9-15%) and *EZH2* (reported as 7-26%).[49]Histone-modifying genes exert their function largely indirectly via co-activation of various transcription factors and thereby their specific role in B-cell oncogenesis and immunological functions is difficult to predict.[51]Gene expression analysis has suggested that mutated *CREBBP* may down-regulate major histocompatibility complex (MHC) class II genes, resulting in impaired T-cell activation and possibly lower T-cell levels in tumor samples.[49] This hypothesis could not be supported in the present study showing no association of *CREBBP* mutation status and total numbers of T-cells or specific subsets except for an association of *CREBBP* mutated status with higher numbers of PD1 positive T-cells. It should be noted, however, that the differences, albeit statistically significant, take place in a very narrow dynamic range. *KMT2D*, that was mutated in 70% of both EF and LR cases, showed a strong correlation to both CD8 and CD163 with high levels of both markers in wild-type cases. *KMT2D* is known to decrease apoptosis and increase B-cell proliferation both directly and indirectly in germinal center B-cells.[52]Conditional mouse models indicate a role in plasma cell and germinal center differentiation.[53] Regulatory alterations, impacting on immunological interactions with T-cells or macrophages have not been described, however. In that line, it is less remarkable that the mutation status of *TNFRSF14*, a protein that is directly involved in immune response regulation, does correlate with CD4+ and CD8+ T-cell infiltration in tumor samples.

By shallow whole genome sequencing, copy number profiles of all tumors were studied in both prognostic groups. Of all previously published numerical alterations in FL, only gain of chromosome 18 stood out as an independent prognostic marker.

Our results confirm *EZH2* as a strong prognostic markers in FL with wild-type gene status associated with poor disease outcome (EF),[31, 32]but other markers, such as *EP300* and *TNFSFR14* that have been implicated to have a significant, though minor impact on prognosis, were not substantiated in our study.[31, 54] This is likely due to selection bias and relative underrepresentation of poor prognosis patients in previous series for which our study design was specifically optimized. This LLBC study design precludes integration of a complete multifactorial prognostic model such as the M7-FLIPI index, however, the prognostic trend of *EZH2* as reported by Pastore et al follows the same direction as in our study, where statistical significance is reached and lack of significance of 4 other markers is confirmed.

Question is if these findings on the prognostic value of microenvironment populations and genomic alterations can be translated to application in daily clinical practice. The mutations in *EZH2* are largely clustered in codon Y646 (Supplementary Figure 1) and therefore technically very easily amenable to simple PCR techniques, [55] while chromosomal gains can be monitored using FISH or NGS.[56, 57] This makes that these two markers have a high potential for clinical implementation. In contrast to the macro-environment population markers CD8 and CD163. With the current techniques, even if it is optimized, the absolute quantitative differences are too small between these two extreme cohorts to become a powerful and clinically useful tool for the scores around the cut point. At best the prediction of the extremes can be used for this purpose.

In conclusion, the literature with regard to IHC prognostic markers in FL has produced highly conflicting results, and for mutation analysis only very limited data are currently available on prognostic impact. By its unique design in a homogeneously rituximab-chemotherapy treated group of patients, we confirm that lower percentages of CD8+ T-cells, CD163+ M2 macrophage areas, *EZH2* wild-type status and gain of chromosome 18 in the initial tumor biopsy specimen predict a poor prognosis in FL for this treatment cohort. Equally important, in this study, we could not substantiate the previously reported claim on the prognostic impact of other most commonly mutated genes such as *TNFRSF14* and *EP300*, of T-cell populations and macrophages classes, as well as a perifollicular distribution of FOXP3+ T-cells for patients treated with R-CHOP (like).[14, 16, 18, 22, 24, 31, 39-41, 54] Moreover, this study provides further insight into the relationship between gene mutation status and most relevant micro-environment populations in FL.

Contributors

The Lunenburg Lymphoma Biomarker Consortium (LLBC) is a collaboration of 10 international lymphoma research groups, each represented by a clinical investigator and one or more hematopathologists and supported by a team of statisticians. Foundation of the LLBC was made possible with a grant from the Van Vlissingen Lymphoma Foundation. EORTC Lymphoma group: Daphne de Jong, John Raemaekers. HOVON Lymphoma group: Daphne de Jong, Marie-José Kersten, Anton Hagenbeek. LYSA: Philippe Gaulard, Gilles Salles, Luc Xerri. British Columbia Cancer Agency: Randy D. Gascoyne, Laurie Sehn. ECOG: Randy D. Gascoyne

GLSG: Andreas Rosenwald, Wolfram Klapper, Michael Pfreundschuh, Wolfgang Hiddemann, Eva Hoster. NLG: Birgitta Sander, Eva Kimby. Barts Cancer Institute: Andrew J. Clear, Maria Calaminici, John Gribben. Leeds Registry: Andrew Jack

Stanford: Yasodha Natkunam, Ranjana Advani. Dana-Farber Cancer Institute, Boston, USA: Edie Weller, Robert Redd

Funding

This study was supported by unrestricted grants from: Genentech/Roche, GlaxoSmithKline, Pfizer Pharma, Teva, Pharmaceuticals/Cephalon and Millenium Pharmaceuticals Inc, Celgene

Acknowledgment

The authors would like to thank Daoud Sie for his advice and providing genomics and compute infrastructure.

References

1. Swenson WT, Wooldridge JE, Lynch CF, Forman-Hoffman VL, Chrischilles E, Link BK. Improved survival of follicular lymphoma patients in the United States. J Clin Oncol. 2005;23(22):5019-5026.
2. Marcus R, Imrie K, Belch A, et al. CVP chemotherapy plus rituximab compared with CVP as first-line treatment for advanced follicular lymphoma. Blood. 2005;105(4):1417-1423.
3. Hiddemann W, Kneba M, Dreyling M, et al. Frontline therapy with rituximab added to the combination of cyclophosphamide, doxorubicin, vincristine, and prednisone (CHOP) significantly improves the outcome for patients with advanced-stage follicular lymphoma compared with therapy with CHOP alone: results of a prospective randomized study of the German Low-Grade Lymphoma Study Group. Blood. 2005;106(12):3725-3732.
4. Salles G, Mounier N, de Guibert S, et al. Rituximab combined with chemotherapy and interferon in follicular lymphoma patients: results of the GELA-GOELAMS FL2000 study. Blood. 2008;112(13):4824-4831.
5. Salles G, Seymour JF, Offner F, et al. Rituximab maintenance for 2 years in patients with high tumour burden follicular lymphoma responding to rituximab plus chemotherapy (PRIMA): a phase 3, randomised controlled trial. Lancet. 2011;377(9759):42-51.
6. Bachy E, Houot R, Morschhauser F, et al. Long-term follow up of the FL2000 study comparing CHVP-interferon to CHVP-interferon plus rituximab in follicular lymphoma. Haematologica. 2013;98(7):1107-1114.
7. Freedman A. Follicular lymphoma: 2011 update on diagnosis and management. Am J Hematol. 2011;86(9):768-775.
8. Solal-Celigny P, Roy P, Colombat P, et al. Follicular lymphoma international prognostic index. Blood. 2004;104(5):1258-1265.
9. Montoto S, Lopez-Guillermo A, Altes A, et al. Predictive value of Follicular Lymphoma International Prognostic Index (FLIPI) in patients with follicular lymphoma at first progression. Ann Oncol. 2004;15(10):1484-1489.
10. Federico M, Bellei M, Marcheselli L, et al. Follicular lymphoma international prognostic index 2: a new prognostic index for follicular lymphoma developed by the international follicular lymphoma prognostic factor project. J Clin Oncol. 2009;27(27):4555-4562.
11. Dave SS, Wright G, Tan B, et al. Prediction of survival in follicular lymphoma based on molecular features of tumor-infiltrating immune cells. N Engl J Med. 2004;351(21):2159-2169.
12. Glas AM, Kersten MJ, Delahaye LJ, et al. Gene expression profiling in follicular lymphoma to assess clinical aggressiveness and to guide the choice of treatment. Blood. 2005;105(1):301-307.
13. Ott G, Katzenberger T, Lohr A, et al. Cytomorphologic, immunohistochemical, and cytogenetic profiles of follicular lymphoma: 2 types of follicular lymphoma grade 3. Blood. 2002;99(10):3806-3812.
14. Lee AM, Clear AJ, Calaminici M, et al. Number of CD4+ cells and location of forkhead box protein P3-positive cells in diagnostic follicular lymphoma tissue microarrays correlates with outcome. J Clin Oncol. 2006;24(31):5052-5059.
15. Alvaro T, Lejeune M, Camacho FI, et al. The presence of STAT1-positive tumor-associated macrophages and their relation to outcome in patients with follicular lymphoma. Haematologica. 2006;91(12):1605-1612.
16. Carreras J, Lopez-Guillermo A, Fox BC, et al. High numbers of tumor-infiltrating FOXP3-positive regulatory T cells are associated with improved overall survival in follicular lymphoma. Blood. 2006;108(9):2957-2964.

17. Canioni D, Salles G, Mounier N, et al. High numbers of tumor-associated macrophages have an adverse prognostic value that can be circumvented by rituximab in patients with follicular lymphoma enrolled onto the GELA-GOELAMS FL-2000 trial. J Clin Oncol. 2008;26(3):440-446.
18. Glas AM, Knoops L, Delahaye L, et al. Gene-expression and immunohistochemical study of specific T-cell subsets and accessory cell types in the transformation and prognosis of follicular lymphoma. J Clin Oncol. 2007;25(4):390-398.
19. Carreras J, Lopez-Guillermo A, Roncador G, et al. High numbers of tumor-infiltrating programmed cell death 1-positive regulatory lymphocytes are associated with improved overall survival in follicular lymphoma. J Clin Oncol. 2009;27(9):1470-1476.
20. Clear AJ, Lee AM, Calaminici M, et al. Increased angiogenic sprouting in poor prognosis FL is associated with elevated numbers of CD163+ macrophages within the immediate sprouting microenvironment. Blood. 2010;115(24):5053-5056.
21. Klapper W, Hoster E, Rolver L, et al. Tumor sclerosis but not cell proliferation or malignancy grade is a prognostic marker in advanced-stage follicular lymphoma: the German Low Grade Lymphoma Study Group. J Clin Oncol. 2007;25(22):3330-3336.
22. Wahlin BE, Aggarwal M, Montes-Moreno S, et al. A unifying microenvironment model in follicular lymphoma: outcome is predicted by programmed death-1--positive, regulatory, cytotoxic, and helper T cells and macrophages. Clin Cancer Res. 2010;16(2):637-650.
23. Wahlin BE, Sundstrom C, Holte H, et al. T cells in tumors and blood predict outcome in follicular lymphoma treated with rituximab. Clin Cancer Res. 2011;17(12):4136-4144.
24. Farinha P, Al-Tourah A, Gill K, Klasa R, Connors JM, Gascoyne RD. The architectural pattern of FOXP3-positive T cells in follicular lymphoma is an independent predictor of survival and histologic transformation. Blood. 2010;115(2):289-295.
25. de Jong D, Koster A, Hagenbeek A, et al. Impact of the tumor microenvironment on prognosis in follicular lymphoma is dependent on specific treatment protocols. Haematologica. 2009;94(1):70-77.
26. de Jong D, Rosenwald A, Chhanabhai M, et al. Immunohistochemical prognostic markers in diffuse large B-cell lymphoma: validation of tissue microarray as a prerequisite for broad clinical applications--a study from the Lunenburg Lymphoma Biomarker Consortium. J Clin Oncol. 2007;25(7):805-812.
27. Sander B, de Jong D, Rosenwald A, et al. The reliability of immunohistochemical analysis of the tumor microenvironment in follicular lymphoma: a validation study from the Lunenburg Lymphoma Biomarker Consortium. Haematologica. 2014;99(4):715-725.
28. Pasqualucci L, Khiabanian H, Fangazio M, et al. Genetics of follicular lymphoma transformation. Cell reports. 2014;6(1):130-140.
29. Okosun J, Bodor C, Wang J, et al. Integrated genomic analysis identifies recurrent mutations and evolution patterns driving the initiation and progression of follicular lymphoma. Nature genetics. 2014;46(2):176-181.
30. Green MR, Gentles AJ, Nair RV, et al. Hierarchy in somatic mutations arising during genomic evolution and progression of follicular lymphoma. Blood. 2013;121(9):1604-1611.
31. Pastore A, Jurinovic V, Kridel R, et al. Integration of gene mutations in risk prognostication for patients receiving first-line immunochemotherapy for follicular lymphoma: a retrospective analysis of a prospective clinical trial and validation in a population-based registry. The lancet oncology. 2015;16(9):1111-1122.

32. Jurinovic V, Kridel R, Staiger AM, et al. Clinicogenetic risk models predict early progression of follicular lymphoma after first-line immunochemotherapy. Blood. 2016;
33. Casulo C, Byrtek M, Dawson KL, et al. Early Relapse of Follicular Lymphoma After Rituximab Plus Cyclophosphamide, Doxorubicin, Vincristine, and Prednisone Defines Patients at High Risk for Death: An Analysis From the National LymphoCare Study. J Clin Oncol. 2015;33(23):2516-2522.
34. Scheinin I, Sie D, Bengtsson H, et al. DNA copy number analysis of fresh and formalin-fixed specimens by shallow whole-genome sequencing with identification and exclusion of problematic regions in the genome assembly. Genome research. 2014;24(12):2022-2032.
35. Koboldt DC, Zhang Q, Larson DE, et al. VarScan 2: somatic mutation and copy number alteration discovery in cancer by exome sequencing. Genome research. 2012;22(3):568-576.
36. Brennan RL, Prediger DJ. Coefficient Kappa - Some Uses, Misuses, and Alternatives. Educ Psychol Meas. 1981;41(3):687-699.
37. Mackay A, Weigelt B, Grigoriadis A, et al. Microarray-Based Class Discovery for Molecular Classification of Breast Cancer: Analysis of Interobserver Agreement. Journal of the National Cancer Institute. 2011;103(8):662-673.
38. R Core Team R. A language and environment for statistical computing. R Foundation for Statistical Computering, Vienna, Austria 2013 [cited; Available from: http://www.R-project.org
39. Richendollar BG, Pohlman B, Elson P, Hsi ED. Follicular programmed death 1-positive lymphocytes in the tumor microenvironment are an independent prognostic factor in follicular lymphoma. Human pathology. 2011;42(4):552-557.
40. Koch K, Hoster E, Unterhalt M, et al. The composition of the microenvironment in follicular lymphoma is associated with the stage of the disease. Human pathology. 2012;43(12):2274-2281.
41. Takahashi H, Tomita N, Sakata S, et al. Prognostic significance of programmed cell death-1-positive cells in follicular lymphoma patients may alter in the rituximab era. Eur J Haematol. 2013;90(4):286-290.
42. Kridel R, Xerri L, Gelas-Dore B, et al. The Prognostic Impact of CD163-Positive Macrophages in Follicular Lymphoma: A Study from the BC Cancer Agency and the Lymphoma Study Association. Clin Cancer Res. 2015;21(15):3428-3435.
43. Coiffier B, Li W, Henitz ED, et al. Prespecified candidate biomarkers identify follicular lymphoma patients who achieved longer progression-free survival with bortezomib-rituximab versus rituximab. Clin Cancer Res. 2013;19(9):2551-2561.
44. Farinha P, Masoudi H, Skinnider BF, et al. Analysis of multiple biomarkers shows that lymphoma-associated macrophage (LAM) content is an independent predictor of survival in follicular lymphoma (FL). Blood. 2005;106(6):2169-2174.
45. Taskinen M, Karjalainen-Lindsberg ML, Nyman H, Eerola LM, Leppa S. A high tumor-associated macrophage content predicts favorable outcome in follicular lymphoma patients treated with rituximab and cyclophosphamide-doxorubicin-vincristine-prednisone. Clin Cancer Res. 2007;13(19):5784-5789.
46. Wahlin BE, Sander B, Christensson B, et al. Entourage: the immune microenvironment following follicular lymphoma. Blood cancer journal. 2012;2(1):e52.
47. Saifi M, Maran A, Raynaud P, et al. High ratio of interfollicular CD8/FOXP3-positive regulatory T cells is associated with a high FLIPI index and poor overall survival in follicular lymphoma. Experimental and therapeutic medicine. 2010;1(6):933-938.

48. Morin RD, Mendez-Lago M, Mungall AJ, et al. Frequent mutation of histone-modifying genes in non-Hodgkin lymphoma. Nature. 2011;476(7360):298-303.
49. Green MR, Kihira S, Liu CL, et al. Mutations in early follicular lymphoma progenitors are associated with suppressed antigen presentation. Proceedings of the National Academy of Sciences of the United States of America. 2015;112(10):E1116-1125.
50. Morin RD, Johnson NA, Severson TM, et al. Somatic mutations altering EZH2 (Tyr641) in follicular and diffuse large B-cell lymphomas of germinal-center origin. Nature genetics. 2010;42(2):181-185.
51. Jiang Y, Hatzi K, Shaknovich R. Mechanisms of epigenetic deregulation in lymphoid neoplasms. Blood. 2013;121(21):4271-4279.
52. Zhang J, Dominguez-Sola D, Hussein S, et al. Disruption of KMT2D perturbs germinal center B cell development and promotes lymphomagenesis. Nature medicine. 2015;21(10):1190-1198.
53. Ortega-Molina A, Boss IW, Canela A, et al. The histone lysine methyltransferase KMT2D sustains a gene expression program that represses B cell lymphoma development. Nature medicine. 2015;21(10):1199-1208.
54. Cheung KJ, Johnson NA, Affleck JG, et al. Acquired TNFRSF14 mutations in follicular lymphoma are associated with worse prognosis. Cancer research. 2010;70(22):9166-9174.
55. Bodor C, Grossmann V, Popov N, et al. EZH2 mutations are frequent and represent an early event in follicular lymphoma. Blood. 2013;122(18):3165-3168.
56. Macintyre G, Ylstra B, Brenton JD. Sequencing Structural Variants in Cancer for Precision Therapeutics. Trends in genetics : TIG. 2016;32(9):530-542.
57. Hastings RJ, Bown N, Tibiletti MG, et al. Guidelines for cytogenetic investigations in tumours. European journal of human genetics : EJHG. 2016;24(1):6-13.

Supplementary methods

DNA isolation and Library preparation

FFPE tissue cores were cut vertically into several smaller fragments to increase surface exposure, followed by DNA extraction with a QIAamp DNA FFPE Tissue Kit (Qiagen, Hilden, Germany) as previously described.[1] Double-stranded genomic DNA was quantified using a Qubit 2.0 Fluorometer (Thermo Fisher Scientific, Carlsbad CA, USA) and 250 ng was fragmented by ultrasonification with a Covaris S2 (Covaris Inc, Woburn MA, USA), with optimized settings for DNA isolated from FFPE tissue.[2] Library preparation of the fragmented DNA was performed with a KAPA Library Preparation kits (KAPA Biosystems, Wilmington MA, USA). Uniquely 8-bp indexed adapters (Roche Nimblegen, Madison WI, USA.) were ligated to the FFPE-extracted DNA followed by purification using AMPure XP beads (Beckman Coulter, Brea CA, USA), which resulted in a fragment size between 150 and 400 basepairs. Subsequently, a PCR amplification was performed with 7 cycles and library yield was assessed by measuring the DNA concentration using an Agilent Bioanalyzer DNA 1000 assay (Agilent Technologies, Santa Clara, CA, USA). Libraries with yield below 50ng were excluded for further analysis.

Shallow whole genome sequencing (WGS) for genome-wide DNA copy number analysis

For shallow WGS, up to 24 barcoded samples libraries were equimolarly pooled and 12.5pM was loaded per lane of a HiSeq Single End Flowcell (Illumina, San Diego CA, USA), followed by cluster generation on a cBot (Illumina, San Diego CA, USA). Sequencing was performed on a HiSeq2000 (Illumina, San Diego CA, USA) in a single-read 50-cycle run mode (SR50).

Shallow WGS reads were analyzed with the Bioconductor package QDNAseq (v1.5.1) [2] which infers copy numbers by a depth of coverage approach without the use of an external reference signal. QDNAseq aligns sequence reads to the human reference genome (GRCh37/hg19) with BWA (v0.7.5), [3] while removing PCR duplicates and reads with mapping qualities below 37 and concurrently dividing the genome into equally sized bins of 30k base pairs. A 2-dimensional Loess correction for GC content and sequence map ability is performed and a blacklist applied based on the 1000 Genomes Project [4] to filter out problematic regions and common regions of germ-line copy number variants.

The resulting copy number profiles were dewaved [5] and segmented. [6] Next, copy number aberrations (CNAs) were called into five discreet categories (homozygous deletion, loss,

normal, gain, or amplification) accounting for sample-specific tumor cell percentages with the Bioconductor package CGHcall (v2.30.0).[7] To reduce dimensions of the data set of 84 000 bins without losing information, CGHregions (v1.26.0; averror setting = 0.0075)[8] was used resulting in 142 chromosomal subregions. A Wilcoxon rank-sum test using 10 000 permutations was performed with CGHtest (v1.1)[9] to compare the distribution of CNAs for each chromosomal subregion. This test includes a permutation-based false discovery rate (FDR) correction for multiple testing. Separate analyses were performed for gains and losses, and chromosomal regions were considered significantly different between cohorts if $P < 0.05$ and $FDR < 0.1$.

Deep targeted sequencing for somatic mutations analysis

For target enrichment, sequence libraries were equimolarly pooled with 8 barcoded samples to a total mass of 1µg DNA. If this amount could not be reached i.e. due to poor DNA quality, a standard of 50ng per patient sample was taken. Libraries were enriched by double hybrid capture for a custom targeted panel using SeqCap EZ choice library capture reagents according to manufacturer's procedures (Roche Nimblegen, Madison WI, USA), covering 122 exons (~50.000 base pairs) of 11 frequently mutated genes in FL (Supplementary table S2). In case a total amount of 1ug DNA could not be reached, the amount of blocking oligonucleotides and EZ enrichment library was adjusted in a linear fashion. Enriched sequence libraries were multiplexed with a maximum of 24 libraries per lane and sequenced on a HiSeq 2000 (Illumina, San Diego CA, USA) in a paired-end 125-cycle mode.

NGS reads were de-multiplexed by Bcl2fastq (Illumina) and adapter sequences trimmed by Cutadapt (v1.6).[8] Subsequently, paired-end reads were aligned to the human reference genome (GRCh37/hg19) with BWA (v0.7.5).[3] Mapped reads were then marked for duplicates with Picard tools (v1.61) [(picard.sourceforge.net)]. Mutation calling was performed with VarScan2 (v2.3.7)[9] according to the following criteria: coverage depth > 20X, average read quality > 20, variant supporting reads >5 and variant allele frequency (VAF) > 10. Mismatches near a stretch of minimally 6 identical nucleotides were neglected. Functional annotation and effect prediction of called variants was performed with SnpEff (v4.1b)[10] Single nucleotide variants (SNVs) and small indels were labeled somatic if impact prediction was 'high' or if impact prediction was 'moderate' and the variant single nucleotide variant (SNV) was tagged as 'uncommon' according to the Single Nucleotide Polymorphism database (dbSNP build 142).[11] This classification eliminated germline SNVs, any synonymous mutation and intronic mutations with low predicted

impact. For BCL2, all SNVs except for those with a 'common' dbSNP label were considered aberrant somatic hypermutation (aSHM). All downstream analyses were performed in the programming language R (version 3.2.1) with custom scripts.

Data availability

All sequence data has been uploaded to the European Genome-phenome Archive (EGA; accession number EGAS00001002049).

Supplementary references

1. van Essen HF, Ylstra B. High-resolution copy number profiling by array CGH using DNA isolated from formalin-fixed, paraffin-embedded tissues. Methods in molecular biology. 2012;838(329-341.
2. Scheinin I, Sie D, Bengtsson H, et al. DNA copy number analysis of fresh and formalin-fixed specimens by shallow whole-genome sequencing with identification and exclusion of problematic regions in the genome assembly. Genome research. 2014;24(12):2022-2032.
3. Li H, Durbin R. Fast and accurate short read alignment with Burrows-Wheeler transform. Bioinformatics. 2009;25(14):1754-1760.
4. Genomes Project C, Abecasis GR, Auton A, et al. An integrated map of genetic variation from 1,092 human genomes. Nature. 2012;491(7422):56-65.
5. van de Wiel MA, Brosens R, Eilers PH, et al. Smoothing waves in array CGH tumor profiles. Bioinformatics. 2009;25(9):1099-1104.
6. Venkatraman ES, Olshen AB. A faster circular binary segmentation algorithm for the analysis of array CGH data. Bioinformatics. 2007;23(6):657-663.
7. van de Wiel MA, Kim KI, Vosse SJ, van Wieringen WN, Wilting SM, Ylstra B. CGHcall: calling aberrations for array CGH tumor profiles. Bioinformatics. 2007;23(7):892-894.
8. van de Wiel MA, Wieringen WN. CGHregions: dimension reduction for array CGH data with minimal information loss. Cancer informatics. 2007;3(55-63.
9. van de Wiel MA, Smeets SJ, Brakenhoff RH, Ylstra B. CGHMultiArray: exact P-values for multi-array comparative genomic hybridization data. Bioinformatics. 2005;21(14):3193-3194.
10. Martin M. Cutadapt removes adapter sequences from high- throughput sequencing reads. EMBnet Journal 2011;17(1):10-12.
11. Sherry ST, Ward MH, Kholodov M, et al. dbSNP: the NCBI database of genetic variation. Nucleic acids research. 2001;29(1):308-311.

Supplementary tables

Table S1. Antibodies used for immunohistochemistry for T-cell subsets, macrophage subsets and tumorcell markers.

Antibody	Company	Working dilution
CD3	Labvision CD3-SP7	20:10 000
CD4	NCL-CD4-268	20:10 000
00CD8	Dako M7103clone CD8/144B	1:500
FOXp3	Abcam	10:1 000
PD1	Abcam	1:100
CD68KP1	Daco code M0814 clone KP1	2:16 000
CD163	Novacastra NCL-L-CD163	20:50 000
P53	Dako code M7001 clone D07	1:3 000
CD20	Dako code M0755 clone L26	10:20 000

Table S2. Custom LLBC hybrid-capture target enrichment panel.

Gene	Target
KMT2D/MLL2	Entire CDS
CREBBP	Entire CDS
MEF2B	Exons 2, 3, 4, 9
EZH2	Exons 16, 18
EP300	HAT domain (exons 24-30)
BCL2	2800bp around TSS
FAS	Exon 7-9
TNFRSF14	Entire CDS
CARD11	Exon 5-9
TNFAIP3	Entire CDS
MYD88	Exons 3-5

Table S3. number of cases per immunohistochemical markers, which could be scored in the TMA (n=122), in 105 patients all immunohistochemical markers were scored on either core.

Marker	No. of patients with core 1 not scored	No. of patients with core 2 not scored	No. of patients with both cores not scored	No. of patients with either core scored
CD3	20	18	12	110
CD4	17	20	12	110
CD8	18	18	13	109
FOXP3	21	18	13	109
PD1	24	19	15	107
P53	20	18	12	110
CD163	20	15	11	111
CD68	18	16	11	111

Table S4. Clinical characteristics of all 122 patients with immunohistochemical and/or molecular markers available.

	Total	Early failure	Long remission	*p*
	n = 122	**n = 49**	**n = 73**	
Group				*0.08*
Barts	8 (7%)	6 (12%)	2 (3%)	
GLSG	99 (81%)	39 (80%)	60 (82%)	
LYSA	15 (12%)	4 (8%)	11 (15%)	
Age at diagnosis				*0.11*
Median (range)	60 (27 - 75)	62 (27 - 75)	58 (32 - 71)	
≤ 60	61 (50%)	21 (43%)	40 (55%)	
Sex				*0.58*
Female	64 (52%)	24 (49%)	40 (55%)	
Grade				*0.43*
Grade 1, 2	90 (74%)	35 (71%)	55 (75%)	
Grade 3A	7 (6%)	4 (8%)	3 (4%)	
Missing	25 (20%)	10 (20%)	15 (21%)	
Stage				*0.41*
Stage I-II	5 (4%)	2 (4%)	3 (4%)	
Stage III	35 (29%)	11 (22%)	24 (33%)	
Stage IV	81 (66%)	36 (73%)	45 (62%)	
Missing	1 (1%)	0	1 (1%)	
B-symptoms				*0.57*
Absent	73 (60%)	28 (57%)	45 (62%)	
Present	47 (39%)	21 (43%)	26 (36%)	
Missing	2 (2%)	0	2 (3%)	
ECOG PS				*0.23*
0	41 (34%)	14 (29%)	27 (37%)	
1	73 (60%)	29 (59%)	44 (60%)	
2	4 (3%)	3 (6%)	1 (1%)	
3	1 (1%)	1 (2%)	0 (0%)	
Missing	3 (2%)	2 (4%)	1 (1%)	
FLIPI risk categories				*0.009*
Low	12 (10%)	2 (4%)	10 (14%)	
Intermediate	47 (39%)	14 (29%)	33 (45%)	
High	57 (47%)	31 (63%)	26 (36%)	
Missing	6 (5%)	2 (4%)	4 (5%)	
First line therapy				*0.52*
R-CHOP	106 (87%)	44 (90%)	62 (85%)	
R-CHVP-I	16 (13%)	5 (10%)	11 (15%)	

Abbreviations: Barts: Bartholomew's Hospital Registry London, GLSG: German low-grade Lymphoma Study Group, LYSA: the Lymphoma Study Association, ECOG: Eastern Cooperative Oncology Group, PS: performance score, FLIPI: follicular lymphoma international prognostic index. R-CHOP: rituximab, cyclophosphamide, adriamycin, vincristine and prednisone R-CHVP-I: rituximab, cyclophosphamide, adriamycin, etoposide, prednisolone and interferon-alpha2a

Table S5. distribution of investigated markers in the whole core, interfollicular and intrafollicular compartment in the two subgroups (n=96). *P25= 25th percentile, **P75=75th percentile.

Marker		Early failure				Long remission				*P*
		P25 (%)	Median (%)	P75 (%)	Range (%)	P25 (%)	Median (%)	P75 (%)	Range (%)	
CD4	whole core	15.2	19.9	26.7	4 - 48.7	14.8	23.4	31.3	5.6 - 53.4	0.12
	interfollicular	17.2	21.8	29.4	3.7 - 49.3	16.9	26.8	34	6.5 - 56.7	0.13
	intrafollicular	10.6	15.6	21.5	3.6 - 47.4	10.9	18.6	28.6	1.3 - 50.8	0.26
CD8	whole core	5.2	7.9	9.5	1.5 - 24.6	7.2	8.6	14	3.8 - 29.4	0.011
	interfollicular	7	10.4	13.3	1.3 - 22.8	8.8	12.4	16.9	4.2 - 29.8	0.024
	intrafollicular	3.1	4.4	6.6	0.9 - 34.4	3.4	5.1	8.8	1.2 - 29.9	0.12
CD3	whole core	26.9	32.2	38.6	13.9 - 72.9	26.6	32.9	45.4	15.9 - 63.6	0.24
	interfollicular	29.6	35	46.5	11.8 - 71.9	32	39.7	49.4	19 - 63.8	0.42
	intrafollicular	18.3	23.4	28.4	12.9 - 77.5	17.9	23.5	35.4	9.4 - 62.5	0.6
FOXP3	whole core	3.7	6.4	8.6	0.4 - 12.4	4.1	5.8	9.1	1.7 - 21.8	>0.99
PD1	whole core	2.9	5.2	8.7	0.3 - 17.5	3.2	4.9	9.1	0.3 - 18.4	0.9
	interfollicular	1,8	3.3	6.4	0.1 - 18.8	2.4	3.8	7.9	0.3 - 18.3	0.6
	intrafollicular	4,3	7.2	11.6	0.2 - 19.6	4.5	7.5	11.7	0.2 - 20.8	0.7
CD68	whole core	3.9	5.8	7.1	2.4 - 14.2	4.5	5.8	7.8	2.8 - 13.7	0.5
	interfollicular	4.4	6.8	8.8	2.5 - 16.7	5.4	6.4	8.6	2.8 - 13.4	0.9
	intrafollicular	3.2	4.4	6.1	1.9 - 14	3.4	4.7	6.7	2.0 - 15	0.37
CD163	whole core	1.4	3.6	5.5	0.2 - 34.7	2.3	5.2	10.1	0.1 - 39.4	0.038
	interfollicular	1.7	4.2	7.9	0.4 - 36.2	3.3	7.4	15.5	0.1 - 39.4	0.031
	intrafollicular	0.8	1.7	2.8	0.1 - 30.8	1.3	1.9	4.7	0.1 - 39.7	0.17
P53	whole core	0.1	0.2	0.7	0 - 19.1	0.1	0.2	0.6	0 - 5.6	0.8
	interfollicular	0	0.2	0.5	0 - 12.6	0.1	0.2	0.5	0 - 3.7	0.8
	intrafollicular	0.1	0.3	0.7	0 - 22.1	0.1	0.4	0.8	0 - 7.1	0.5

Table S6. distribution of investigated markers in the whole core, interfollicular and intrafollicular compartment in the two subgroups (n=105). (*this table can be found on the website of Haematologica*).

Table S7. Odds ratio (OR) (95% CI) for a 10% change in the IHC markers from univariate analysis, and multivariate analysis without and with the FLIPI of the whole core (n=96).

	Univariate		**Multivariate without FLIPI**		**Multivariate with FLIPI**	
	OR	**P**	**OR**	**P**	**OR**	**P**
	(95% CI)		**(95% CI)**		**(95% CI)**	
%CD4	1.36	0.13	1.2	*0.6*	1.21	*0.5*
	(0.92 2.06)		(0.7, 2.2)		(0.65, 2.28)	
%CD8	3.86	*0.011*	4.5	*0.041*	3.63	*0.084*
	(1.48, 12.13)		(1.1, 21.2)		(0.89, 17.08)	
%P53	0.15	*0.16*	0.9	*0.27*	0.84	*0.23*
	(0.0, 1.10)		(0.6, 1.1)		(0.57, 1.06)	
%PD1	1.00	*>0.99*	1.0	*>0.99*	1.13	*0.9*
	(0.39, 2.58)		(0.3, 3.3)		(0.32, 4.06)	
%CD163	2.01	*0.042*	1.74	*0.17*	1.69	*0.19*
	(1.11, 4.37)		(0.9, 4.2)		(0.83, 4.17)	
%CD68	1.33	*0.7*	0.8	*0.8*	1.24	*0.8*
	(0.31, 6.09)		(0.1, 5.7)		(0.16, 9.38)	
%FOXP3	1.45	*0.5*	0.9	*0.9*	1.13	*0.9*
	(0.47, 4.85)		(0.2, 4.1)		(0.25, 5.53)	
%CD3	1.30	*0.16*	0.8	*0.37*	0.70	*0.31*
	(0.91, 1.91)		(0.4, 1.4)		(0.34, 1.39)	
FLIPI, high	0.28	*0.005*			0.31	*0.016*
	(0.11, 0.66)				(0.12, 0.79)	

Table S8. OR (95% CI) for a 10% change in the markers from univariate analysis, and multivariate analysis without and with the FLIPI of the interfollicular compartment (n=96).

	Univariate		**Multivariable without FLIPI**		**Multivariable with FLIPI**	
	OR (95% CI)	***p***	**OR (95% CI)**	***p***	**OR (95% CI)**	***p***
%CD4	1.33 (0.91, 1.99)	0.14	1.37 (0.80, 2.4)	0.26	1.34 (0.77, 2.41)	0.30
%CD8	2.59 (1.16, 6.36)	0.03	3.72 (1.18, 13.52)	< 0.01	3.18 (0.98, 11.81)	0,07
%P53	0.08 (0.00, 1.41)	0.19	0.11 (0.00, 2.26)	0.23	0.08 (0.00, 2.09)	0.20
%PD1	1.10 (0.42, 2.95)	0.85	1.24 (0.35, 4.52)	0.74	1.22 (0.32, 4.7)	0.77
%CD163	1.92 (1.14, 3.63)	0.03	1.67 (0.92, 3.4)	0.12	1.59 (0.85, 3.31)	0.17
%CD68	0.81 (0.23, 2.92)	0.75	0.50 (0.09, 2.56)	0.41	0.68 (0.11, 3.78)	0.66
%CD3	1.15 (0.82, 1.63)	0.42	0.68 (0.37, 1.21)	0.20	0.71 (0.38, 1.27)	0.26
FLIPI, high	0.28 (0.11, 0.66)	< 0.01			0.33 (0.12, 0.83)	< 0.01

Table S9. OR (95% CI) for a 10% change in the markers from univariate analysis, and multivariate analysis without and with the FLIPI of the intrafollicular compartment (n=96).

	Univariate		Multivariable without FLIPI		Multivariable with FLIPI	
	OR (95% CI)	*p*	OR (95% CI)	*p*	OR (95% CI)	*p*
%CD4	1.36 (0.94, 2.04)	0.12	1.58 (0.90, 2.91)	0.12	1.64 (0.91, 3.11)	0.11
%CD8	2.03 (0.91, 5.94)	0.13	2.28 (0.65, 9.46)	0.22	1.98 (0.53, 8.79)	0.33
%P53	0.27 (0.02, 1.16)	0.16	0.24 (0.02, 1.12)	0.14	0.22 (0.01, 1.18)	0.15
%PD1	1.16 (0.53, 2.55)	0.71	1.41 (0.51, 4.09)	0.51	1.58 (0.53, 4.98)	0.42
%CD163	1.54 (0.82, 3.73)	0.24	1.21 (0.58, 3.16)	0.64	1.26 (0.59, 3.34)	0.58
%CD68	1.72 (0.37, 9.15)	0.50	1.43 (0.20, 11.21)	0.73	2.51 (0.31, 22.75)	0.39
%CD3	1.18 (0.84, 1.72)	0.37	0.58 (0.26, 1.23)	0.16	0.55 (0.23, 1.21)	0.15
FLIPI, high	0.28 (0.11, 0.66)	< 0.01			0.26 (0.10, 0.65)	< 0.01

Table S10. FOXP3 perifollicular patterns by cohort based on agreement scores of three independent pathologists

FOXP3 perifollicular pattern	Total n=96	Early failure n=39	Long remission n=57	P
Positive	21 (22%)	10 (26%)	11 (19%)	0.46
Negative	75 (78%)	29 (74%)	46 (81%)	

Table S11. Frequencies and statistics of copy number gains and losses per chromosomal region by subgroup (*this table can be found on the website of Haematologica*).

Table S12. Somatic variants from targeted resequencing (*this table can be found on the website of Haematologica*).

Table S13. Distribution of gene mutation status by subgroup (n=111)

	Total n=111 (%)	Early failure n=47 (%)	Long remission n=64 (%)	OR [95% CI]	*p (unadjusted)*
BCL2					
Mutated	103 (93)	45 (96)	58 (91)	0.43 [0.04 - 2.57]	*0.46*
Unmutated	8 (7)	2 (4)	6 (9)		
KMT2D					
Mutated	80 (72)	35 (74)	45 (70)	0.81 [0.31 - 2.04]	*0.7*
Unmutated	31 (28)	12 (26)	19 (30)		
CREBBP					
Mutated	72 (65)	34 (72)	38 (59)	0.56 [0.23 - 1.35]	*0.17*
Unmutated	39 (35)	13 (28)	26 (41)		
TNFRSF14					
Mutated	33 (30)	13 (28)	20 (31)	1.19 [0.48 - 2.99]	*0.8*
Unmutated	78 (70)	34 (72)	44 (69)		
MEF2B					
Mutated	12 (11)	5 (11)	7 (11)	1.03 [0.26 - 4.42]	*> 0.99*
Unmutated	99 (89)	42 (89)	57 (89)		
EZH2					
Mutated	23 (21)	4 (9)	19 (30)	4.48 [1.34 - 19.59]	*0.008*
Unmutated	88 (79)	43 (91)	45 (70)		
TNFAIP3					
Mutated	9 (8)	2 (4)	7 (11)	2.74 [0.49 - 28.30]	*0.30*
Unmutated	102 (92)	45 (96)	57 (89)		
EP300					
Mutated	7 (6)	2 (4)	5 (8)	1.90 [0.29 - 20.78]	*0.7*
Unmutated	104 (94)	45 (96)	59 (92)		
CARD11					
Mutated	9 (8)	4 (9)	5 (8)	0.91 [0.18 - 4.88]	*> 0.99*
Unmutated	102 (92)	43 (91)	59 (92)		
FAS					
Mutated	4 (4)	4 (9)	0 (0)	0.00 [0.00 - 1.08]	*0.030*
Unmutated	107 (96)	43 (91)	64 (100)		
MYD88					
Mutated	2 (2)	1 (2)	1 (2)	0.73 [0.01 - 58.52]	*> 0.99*
Unmutated	109 (98)	46 (98)	63 (98)		

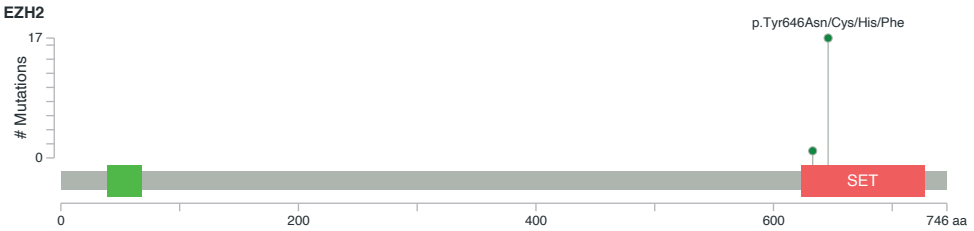

Figure S1. Y646 hotspot in EZH2. All mutations in EZH2. Missense mutations are depicted in green. Mutations are visualized by Mutation Mapper from cBioPortal.

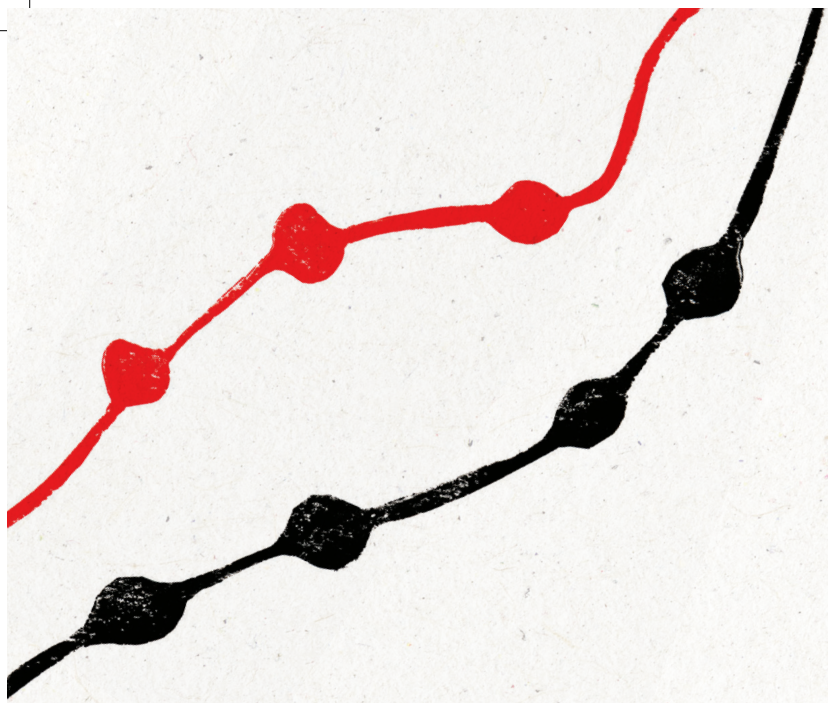

Chapter 7

Aggressive genomic features in clinically indolent primary HHV8-negative effusion-based lymphoma

Matias Mendeville, Margaretha G.M. Roemer, Mari F.C.M. van den Hout, G.Tjitske Los-de Vries, Reno Bladergroen, Phylicia Stathi, Nathalie J. Hijmering, Andreas Rosenwald, Bauke Ylstra, Daphne de Jong

Blood. 2019;133(4):377-380

In rare instances, malignant lymphomas present as a body-cavity based effusion, without an identifiable tumor mass. Most frequently, this concerns primary effusion lymphoma (PEL), a Human Herpes Virus-8 (HHV8)-positive B-cell lymphoma, that typically occurs in Human Immunodeficiency Virus (HIV)-positive patients. PEL has a characteristic phenotype, lacking pan-B-cell markers (CD19, CD20, CD79a), but often positive for activation and plasma cell-related markers (CD30, CD38, CD138) and generally co-infected with Epstein-Barr Virus (EBV). Prognosis is poor with a median overall survival (OS) of 6 months.[1]

Recently, HHV8-negative effusion-based lymphoma (HHV8-negative EBL) has been described that has a very different epidemiology, generally presenting in patients over 70 years of age and outside the HIV-context.[2] The majority of these patients have an underlying condition causing fluid overload, such as chronic heart failure, renal insufficiency or liver cirrhosis. The disease course of HHV8-negative EBL is mild and survival is largely determined by co-morbidity and high age at diagnosis. In contrast to HHV8-positive PEL, HHV8-negative EBL has a complete mature B-cell phenotype and is generally EBV-negative, similar to conventional DLBCL. Therefore, the differential diagnosis with DLBCL may be challenging and largely depends on staging information, excluding the presence of disseminated disease at time of diagnosis.

Thus far, a limited number of HHV8-negative EBL cases have been reported.[2–5] In these documented cases, treatment varied from drainage alone to chemotherapy and stem cell transplantation, with remarkable good outcome in those treated with drainage only. This underpins the importance to distinguish HHV8-negative EBL from secondary effusion of DLBCL, which has a poor prognosis and requires an essentially different therapeutic approach.[6]

Genomic data of a limited number of HHV8-negative EBL has been reported that do not show a consistent or characteristic pattern[2–5], precluding conclusions on their role in oncogenesis. In this study, we aim to delineate the genomic landscape of HHV8-negative EBL using established next-generation sequencing (NGS) procedures.

All cytological aspiration specimens of pleural, pericardial and abdominal effusions with a recorded diagnosis of lymphoma diagnosed between 2000 and 2017 (n=81) were selected from the VU University Medical Center Amsterdam. All secondary lymphoma effusions based on clinical staging information or histological diagnosis were excluded. Complete pathology workup was performed (supplemental Table 1), identifying 10 fully diagnostic cases of HHV8-negative EBL. One additional case was received from the University of Würzburg, Germany. Cell-of-Origin (COO) was determined using the Hans and Tally algorithms.[7]

Genomic DNA was extracted with QIAamp DNA FFPE Tissue and Mini Kits (Qiagen, Hilden, Germany), according to the manufacturers recommendation. NGS library preparation was done using KAPA Library Preparation (KAPA Biosystems, Wilmington MA, USA). Single-read 50bp shallow Whole Genome Sequencing (WGS) for copy number analysis and paired-end 150bp targeted sequencing with SeqCapEZ probes (Roche Nimblegen, Madison WI, USA) for mutation and translocation analysis was performed on a HiSeq 2500 (Illumina, San Diego CA, USA). Sequencing reads were aligned and duplicates removed. Copy number analysis was performed using QDNAseq[8] and LoFreq[9] was used for mutation calling. For translocation detection, BreaKmer, GRIDDS, Wham and novoBreak were used.[10–13] Translocations detected by at least two tools were selected.

All sequence data has been deposited at the European Genome-phenome Archive under accession number EGAS00001002743. For more detailed information see Supplemental Methods.

We studied a series of 11 cases of HHV8-negative EBL with clinicopathological features as listed in Table 1. The mean age of patients at diagnosis was 83 years (range 60-92 years). Six patients presented with pleural effusions causing dyspnea and one as a pericardial effusion causing a cardiac tamponade. Seven patients had a history of chronic heart failure, supporting the concept that chronic fluid overload states are an important pathogenic factor in HHV8-negative EBL. At the time of primary diagnosis, the majority of the patients was diagnosed as DLBCL. However, none of the patients were treated as such, due to comorbidity and/or personal preference because of advanced age. Six patients died of their underlying disease within 7 months, 4 patients survived for 14-99 months (mean: 42 months), of which 3 are still alive. For 1 patient the vital status is unknown. No patient died of lymphoma, underpinning the indolent behavior of HHV8-negative EBL. Of 10 available cases, 9 were classified as nonGCB and 1 as GCB.

For 8/11 cases, genomic profiles were derived using shallow WGS and targeted sequencing (supplemental Figure 1). We observed a high number of mutations, including characteristic patterns of somatic hypermutation (*PIM1*, *BCL2*, *KLHL14*)[14] in 4/8 cases, indicating a (post-) germinal center character (Figure 1). The most recurrent mutations were found in *HIST1H1E* and *MYD88*. Of the 4 *MYD88* mutations, 3 affected *MYD88*^{L265P} and co-mutation with *CD79B* was found in one case. These aberrations are typically found in ABC-type DLBCLs, and enriched in extranodal (testis, CNS) DLBCL.[15] In 6/8 cases, truncating mutations were found in *BTG1* and/or *BTG2*. *IRF4* and *SYNE1* were mutated in 4/8 cases. Other recurrently mutated genes included chromatin modifying genes (e.g. *CREBBP*, *KMT2D*, *MEF2B*), which are more frequently found in GCB-type DLBCLs.[16]

Table 1. Clinicopathological features of 11 HHV8-negative EBL cases.

ID	age	sex	effusion site	treatment	follow-up	vital status	EBER	HHV8	CD20	CD79a	CD138	COO
001	85	M	pericardium	aspiration	4	DOOC	-	-	+	-	-	nonGCB
002	77	F	pleural	aspiration	14	alive, NED	-	-	+	+	-	nonGCB
003	86	F	pleural	aspiration, pleuradesis	39	alive, NED	-	-	+	+	-	nonGCB
004	83	F	pleural	R-chlorambucil	99	alive, NED	-	-	+	+	-	nonGCB
005	91	F	pleural	aspiration	1	DOOC	-	-	-	-	+	nonGCB
006	75	F	pleural	no treatment	16	DOOC, NED	-	-	+	+	-	GCB
007	92	M	pleural	aspiration	1	DOOC	-	-	+	+	-	nonGCB
008	60	F	pleural	aspiration	4	not known	-	-	+	+	-	nonGCB
009	88	M	pleural	aspiration	1	DOOC	-	-	+	+	-	nonGCB
010	85	F	pleural	chlorambucil, prednisone	3	DOOC	-	-	+	nd	nd	nd
011	88	M	pleural	no treatment	7	DOOC	-	-	+	-	-	nonGCB

DOOC: died of other causes; NED: no evidence of disease. EBER: Epstein-Barr virus (EBV)-encoded small RNA; HHV-8: human herpesvirus-8; nd: not determined; COO: Cell-of-origin.

HHV8-negative EBL showed an overall complex copy number landscape with a mean of 33.6 copy number aberrations (CNAs) per case (range: 6-133, stdev: 34.7). This number of CNAs is similar to that reported for conventional DLBCL.[17] Large CNAs that occurred in at least 2/8 cases included gains of chromosomes 1q, 2q, 7, 8q, 10p, 12q, 13q and 18q, and losses of chromosomes 6q and 15p (Figure 1; supplemental Figure 2; supplemental Table 2). These findings are in line with classical karyotyping and comparative genomic analysis in the reported HHV8-negative EBL cases.[2–5]

The copy number landscape of HHV8-negative EBL showed a remarkable enrichment of focal CNAs. Specifically, focal deletions at 3p14.2 and 6q21 were present in 6/8 cases (supplemental Figure 2; supplemental Table 3). Both loci were heterozygously deleted in 5 cases, and homozygously deleted in 1 case. Focal deletion of chromosome 6q21 has not been described for HHV8-positive PEL, but is observed in DLBCL, albeit at relatively lower frequency (57/304 [19%])[15]. The 6q21 locus contains *PRDM1*/*Blimp-1*, a master regulator of plasma cell differentiation.[18] Furthermore, *PRDM1* was mutated in 2 cases that had a heterozygous deletion of 6q21, resulting in bi-allelic inactivation of *PRDM1* in 3/8 cases (Figure 1; supplemental Figure 1). The 3p14.2 focal deletion has been described in a subset of DLBCLs (7/57 [12%])[19], but it occurred at a significantly higher frequency in HHV8-negative EBL (6/8 [75%], p=0.0005). In HHV8-positive PEL, a similar frequency (85%) of *FHIT* deletions is reported.[20] *FHIT* is involved in maintaining genome stability, and disruption may lead to an accumulation of genomic damage. [21]

The most frequent translocations were observed at the *MYC*, *BCL2* and *BCL6* loci. The presence of these translocations has been previously described in a subset of HHV8-negative EBL.[2–5] We demonstrated the involvement of non-Ig translocation partners in addition to Ig translocation partners. Furthermore, previously undescribed translocations involving *TP63, EXOC2* and *KMT2D* were identified (supplemental Figure 1).

Analogous to findings in other clinically indolent B-cell lymphomas, we expected HHV8-negative EBL to have a relatively simple genomic landscape with low levels of mutations and CNAs.[22] However, we observed that HHV8-negative EBL is characterized by a complex genomic landscape with frequent mutations, copy number aberrations and translocations, often found in aggressive ABC- and GCB-type DLBCL and PEL. Despite an abundance of known adverse prognostic features in HHV8-negative EBL, such as *MYC* translocations, the clinical course is remarkably indolent. The non-aggressive behavior of these tumor cells may be caused by the micro/macro-environment in the primary anatomical localization, restraining progression.[23] For daily practice, clinicopathologic correlation, excluding the presence of disseminated disease, remains essential.

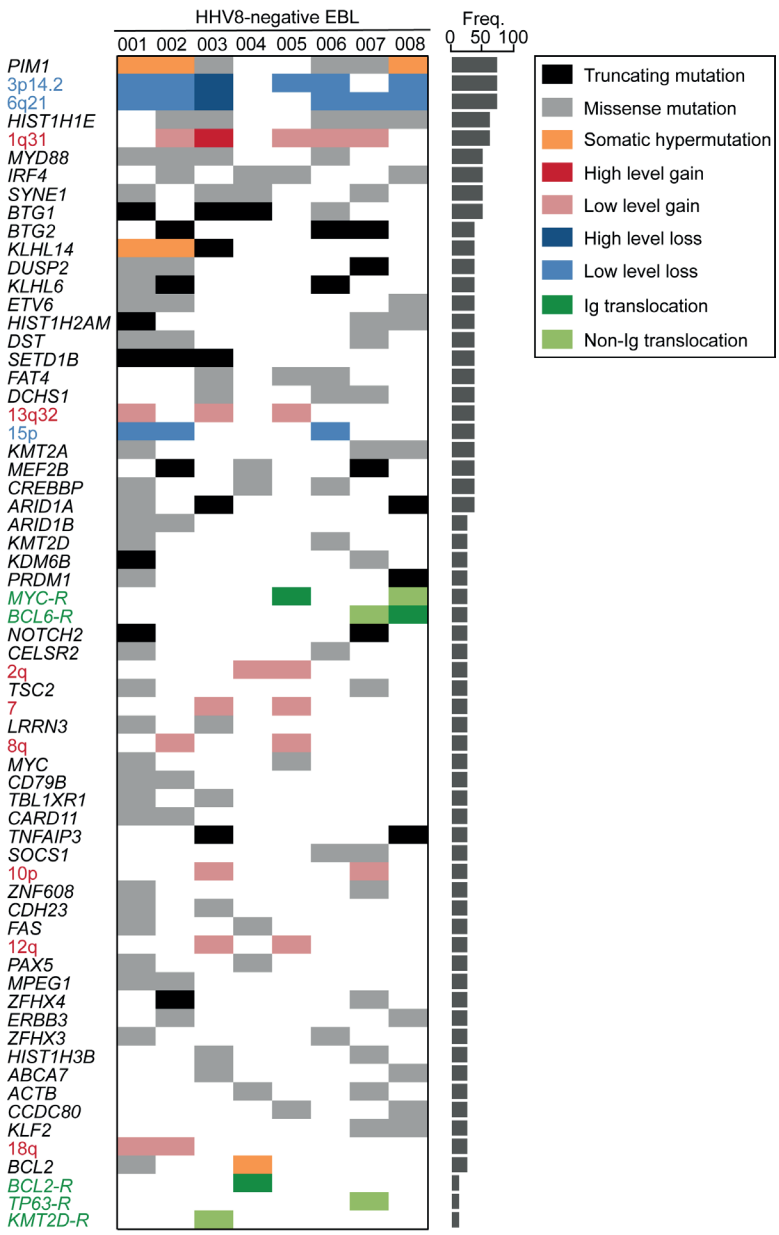

Figure 1. Distribution of genomic aberrations in HHV8-negative EBL. Each column represents an individual case (HHV8-negative EBL 001-008). Rows depict genomic aberrations, including mutations, copy number aberrations and translocations. The bar graph on the right shows the percentage of each aberration in the full cohort. Variant categories include missense mutations (grey), truncating mutations (black), low level copy number gains (red), high level copy number gains (dark red), low level copy number losses (blue), high level copy number losses (dark blue), translocations with Ig partners (dark green) and translocations with non-Ig partners (light green).

Acknowledgments

The authors would like to thank Paul P. Eijk (Department of Pathology, Amsterdam UMC, Location VUmc, Amsterdam) for providing administrative and material support and Daoud Sie PhD (Clinical Genetics, Amsterdam UMC, Location VUmc, Amsterdam), for providing genomics and computational infrastructure. This work was supported by the Dutch Cancer Society (Grant No. KWF 2015-7925 and KWF 2012-5711).

Authorship contributions

M.M. designed and performed the research, analyzed and interpreted the data, and wrote the paper. M.G.M.R. analyzed and interpreted the data, and wrote the paper. M.F.C.M.H. designed and performed the research, analyzed and interpreted the data. G.T.LdV. performed research, analyzed and interpreted the data. R.B, P.S., N.J.H. performed research. A.R. provided samples and reviewed the manuscript. B.Y., D.D.J., designed the research, analyzed and interpreted the data, and wrote the paper.

Conflict-of-interest disclosure: All authors declare no competing financial interests.

References

1. Simonelli C, Spina M, Cinelli R, et al. Clinical features and outcome of primary effusion lymphoma in HIV-infected patients: a single-institution study. *J. Clin. Oncol.* 2003;21(21):3948–3954.
2. Alexanian S, Said J, Lones M, Pullarkat ST. KSHV/HHV8-negative effusion-based lymphoma, a distinct entity associated with fluid overload states. *Am. J. Surg. Pathol.* 2013;37(2):241–249.
3. Wu W, Youm W, Rezk SA, Zhao X. Human herpesvirus 8-unrelated primary effusion lymphoma-like lymphoma report of a rare case and review of 54 cases in the literature. *Am. J. Clin. Pathol.* 2013;140(2):258–273.
4. Xiao J, Selvaggi SM, Leith CP, Fitzgerald SA, Stewart J. Kaposi sarcoma herpesvirus/human herpesvirus-8-negative effusion-based lymphoma: Report of 3 cases and review of the literature. *Cancer Cytopathol.* 2013;121(11):661–669.
5. Zaimoku Y, Takahashi W, Iwaki N, et al. Human herpesvirus-8-unrelated primary effusion lymphoma of the elderly not associated with an increased serum lactate dehydrogenase level: A benign sub-group of effusion lymphoma without chemotherapy. *Leuk. Lymphoma*. 2016;57(7):1625–1632.
6. Chen Y-P, Huang H-Y, Lin K-P, et al. Malignant effusions correlate with poorer prognosis in patients with diffuse large B-cell lymphoma. *Am. J. Clin. Pathol.* 2015;143(5):707–715.
7. Coutinho R, Clear AJ, Owen A, et al. Poor concordance among nine immunohistochemistry classifiers of cell-of-origin for diffuse large b-cell lymphoma: Implications for therapeutic strategies. *Clin. Cancer Res.* 2013;19(24):6686–6695.
8. Scheinin I, Sie D, Bengtsson H, et al. DNA copy number analysis of fresh and formalin-fixed specimens by shallow whole-genome sequencing with identification and exclusion of problematic regions in the genome assembly. *Genome Res.* 2014;24(12):2022–2032.
9. Wilm A, Aw PPK, Bertrand D, et al. LoFreq: A sequence-quality aware, ultra-sensitive variant caller for uncovering cell-population heterogeneity from high-throughput sequencing datasets. *Nucleic Acids Res.* 2012;40(22):11189–11201.
10. Abo RP, Ducar M, Garcia EP, et al. BreaKmer: detection of structural variation in targeted massively parallel sequencing data using kmers. *Nucleic Acids Res.* 2015;43(3):e19.
11. Cameron DL, Schröder J, Penington JS, et al. GRIDSS: Sensitive and specific genomic rearrangement detection using positional de Bruijn graph assembly. *Genome Res.* 2017;27(12):2050–2060.
12. Kronenberg ZN, Osborne EJ, Cone KR, et al. Wham: Identifying Structural Variants of Biological Consequence. *PLoS Comput. Biol.* 2015;11(12):1–19.
13. Chong Z, Ruan J, Gao M, et al. NovoBreak: Local assembly for breakpoint detection in cancer genomes. *Nat. Methods*. 2016;14(1):65–67.
14. Pasqualucci L, Neumeister P, Goossens T, et al. Hypermutation of multiple proto-oncogenes in B-cell diffuse large-cell lymphomas. *Nature*. 2001;412(6844):341–346.
15. Chapuy B, Stewart C, Dunford A, et al. Molecular subtypes of Diffuse Large B-cell Lymphoma are associated with distinct pathogenic mechanisms and outcomes. *Nat. Med.* 2018;24(5):679–690.
16. Morin RD, Mendez-Lago M, Mungall AJ, et al. Frequent mutation of histone-modifying genes in non-Hodgkin lymphoma. *Nature*. 2011;476(7360):298–303.
17. Monti S, Chapuy B, Takeyama K, et al. Integrative Analysis Reveals an Outcome-Associated and Targetable Pattern of p53 and Cell Cycle Deregulation in Diffuse Large B Cell Lymphoma. *Cancer Cell*. 2012;22(3):359–372.

18. Mandelbaum J, Bhagat G, Tang H, et al. BLIMP1 Is a Tumor Suppressor Gene Frequently Disrupted in Activated B Cell-like Diffuse Large B Cell Lymphoma. *Cancer Cell*. 2010;18(6):568–579.
19. Kameoka Y, Tagawa H, Tsuzuki S, et al. Contig array CGH at 3p14.2 points to the FRA3B/FHIT common fragile region as the target gene in diffuse large B-cell lymphoma. *Oncogene*. 2004;23(56):9148–9154.
20. Roy D, Sin SH, Damania B, Dittmer DP. Tumor suppressor genes FHIT and WWOX are deleted in primary effusion lymphoma (PEL) cell lines. *Blood*. 2011;118(7):32–40.
21. Pekarsky Y, Zanesi N, Palamarchuk A, Huebner K, Croce CM. FHIT: from gene discovery to cancer treatment and prevention. *Lancet. Oncol.* 2002;3(12):748–754.
22. Stevens WBC, Mendeville M, Redd R, et al. Prognostic relevance of CD163 and CD8 combined with EZH2 and gain of chromosome 18 in follicular lymphoma: A study by the Lunenburg Lymphoma Biomarker Consortium. *Haematologica*. 2017;102(8):1413–1423.
23. Bissell MJ, Hines WC. Why don't we get more cancer? A proposed role of the microenvironment in restraining cancer progression. *Nat. Med.* 2011;17(3):320–329.

Supplemental Data

1. Supplemental Methods

2. Supplemental Figures

Supplemental Figure 1 – Circular representation of HHV8-negative EBL genomic profiles
Supplemental Figure 2 – Copy number gains and losses in HHV8-negative EBL

3. Supplemental Tables

Supplemental Table 1. Immunohistochemical stainings of 11 HHV8-negative EBL cases.
Supplemental Table 2 – Large CNAs present in at least 2 of 8 HHV8-negative EBL cases. (provided as separate excel)
Supplemental Table 3 – Focal CNAs present in at least 3 of 8 HHV8-negative EBL cases. (provided as separate excel)

Supplemental Methods

Patients and materials

From the files of the department of Pathology, VU University Medical Center Amsterdam (VUmc), all cytological aspiration specimens of pleural, pericardial and abdominal effusions with a recorded diagnosis of lymphoma of any class diagnosed between 2000 and 2017 (n=81) were selected. First, all secondary lymphoma effusions based on clinical staging information and/or a recorded previous or subsequent histological diagnosis of lymphoma at a lymph node or organ site were excluded. Complete pathology workup for all remaining cases was performed according to standard procedures, including immunohistochemistry (CD20, CD79a, PAX5, CD3, BCL2, BCL6, CD10, CD138, MUM1, CD30, MYC, HHV8), EBER in situ hybridization and immunoglobulin heavy and light chain clonality analysis (BIOMED2), identifying 10 fully diagnostic cases of HHV8-negative EBL. One additional fresh-frozen case was received from the Institute of Pathology, University of Würzburg, Germany. To determine Cell-of-Origin (COO) status, Hans classification was used.[1] On cases that scored as GCB (n=3), additional Tally classification was done using GCET, LMO2 and FOXP1 immunhistochemistry.[2] Pathological revisions excluded 3 out of 11 cases for further genomic profiling due to low tumor cell content, precluding sufficient DNA yield.

DNA isolation and Library preparation

Genomic DNA was extracted from all VUmc tumor biopsies with a QIAamp DNA FFPE Tissue Kit (Qiagen, Hilden, Germany) and quantified using a Qubit 2.0 Fluorometer (Thermo Fisher Scientific, Carlsbad CA, USA). The additional fresh-frozen case was isolated with the QIAamp DNA Mini Kit (Qiagen, Hilden, Germany). For each patient sample, DNA was sheared by ultrasound with a Covaris S2 (Covaris Inc, Woburn MA, USA), with settings adjusted to DNA from FFPE tissue, as previously described.[3] NGS-libraries were prepared with an input of 250ng sheared DNA using KAPA Library Preparation (KAPA Biosystems, Wilmington MA, USA). In short, uniquely 8-bp indexed adapters (IDT, Coralville IA, USA) were ligated to the FFPE-extracted DNA, followed by size selection of fragments in the range of 150 to 400bp.

Shallow whole genome sequencing (WGS) and copy number analysis

For shallow WGS, 125ng of the created NGS-libraries were equimolarly pooled and 12.5pM was loaded on one lane of a HiSeq Single End Flowcell (Illumina, San Diego CA, USA).

Sequencing was performed on a HiSeq 2500 (Illumina, San Diego CA, USA) in a single-read 50-cycle run mode (SR50). Copy number analysis was performed as described previously.[4] Shallow WGS reads were aligned to the human reference genome build GRCh37/hg19[5] with BWA 0.5.9[6]. PCR duplicates were marked with Picard 1.61, and filtered out with SAMtools 0.1.18[7], together with reads with mapping qualities lower than 37. The Bioconductor package QDNAseq 1.5.1[3] was used to divide the genome into nonoverlapping bins of 100kb, followed by correction of GC content and mappability, and filtering of problematic regions and regions of common germ-line copy number variants based on the 1000 Genomes Project[8]. Subsequently, the resulting copy numbers were segmented using DNAcopy[9] and called into five discrete categories (high level gain, low level gain, normal, low level loss, or high level loss) using CGHcall 2.30.0[10]. Segments with more than 2 extra copies were labelled as high level gains, segments with 1 or 2 extra copies were labelled as low level gains. Segments with 1 lost copy were labelled low level loss, and segments with 2 lost copies were labelled as high level loss. Recurrent copy number aberrations (CNAs) were visualised in a frequency plot (supplemental Figure 2). For each focal CNA region, here defined as <15 Mb[11], that occurred in at least 3 of 8 cases (37,5%) all human genes were retrieved from Ensembl v74[5]. Next, the Catalogue of Somatic Mutations (COSMIC v76)[12] was used to annotate these recurrent regions of CNAs with potential oncogenic genes (supplemental Table 2).

Panel design, targeted capture and deep sequencing for mutation and translocation analysis.

To detect mutations and translocations of interest, a custom targeted panel was designed using NimbleGen design software (Roche). The capture panel targets all exons of 369 genes and 12 translocation targets, including genic and intergenic regions (Roche ID 43712). The capture was performed according to NimbleGen EZ SeqCap library protocol (Roche Nimblegen, Madison WI, USA). From all 8 NGS-libraries, 125ng was used to create equimolar pools with a total mass of 1μg DNA. The captured NGS-libraries were sequenced on a HiSeq 2500 (Illumina, San Diego CA, USA) in a paired-end 150bp mode. This resulted in a mean target coverage of 617x. Paired-end 150bp reads were de-multiplexed by Bcl2fastq (Illumina) and adapter sequences trimmed by Seqpurge.[13] Next, paired-end reads were aligned to the human reference genome (GRCh37/hg19) with BWA mem (v0.7.12).[3] Mapped reads were realigned with ABRA (v0.96)[14] and duplicate reads were flagged with picardtools MarkDuplicates (v2.4.1). Mutation calling was performed with LoFreq (v2.3.7).[15] Functional annotation and effect prediction of called variants was performed with SnpEff (v4.1b)[10]. Single nucleotide variants (SNVs) and small indels were

labeled somatic if impact prediction was 'high' or if impact prediction was 'moderate' and the variant single nucleotide variant (SNV) was tagged as 'uncommon' according to the Single Nucleotide Polymorphism database (dbSNP build 142).[8] For translocation detection, four bioinformatic tools were combined including BreaKmer, GRIDDS, Wham and novoBreak.[16–19] Translocations detected by at least two tools were selected for visual confirmation using the Integrative Genome Viewer (IGV).[20]

All downstream analyses were performed in the programming language R (version 3.2.1) with custom scripts.

Data availability

All sequence data has been uploaded to the European Genome-phenome Archive (EGA; accession number EGAS00001002743).

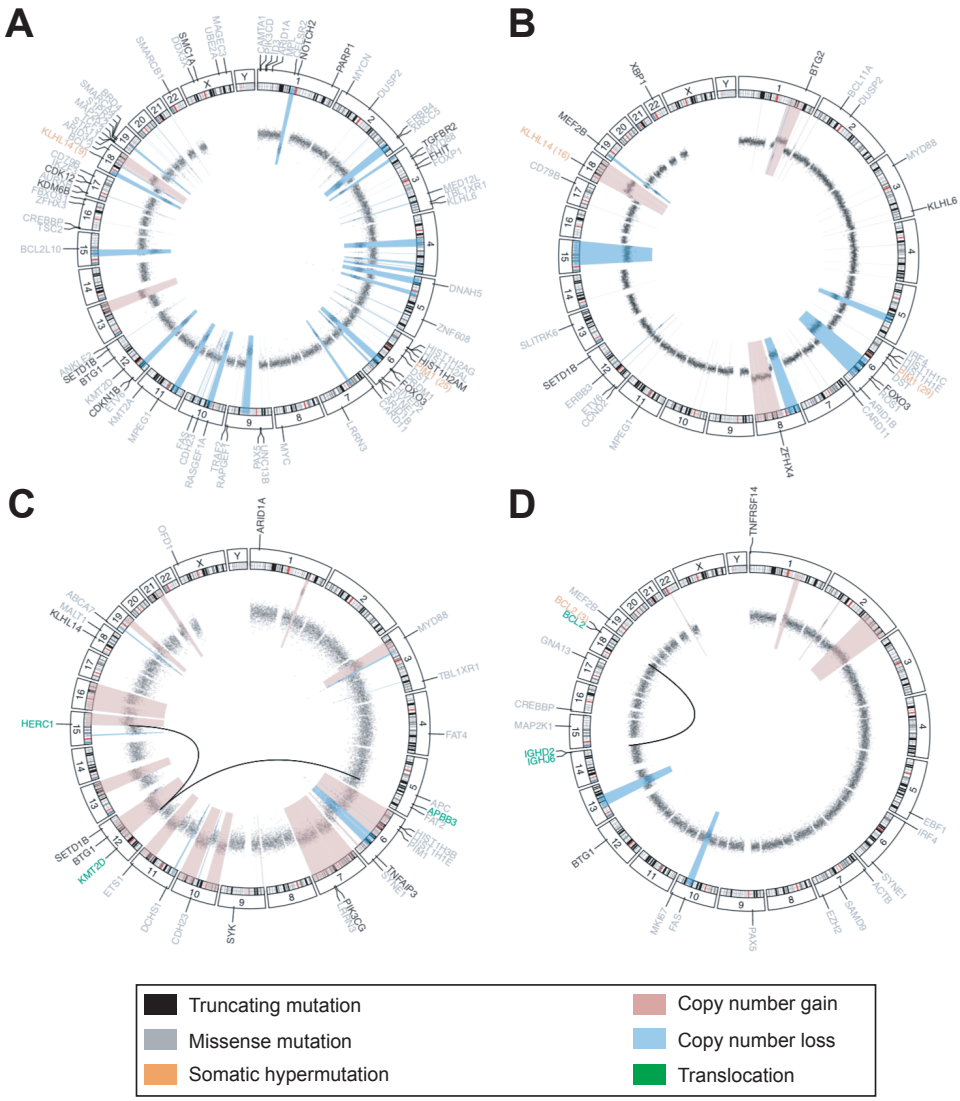
A
B
C
D
Truncating mutation
Missense mutation
Somatic hypermutation
Copy number gain
Copy number loss
Translocation

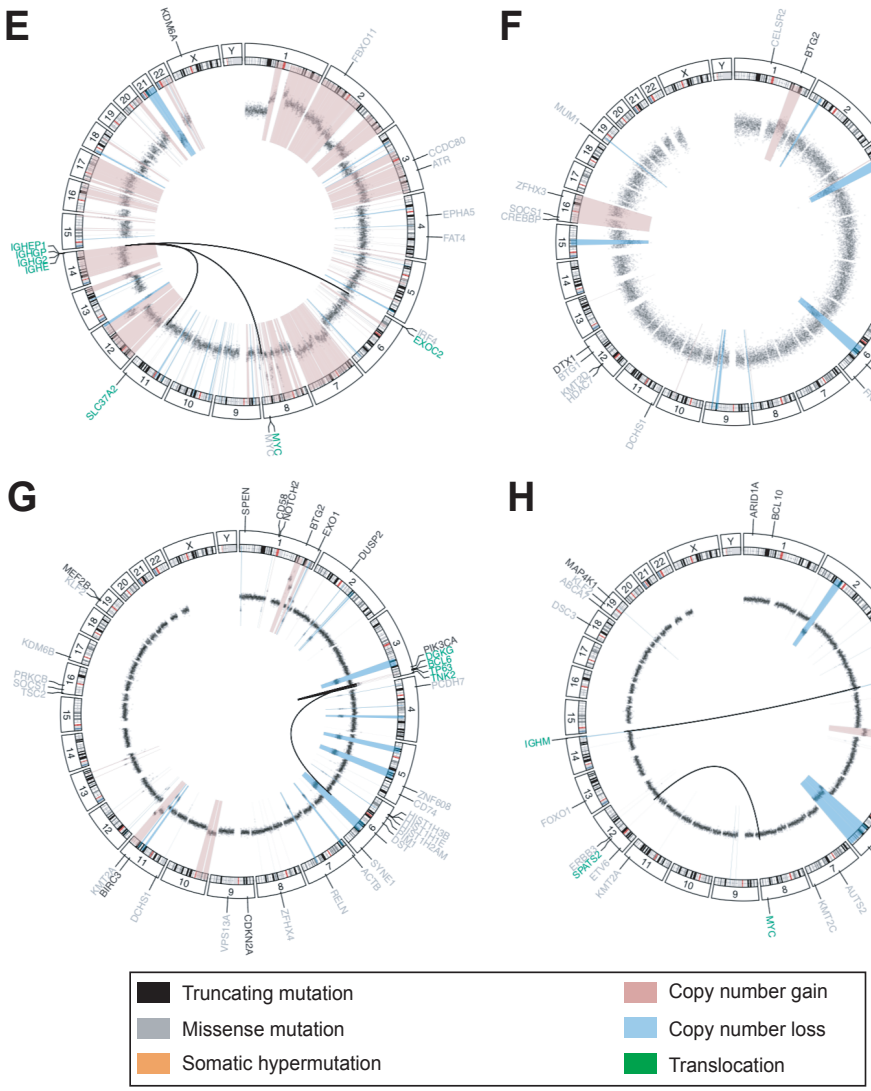

Supplemental Figure 1. Circular representation of HHV8-negative EBL genomic profiles. A) Circular representation of all detected genomic aberrations in HHV8-negative EBL case #1, including regions of copy number gains (light red), regions of copy number losses (light blue), truncating mutations (black), missense mutations (grey), genes targeted by somatic hypermutation (orange; with number of mutations between parantheses) and translocations (green). Black lines connect translocation partners. B) Circular representation of all detected genomic aberrations of in HHV8-negative EBL case #2, details as in A. C) Circular representation of all detected genomic aberrations of in HHV8-negative EBL case #3, details as in A. D) Circular representation of all detected genomic aberrations of in HHV8-negative EBL case #4, details as in A. E) Circular representation of all detected genomic aberrations of in HHV8-negative EBL case #5, details as in A. F) Circular representation of all detected genomic aberrations of in HHV8-negative EBL case #6, details as in A. G) Circular representation of all detected genomic aberrations of in HHV8-negative EBL case #7, details as in A. H) Circular representation of all detected genomic aberrations of in HHV8-negative EBL case #8, details as in A.

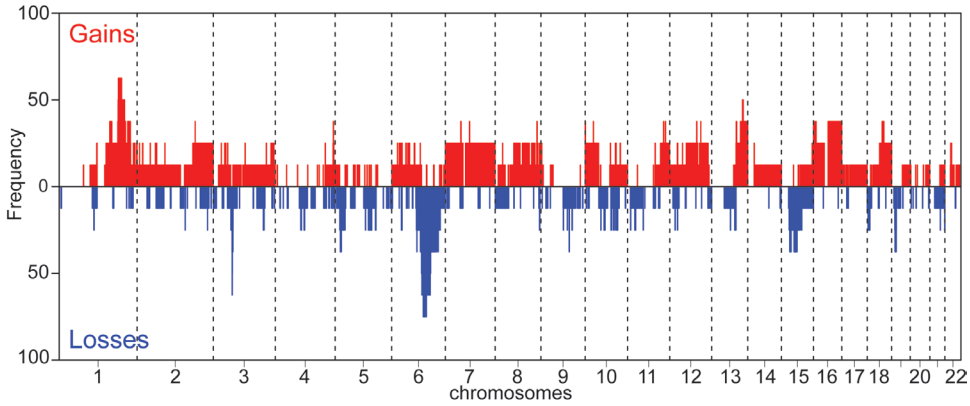

Supplemental Figure 2. Copy number gains and losses in HHV8-negative EBL. Distribution and percentage of copy number gains (red) and losses (blue) in 8 HHV8-negative EBL cases. X-axis: chromosomal regions, ordered by genomic coordinates of chromosomes 1 to 22. Y-axis: percentage of cases showing CNAs. Vertical dotted lines: boundaries between chromosomes.

Supplemental Tables

Supplemental Table 1. Immunohistochemical stainings of 11 HHV8-negative EBL cases.

ID	EBER	HHV8	CD20	CD79a	CD138	CD10	BCL6	MUM1	GCET	LMO2	FOXP1	BCL2	MYC-IHC	CD30
001	-	-	+	-	-	-	-	nd	nd	nd	nd	weak	20%	-
002	-	-	+	+	-	+	+	+	-	-	+	+	<10%	weak
003	-	-	+	+	-	+	+	+	-	-	+	+	25%	-
004	-	-	+	+	-	-	-	-	nd	nd	nd	weak	-	-
005	-	-	-	-	+	-	+	+	nd	nd	nd	-	60%	-
006	-	-	+	+	-	-	+	-	+	+	+	-	<10%	-
007	-	-	+	+	-	-	-	+	nd	nd	nd	-	-	weak
008	-	-	+	+	-	-	+	+	nd	nd	nd	+	70%	nd
009	-	-	+	+	-	-	+	+	nd	nd	nd	weak	<10%	-
010	-	-	+	nd	nd	nd	nd	nd	nd	nd	nd	nd	nd	nd
011	-	-	+	-	-	-	-	+	nd	nd	nd	-	-	-

Supplemental References

1. Hans CP, Weisenburger DD, Greiner TC, et al. Confirmation of the molecular classification of diffuse large B-cell lymphoma by immunohistochemistry using a tissue microarray. 2017;103(1):275–283.
2. Meyer PN, Fu K, Greiner TC, et al. Immunohistochemical methods for predicting cell of origin and survival in patients with diffuse large B-cell lymphoma treated with rituximab. *J. Clin. Oncol.* 2011;29(2):200–207.
3. Scheinin I, Sie D, Bengtsson H, et al. DNA copy number analysis of fresh and formalin-fixed specimens by shallow whole-genome sequencing with identification and exclusion of problematic regions in the genome assembly. *Genome Res.* 2014;24(12):2022–2032.
4. Stevens WBC, Mendeville M, Redd R, et al. Prognostic relevance of CD163 and CD8 combined with EZH2 and gain of chromosome 18 in follicular lymphoma: A study by the Lunenburg Lymphoma Biomarker Consortium. *Haematologica*. 2017;102(8):1413–1423.
5. Flicek P, Ahmed I, Amode MR, et al. Ensembl 2013. *Nucleic Acids Res.* 2013;41(D1):.
6. Li H, Durbin R. Fast and accurate short read alignment with Burrows – Wheeler transform. *Bioinformatics*. 2009;25(14):1754–1760.
7. Li H, Handsaker B, Wysoker A, et al. The Sequence Alignment / Map (SAM) Format and SAMtools 1000 Genome Project Data Processing Subgroup. *Bioinformatics*. 2009;25(16):1–2.
8. 1000 Genomes Project Consortium T 1000 GP, Abecasis GR, Auton A, et al. An integrated map of genetic variation from 1,092 human genomes. *Nature*. 2012;491(7422):56–65.
9. Venkatraman ES, Olshen AB. A faster circular binary segmentation algorithm for the analysis of array CGH data. *Bioinformatics*. 2007;23(6):657–663.
10. van de Wiel MA, Kim KI, Vosse SJ, et al. CGHcall: Calling aberrations for array CGH tumor profiles. *Bioinformatics*. 2007;23(7):892–894.
11. Krijgsman O, Carvalho B, Meijer G a., Steenbergen RDM, Ylstra B. Focal chromosomal copy number aberrations in cancer-Needles in a genome haystack. *Biochim. Biophys. Acta - Mol. Cell Res.* 2014;1843(11):2698–2704.
12. Forbes SA, Bhamra G, Bamford S, et al. The catalogue of somatic mutations in cancer (COSMIC). *Curr. Protoc. Hum. Genet.* 2008;(SUPPL. 57):
13. Sturm M, Schroeder C, Bauer P. SeqPurge: Highly-sensitive adapter trimming for paired-end NGS data. *BMC Bioinformatics*. 2016;17(1):.
14. Mose LE, Wilkerson MD, Neil Hayes D, Perou CM, Parker JS. ABRA: Improved coding indel detection via assembly-based realignment. *Bioinformatics*. 2014;30(19):2813–2815.
15. Wilm A, Aw PPK, Bertrand D, et al. LoFreq: A sequence-quality aware, ultra-sensitive variant caller for uncovering cell-population heterogeneity from high-throughput sequencing datasets. *Nucleic Acids Res.* 2012;40(22):11189–11201.
16. Abo RP, Ducar M, Garcia EP, et al. BreaKmer: detection of structural variation in targeted massively parallel sequencing data using kmers. *Nucleic Acids Res.* 2015;43(3):e19.
17. Cameron DL, Schröder J, Penington JS, et al. GRIDSS: Sensitive and specific genomic rearrangement detection using positional de Bruijn graph assembly. *Genome Res.* 2017;27(12):2050–2060.
18. Kronenberg ZN, Osborne EJ, Cone KR, et al. Wham: Identifying Structural Variants of Biological Consequence. *PLoS Comput. Biol.* 2015;11(12):1–19.

19. Chong Z, Ruan J, Gao M, et al. NovoBreak: Local assembly for breakpoint detection in cancer genomes. *Nat. Methods*. 2016;14(1):65–67.
20. Thorvaldsdóttir H, Robinson JT, Mesirov JP. Integrative Genomics Viewer (IGV): High-performance genomics data visualization and exploration. *Brief. Bioinform.* 2013;14(2):178–192.

Chapter 8

Summary and Discussion

Summary

In **Chapter 1**, the field of translational oncology in general is introduced, with a focus on computational approaches to study molecular alterations in non-Hodgkin lymphoma. This chapter concludes with a description of the aims of this thesis.

Chapter 2 reviews the current state of the art of molecular subtyping of DLBCL and investigates potential avenues for harmonization of the presently available molecular subtypes. To this end, we examine how consensus molecular classifications have been established in other malignancies, such as breast, central nervous system and colorectal tumors. This chapter concludes with proposed suggestions for laboratory infrastructure required for successful clinical implementation.

Chapter 3 evaluates the two recently proposed DNA-based classifications for DLBCL from a computational perspective and thereby takes the questions lead out in chapter 2 one step further. We show that irrespective of the computational methods 70% of DLBCL can be robustly assigned to one of the 5 DLBCL clusters, while the other 30% have not sufficient specific characteristics to be consistently assigned to a subtype, indicative of underlying heterogeneous biology of the disease as a cause. In this opinion paper, we argue why a consensus approach is required in order to develop a molecular DLBCL classification to meaningfully evaluate new treatment modalities for DLBCL and examine the computational challenges that will be encountered in that process.

In **Chapter 4**, we perform extensive genomic profiling on 2 large cohorts of DLBCL patients to recapitulate the novel molecular subtyping systems described in **Chapter 2** and **3**. The aim of this retrospective study is to explore if molecular subtyping has added value for outcome prediction of DLBCL patients by integration with the established outcome prediction parameters International Prognostic Index (IPI) and disease activity monitoring by PET/CT during and after conclusion of standard treatment. We identify a group of patients with a particular DNA subtype (C5/MCD), which have an unfavorable prognosis and moreover in which complete metabolic response as demonstrated by a negative PET/CT scan is not sufficiently predictive of favorable outcome to standard immunochemotherapy in contrast to the other molecular subtypes. These findings, which we validate in 2 independent DLBCL cohorts, demonstrate that risk stratification of DLBCL patients is improved through integration of upfront molecular profiling and PET/CT imaging as disease monitor during and at end of treatment. Moreover, this data supports the notion that current treatment protocols are insufficient for C5/MCD patients and that these patients therefore may be eligible for additional treatment even after apparently reaching complete remission as concluded from a negative PET/CT scan.

In **Chapter 5** we have developed a computational approach for estimation of absolute copy numbers from shallow whole-genome sequencing data which method we called "ACE". This bioinformatic tool, which is made available as a R-package in Bioconductor and Github, scales relative copy number signals from chromosomal segments to optimally fit absolute copy numbers, without the need for additional genetic information. In doing so, ACE provides an accurate estimate of tumor purity and ploidy, which can help to improve interpretation of somatic mutations from bulk tumor tissue. ACE was also used as a quality control in **Chapter 4,** samples that had less than 20% tumor cell content based on ACE and variant allele frequencies of mutations below 10% were excluded.

Chapter 6 is a study on prognostic biomarkers in biopsy specimens from patients with Follicular Lymphoma (FL), an incurable and indolent form of non-Hodgkin lymphoma characterized by multiple relapses with variable remission rates. Through investigation of microenvironment-related markers with immunohistochemistry and tumor cell-related markers with shallow-WGS and a small gene panel, we identify four genomic features related to *early failure* (i.e., progression of lymphoma-related death < 2 years) in FL patients treated with standard immunochemotherapy: EZH2 wild-type, gain of chromosome 18 and low percentages of CD8+ cells and CD163+ areas.

In **Chapter 7**, we perform genomic profiling of 8 cases of HHV8-negative EBL Human herpesvirus 8-negative effusion-based lymphoma (HHV8-negative EBL), a rare and distinct B-cell non-Hodgkin lymphoma (B-NHL) entity related to fluid overload states generally caused by underlying medical conditions. HHV8-negative EBL follows a mild clinical course but is easily misdiagnosed due to a phenotypical resemblance as secondary diffuse large B-cell lymphoma (DLBCL), which follows a more aggressive clinical course, underpinning the importance to differentiate between the two entities. Analogous to other indolent B-cell lymphomas we expected a relatively simple genomic landscape, with low levels of genetic alterations. However, we observed high levels genomic features that are commonly found in more aggressive B-cell lymphomas, like *MYC* translocations and *MYD88* mutations. These seemingly contradictory results in terms of tumor behavior underpin that B-NHL aggressiveness is thus an interplay with the micro/macroenvironment in the primary anatomical localization, which somehow restrains progression for HHV8-negative EBL. Our findings assisted to genetically characterize a distinct lymphoma entity, which is recently included in the 5th edition of the WHO Classification of Haematolymphoid Tumors, under a new name: *fluid-overload associated large B-cell lymphoma* (Alaggio et al. 2022).

Discussion

Challenges in using clinical tumor tissue material for genomics

Formalin-fixation and paraffin-embedding (FFPE) is the worldwide standard of tissue processing for diagnostic pathology. Pathology archives that date decades back provide a wealth of material for translational research and clinico-pathological studies. However, technologies are not always easily and readily applicable to FFPE biopsy material as has been the case for immunohistochemistry in the early 1990s, fluorescent in situ hybridization and techniques such as Southern blotting in the late 1990s and gene-expression profiling in the early 2000s. This is no different for the current NGS technologies for cancer genome studies; FFPE biopsy material has its challenges associated with suboptimal DNA quality and related artifacts, as pointed out in **Chapter 1**. Alternative forms of tissue processing that may provide higher quality DNA for molecular studies may have been regularly discussed but can only be an alternative in very specific settings of (clinical) research.

This thesis shows that the technical difficulties related to FFPE tissue samples can mostly be overcome for targeted NGS experiments that interrogate the cancer genome. Chapters 6 and 7 show that extensive targeted sequencing assays are feasible on FFPE-derived DNA to test all main types of clinically relevant genomic alterations in non-Hodgkin lymphomas. In Chapter 4, an even more comprehensive sequencing yet still targeted assay, whole-exome sequencing, was successfully applied on FFPE samples from a large cohort of DLBCL patients, with only 8% (n=19/235) of cases excluded because of insufficient material for NGS and 5% (n=12/235) due to low tumor purity (<20%). In addition, it has been reported that even WGS, the most extensive NGS application, is technically feasible to FFPE specimens, with 98% of clinically actionable variants detected despite a considerable level of persistent artefacts (Robbe et al. 2018). These developments show that most challenges for the use of FFPE material in diagnostic NGS DNA-based assays for daily practice may be solved at a sufficient level. It should be noted that FFPE is not the only source of artefacts in sequencing data. Other laboratory procedures, such as the deliberate fragmentation of DNA as part of a sequencing library preparation, can also introduce artifacts albeit to a lesser extent, even when applied to FF material (Tanaka et al. 2020). Therefore, rigorous QC steps will always remain pivotal at any step of NGS data processing, irrespective of the source.

Also from a research point of view, FFPE may now arguably be preferred over FF tissue to determine DNA mutations, translocations and CNA, since tumor cell enrichment can

readily be performed (van Essen and Ylstra 2012) such that the background normal DNA fraction gets eliminated. However, for WGS, FF tissue is still the preferred source of DNA, to allow biomarker discovery and to unravel oncogenetic mechanisms. In an ideal scenario and especially where WGS testing is preferred, effort should still be put in building biobanks to optimally fulfill various needs in parallel: intact histo-morphology for detailed architectural and cellular histopathological examination, DNA/RNA quality for the optimal molecular diagnostics and viable cell suspensions for functional studies. Thereby, multiple biopsies may be needed and separately stored. A recent prospective study has shown that such protocols can be successfully implemented in a clinical setting e.g. in a study in which 1200 patients with metastatic cancer were successfully subjected to both forms of tissue processing techniques (Samsom et al. 2022). The additional costs associated with processing and storing both FFPE and FF tissue are dwarfed by the average cost of care for a patient requiring systemic cancer treatment, which in the Netherlands is estimated to be at least 50-100k euro per patient. It is precisely these patients who arguably benefit most from the most advanced molecular diagnostic techniques, such as WGS, which substantiates the need for FF preserved biopsy material and possibly for viable cell suspension biobanking.

Clinical implementation of NGS applications

Translational cancer genomics has the potential to become more routinely available in the clinic, since prices are expected to drop further and even down to $100 per genome in the near future due to more efficient technology and increasing market competition, challenging the existing major player in the field (Almogy et al. 2022).

NGS assays with smaller targeted gene panels of several 10's to 100s of genes have shown to be able to effectively determine genetic alterations on clinical tumor material, including FFPE tissue samples, as shown in **Chapters 4, 6 and 7**. These are currently still most cost-effective and proven to be clinically implementable. In rare instances, it may suffice to screen only for few specific biomarkers that are directly associated with response to specific treatment compounds. However, the molecular basis of cancer is generally much more complex. Extensive and detailed large-scale sequencing efforts that go beyond the analysis of individual mutations, CNAs and translocations are more generally needed to provide meaningful information (Degasperi et al. 2022). Currently, the level of knowledge in malignant lymphoma is relatively disappointing though, and more in-depth knowledge on oncogenesis of large patient populations is needed.

WGS plays an important role in this, by comprehensively analyzing all possible alterations in the DNA, including mutational load, mutational signatures, microsatellite instability, homologous recombination deficiency, viral integration and germline mutations that confer cancer susceptibility (Berger and Mardis 2018). WGS is arguably not required to inform treatment decisions of the majority of current cancer patients, in which situation an NGS panel approach for currently actionable targets would suffice. However, it contributes to the development of knowledge on the long-term, thereby potentially improving disease management of future patients. For this purpose, a self-learning care system is currently implemented in the Netherlands by the Hartwig Medical Foundation (HMF), a non-profit organization that performs WGS in collaboration with Dutch hospitals. A recent study that deployed HMF's infrastructure demonstrated the feasibility, validity, and value of WGS in routine clinical practice by comparing WGS to standard of care (SOC) diagnostics (i.e. SOC assay of choice depended on tumor type) in this specialized referral center on 1200 patients with metastatic cancer (Samsom et al. 2022). In 70% of cases WGS was successfully performed, with low tumor purity (<20%) as the main reason for failure. The performance of WGS compared to SOC in terms of detected biomarkers was similar (both >99% of the in total 896 biomarkers found in regions covered by both tests). Importantly, with an average turnaround time of 11 days, WGS was demonstrated to be feasible within a clinically relevant timeframe.

Besides reduced costs and technical feasibility, the incentives for clinical implementation of NGS applications increase, as the clinical consequences of broad genomic characterization becomes more apparent. Gradually, molecular diagnostics are adopted into the WHO guidelines for tumor classifications. The classification for Central Nervous System tumors (Louis et al. 2021), soft tissue sarcomas (Sbaraglia, Bellan, and Dei Tos 2021) and various pediatric tumors (Pfister et al. 2022) are at the forefront, while hemato-lymphoid cancers lag behind (Alaggio et al. 2022). This is a direct consequence of the lack of knowledge that precludes meaningful dissection of molecularly-based tumor types as well as the lack of predictive marker-treatment combinations. In patients with a metastasis of which the primary cancer is of unknown origin, extensive genetic characterization by NGS has shown its added value both for diagnostic purposes as for identification of actionable targets. A recent study has demonstrated that in 75% of the 62 studied cancers with unknown primary, WGS enabled identification of the primary tissue from which the tumor originated, which led to indications for actionable treatment in half of the patients (Jiao et al. 2020). Targeted treatment in oncology both within and outside clinical trials are increasingly informed by tumor molecular characteristics and growing reference databases of genetically actionable targets and their related compounds/drugs

(Chakravarty et al. 2017). This is exemplified by a study in which WGS was applied to 2520 tumors from patients with metastatic cancer, in which actionable genetic alterations were identified in 62% of patients for which approved therapies or clinical trials are available (Priestley et al. 2019).

Novel insights into the pathology of non-Hodgkin lymphoma

Non-Hodgkin lymphoma encompasses many different entities with a clinical behavior ranging from very indolent to highly aggressive. Diffuse large B-cell lymphoma, not otherwise specified (DLBCL NOS) is not only the most frequent entity in adults, but in respect to molecular classification possibly the most challenging. The 5 molecular classes described by Chapuy and colleagues and the 7 classes described by Wright and colleagues largely overlap, but differ in various essential parameters to preclude sufficient consensus on definitions of classes and driver genes. Thereby, NGS-based classification shows its potential, but is still far away from implementation as discussed in **Chapter 2** and **3**, in which a strategy towards a consensus classification is given.

An anticipated DNA-based consensus classification may not be the final destination in disentangling the molecular heterogeneity in DLBCL. The observation that currently 30-40% of cases cannot unambiguously be assigned to a single molecular subtype and that this is not a result of computational inadequacy, but of underlying biology, may require further multiparameter refined stratification and even larger cohorts (Mendeville et al. 2022). In addition to the genetic alterations of DLBCL, non-malignant cell types in the DLBCL tumor microenvironment (TME) have also been described to impact the observed molecular heterogeneity in this disease entity (Lenz et al. 2008). In a recent study, a large-scale systemic analysis of the DLBCL TME was performed through integration of deconvoluted bulk transcriptome sequencing data and single-cell RNA sequencing (Steen et al. 2021). The authors identified 5 different transcriptional cell states of malignant B-cells and 12 other different cell types that make up the TME. Together, these malignant cell states and TME-related immune cells form multi-cellular communities, called DLBCL ecosystems, that portray unique associations with clinical outcomes.

Contributions of molecular diagnostics for improved disease management for DLBCL and FL

How do we envision the role of molecular diagnostics to shape the near future of disease management for patients with non-Hodgkin lymphoma? As molecular classification will be expected to mature, also in management of malignant lymphoma, multidisciplinary

Molecular Tumor Boards (MTB) that include experts that can translate molecular findings to clinical indications will find their place as so successfully done in solid oncology (Luchini et al. 2020). **Chapter 4** shows already that integration of genomic subtypes combined with existing clinical risk predictors improves outcome prediction and *vice versa* that currently accepted outcome predictors may be interpreted differently depending on genomic subtypes. More reliable assessment of DLBCL patients provides arguments to support treatment intensification for high-risk patients and treatment de-escalation for low-risk patients. Importantly, since the novel proposed DLBCL subtypes are biologically-driven, they have the potential for precision-based therapy, as exemplified by a recent post-hoc analysis of a randomized phase-III trial. Patients under 60 with MCD-and N1-type DLBCLs showed significantly better outcome, with a 100% 3-year event-free survival (EFS) in both subtypes than patients that received R-CHOP alone (3-year EFS 42.9% and 50%, respectively) (Wilson et al. 2021). Importantly, this study was the first to finally describe a predictive value of molecular subtypes, as acclaimed molecular-stratified clinical trials thus far had failed to show any such impact.

Given the yet unresolved heterogeneous behavior of the disease, the next step would be to investigate to what extent the integration of the current DNA-based classification with other molecular characteristics would be of added value to inform patient management for DLBCL. Evaluation of other layers of molecular characteristics, that go beyond the genomic nucleotide code like epigenetic features, could also be considered. The non-coding genome has also been demonstrated to be largely involved in oncogenesis and thus could provide therapeutic relevance also for DLBCL and FL. For example, a recent study identified hypermutation of super-enhancers that deregulate gene targets that have potential therapeutic relevance in DLBCL (Bal et al. 2022). Furthermore, through the improved understanding of the TME, as discussed earlier, new therapeutic possibilities are identified, with several TME-related targets for immunotherapy shown to have promising results in early clinical studies (Sehn and Salles 2021). With this large range of available treatment modalities for DLBCL and the developments of modern prospective clinical trials (Woodcock and LaVange 2017), there is new hope for effective personalized treatment for the 40% of DLBCL patients that respond badly to standard first-line therapy.

For Follicular lymphoma (FL), an indolent yet still incurable disease, the main clinical challenge is to predict the small group of patients (~20%) that have early progression and short overall survival (Casulo et al. 2015). As shown in **Chapter 6**, specific gene mutations and CNAs can inform prognosis, thereby aiding to identify patients at risk of relapse. Others have described similar strategies for risk stratification, through integration of

clinical risk parameters (FLIPI) with the mutation status of 7 genes (Pastore et al. 2015). However, of the FL patients with progression of disease within 24 months after first-line immunochemotherapy, only 50% are correctly predicted by this clinico-genomic risk model (Jurinovic et al. 2016). This warrants further improvement of risk stratification and validation in larger and homogenously treated FL cohorts. Clinical heterogeneity in FL is partly determined by the interaction with the TME, but to date, an unambiguous TME profile in patients related to (poor) outcome has not been identified. A recent study identified 4 populations of infiltrating T-cells that may be linked to survival (Han et al. 2022). Once independent validated this may provide opportunities for targetable immune checkpoints. Despite the fact that no convincing prognostic molecular-informed model for improved risk stratification in FL patients has yet been described, the various studies have led to a renewed understanding of the pathogenicity of FL, allowing new treatment targets to be devised (e.g., EZH2 inhibitors, BCL2 inhibitors).

Concluding Remarks

What have we achieved of the aims that were defined for this thesis?

Aim 1: To develop a comprehensive assay for simultaneous screening of all three types of genomic alterations using a limited amount of input DNA derived from FFPE biopsy samples without the need of matched normal control DNA, optimized to be implemented in clinical practice for lymphoma diagnostics.

We successfully developed an all-in-one targeted NGS assay for FFPE biopsy material, with a bioinformatics pipeline to detect all genetic alterations relevant for lymphoma. Despite the challenges in the clinical setting, including the frequent lack of matched-normal reference samples and the suboptimal DNA quality of FFPE biopsy material, somatic mutations, copy number aberrations and translocations were identified. Therefore, adaptations were customized to the specific needs of FFPE-derived DNA for wet- and drylab procedures. In addition, a new algorithm was introduced, ACE, that allows for an accurate measure of tumor cell percentage, which in turn has been applied to quality select samples on basis of tumor cell percentage. The various drylab implementations have been converted to pipelines and were publicly made available for reuse.

Aim 2: To improve our understanding of the biological basis of the clinical heterogeneity of DLBCL and FL and thereby enable improved risk stratification for these patients. We intend to achieve this by applying the assays developed under aim 1, to large, selected patient cohorts of DLBCL and FL.

We successfully applied the all-in-one assay for several studies as part of this thesis and for studies of colleagues in the research team (Los-De Vries et al. 2020; Los-de Vries et al. 2022). This has led to improved insights into the molecular basis of these diseases with improved risk stratification, and clues for molecular-informed clinical trial designs and tailored treatment approaches as consequences. Our studies of larger patient populations in DLBCL and in selected patients with uncommon presentations of FL show that the *a priori* recognition of a heterogeneous disease course of patients can be improved by molecular profiling. Moreover, in depth molecular characterization of HHV8-negative effusion-based lymphoma has contributed to a more refined definition of the disease and has found its way into the recent 5th edition of the WHO Classification (Alaggio et al. 2022). There is however still room for improvement to disentangle the underlying complex oncogenesis of malignant lymphoma that may go beyond molecular features and to eventually tailor personalized treatment options accordingly.

References

1. Alaggio, Rita, Catalina Amador, Ioannis Anagnostopoulos, Ayoma D. Attygalle, Iguaracyra Barreto de Oliveira Araujo, Emilio Berti, Govind Bhagat, et al. 2022. "The 5th Edition of the World Health Organization Classification of Haematolymphoid Tumours: Lymphoid Neoplasms." *Leukemia* 36 (7). https://doi.org/10.1038/S41375-022-01620-2.
2. Almogy, Authors Gilad, Mark Pratt, Florian Oberstrass, Linda Lee, Dan Mazur, Nate Beckett, Omer Barad, et al. 2022. "Cost-Efficient Whole Genome-Sequencing Using Novel Mostly Natural Sequencing-by-Synthesis Chemistry and Open Fluidics Platform." *BioRxiv*, August, 1–8. https://doi.org/10.1101/2022.05.29.493900.
3. Bal, Elodie, Rahul Kumar, Mohammad Hadigol, Antony B Holmes, Laura K Hilton, Jui Wan Loh, Kostiantyn Dreval, et al. 2022. "Super-Enhancer Hypermutation Alters Oncogene Expression in B Cell Lymphoma." *Nature* 607 (7920). https://doi.org/10.1038/S41586-022-04906-8.
4. Berger, Michael F., and Elaine R. Mardis. 2018. "The Emerging Clinical Relevance of Genomics in Cancer Medicine." *Nature Reviews. Clinical Oncology* 15 (6): 353–65. https://doi.org/10.1038/S41571-018-0002-6.
5. Casulo, Carla, Michelle Byrtek, Keith L. Dawson, Xiaolei Zhou, Charles M. Farber, Christopher R. Flowers, John D. Hainsworth, et al. 2015. "Early Relapse of Follicular Lymphoma after Rituximab plus Cyclophosphamide, Doxorubicin, Vincristine, and Prednisone Defines Patients at High Risk for Death: An Analysis from the National LymphoCare Study." *Journal of Clinical Oncology* 33 (23): 2516–22. https://doi.org/10.1200/JCO.2014.59.7534.
6. Chakravarty, Debyani, Jianjiong Gao, Sarah Phillips, Ritika Kundra, Hongxin Zhang, Jiaojiao Wang, Julia E. Rudolph, et al. 2017. "OncoKB: A Precision Oncology Knowledge Base." *JCO Precision Oncology* 2017 (1): 1–16. https://doi.org/10.1200/PO.17.00011.
7. Degasperi, Andrea, Xueqing Zou, Tauanne Dias Amarante, Andrea Martinez-Martinez, Gene Ching Chiek Koh, João M.L. Dias, Laura Heskin, et al. 2022. "Substitution Mutational Signatures in Whole-Genome-Sequenced Cancers in the UK Population." *Science* 376 (6591). https://doi.org/https://doi.org/10.1126/science.abl9283.
8. Essen, Hendrik F. Hendrik F van, and Bauke Ylstra. 2012. "High-Resolution Copy Number Profiling by Array CGH Using DNA Isolated from Formalin-Fixed, Paraffin-Embedded Tissues." In *Methods in Molecular Biology*, edited by Lars Feuk, 838:329–41. New York, NY: Springer New York. https://doi.org/10.1007/978-1-61779-507-7_16.
9. Han, Guangchun, Qing Deng, Mario L Marques-Piubelli, Enyu Dai, Minghao Dang, Man Chun John Ma, Xubin Li, et al. 2022. "Follicular Lymphoma Microenvironment Characteristics Associated with Tumor Cell Mutations and MHC Class II Expression." *Blood Cancer Discovery*, June. https://doi.org/10.1158/2643-3230.BCD-21-0075.
10. Jiao, Wei, Gurnit Atwal, Paz Polak, Rosa Karlic, Edwin Cuppen, Fatima Al-Shahrour, Gurnit Atwal, et al. 2020. "A Deep Learning System Accurately Classifies Primary and Metastatic Cancers Using Passenger Mutation Patterns." *Nature Communications 2020 11:1* 11 (1): 1–12. https://doi.org/10.1038/s41467-019-13825-8.
11. Jurinovic, Vindi, Robert Kridel, Annette M. Staiger, Monika Szczepanowski, Heike Horn, Martin H. Dreyling, Andreas Rosenwald, et al. 2016. "Clinicogenetic Risk Models Predict Early Progression of Follicular Lymphoma after First-Line Immunochemotherapy." *Blood* 128 (8): 1112–20. https://doi.org/10.1182/BLOOD-2016-05-717355.
12. Lenz, G., G. Wright, S S Dave, W. Xiao, J. Powell, H. Zhao, W. Xu, et al. 2008. "Stromal Gene Signatures in Large-B-Cell Lymphomas." *The New England Journal of Medicine* 359 (22): 2313–23. https://doi.org/10.1056/NEJMoa0802885.

13. Los-De Vries, G. Tjitske, Mintsje de Boer, Erik van Dijk, Phylicia Stathi, Nathalie J. Hijmering, Margaretha G.M. Roemer, Matias Mendeville, et al. 2020. "Chromosome 20 Loss Is Characteristic of Breast Implant–Associated Anaplastic Large Cell Lymphoma." *Blood* 136 (25): 2927–32. https://doi.org/10.1182/blood.2020005372.

14. Los-de Vries, G Tjitske, Wendy B C Stevens, Erik van van Dijk, Carole Langois-Jacques, Andrew James Clear, Phylicia Stathi, Margaretha G M Roemer, et al. 2022. "Genomic and Microenvironmental Landscape of Stage I Follicular Lymphoma, Compared to Stage III/IV." *Blood Advances*, July. https://doi.org/10.1182/BLOODADVANCES.2022008355.

15. Louis, David N., Arie Perry, Pieter Wesseling, Daniel J. Brat, Ian A. Cree, Dominique Figarella-Branger, Cynthia Hawkins, et al. 2021. "The 2021 WHO Classification of Tumors of the Central Nervous System: A Summary." *Neuro-Oncology* 23 (8): 1231–51. https://doi.org/10.1093/NEUONC/NOAB106.

16. Luchini, Claudio, Rita T. Lawlor, Michele Milella, and Aldo Scarpa. 2020. "Molecular Tumor Boards in Clinical Practice." *Trends in Cancer* 6 (9): 738–44. https://doi.org/10.1016/J.TRECAN.2020.05.008.

17. Mendeville, Matias, Jurriaan Janssen, Yongsoo Kim, Erik van Dijk, Daphne de Jong, and Bauke Ylstra. 2022. "A Bioinformatics Perspective on Molecular Classification of Diffuse Large B-Cell Lymphoma." *Leukemia* 36 (9): 2177–79. https://doi.org/10.1038/s41375-022-01670-6.

18. Pastore, Alessandro, Vindi Jurinovic, Robert Kridel, Eva Hoster, Annette M. Staiger, Monika Szczepanowski, Christiane Pott, et al. 2015. "Integration of Gene Mutations in Risk Prognostication for Patients Receiving First-Line Immunochemotherapy for Follicular Lymphoma: A Retrospective Analysis of a Prospective Clinical Trial and Validation in a Population-Based Registry." *The Lancet Oncology* 16 (15): 1111–22. https://doi.org/10.1016/S1470-2045(15)00169-2.

19. Pfister, Stefan M., Miguel Reyes-Múgica, John K.C. Chan, Henrik Hasle, Alexander J. Lazar, Sabrina Rossi, Andrea Ferrari, et al. 2022. "A Summary of the Inaugural WHO Classification of Pediatric Tumors: Transitioning from the Optical into the Molecular Era." *Cancer Discovery* 12 (2): 331–55. https://doi.org/10.1158/2159-8290.CD-21-1094/674743/P/A-SUMMARY-OF-THE-INAUGURAL-WHO-CLASSIFICATION-OF.

20. Priestley, Peter, Jonathan Baber, Martijn P. Lolkema, Neeltje Steeghs, Ewart de Bruijn, Charles Shale, Korneel Duyvesteyn, et al. 2019. "Pan-Cancer Whole-Genome Analyses of Metastatic Solid Tumours." *Nature* 575 (7781): 210–16. https://doi.org/10.1038/s41586-019-1689-y.

21. Robbe, Pauline, Niko Popitsch, Samantha JL Knight, Pavlos Antoniou, Jennifer Becq, Miao He, Alexander Kanapin, et al. 2018. "Clinical Whole-Genome Sequencing from Routine Formalin-Fixed, Paraffin-Embedded Specimens: Pilot Study for the 100,000 Genomes Project." *Genetics in Medicine* 20 (10): 1196–1205. https://doi.org/10.1038/gim.2017.241.

22. Samsom, Kris G., Luuk J. Schipper, Paul Roepman, Linda J.W. Bosch, Ferry Lalezari, Elisabeth G. Klompenhouwer, Adrianus J. de Langen, et al. 2022. "Feasibility of Whole-Genome Sequencing-Based Tumor Diagnostics in Routine Pathology Practice." *Journal of Pathology* 258 (2). https://doi.org/10.1002/path.5988.

23. Sbaraglia, Marta, Elena Bellan, and Angelo P. Dei Tos. 2021. "The 2020 WHO Classification of Soft Tissue Tumours: News and Perspectives." *Pathologica* 113 (2): 70–84. https://doi.org/10.32074/1591-951X-213.

24. Sehn, Laurie H, and Gilles Salles. 2021. "Diffuse Large B-Cell Lymphoma." Edited by Dan L. Longo. *NEJM* 384 (9): 842–58. https://doi.org/10.1017/CBO9780511663369.013.

25. Steen, Chloé B., Bogdan A. Luca, Mohammad S. Esfahani, Armon Azizi, Brian J. Sworder, Barzin Y. Nabet, David M. Kurtz, et al. 2021. "The Landscape of Tumor Cell States and Ecosystems in Diffuse Large B Cell Lymphoma." *Cancer Cell* 39 (10): 1422-1437.e10. https://doi.org/10.1016/j.ccell.2021.08.011.

26. Tanaka, Norio, Akihisa Takahara, Taichi Hagio, Rika Nishiko, Junko Kanayama, Osamu Gotoh, and Seiichi Mori. 2020. “Sequencing Artifacts Derived from a Library Preparation Method Using Enzymatic Fragmentation.” *PLoS ONE* 15 (1). https://doi.org/10.1371/journal.pone.0227427.

27. Wilson, Wyndham H., George W. Wright, Da Wei Huang, Brendan Hodkinson, Sriram Balasubramanian, Yue Fan, Jessica Vermeulen, Martin Shreeve, and Louis M. Staudt. 2021. “Effect of Ibrutinib with R-CHOP Chemotherapy in Genetic Subtypes of DLBCL.” *Cancer Cell* 39 (12): 1643-1653.e3. https://doi.org/10.1016/J.CCELL.2021.10.006.

28. Woodcock, Janet, and Lisa M. LaVange. 2017. “Master Protocols to Study Multiple Therapies, Multiple Diseases, or Both.” *New England Journal of Medicine* 377 (1): 62–70. https://doi.org/10.1056/NEJMRA1510062/SUPPL_FILE/NEJMRA1510062_DISCLOSURES.PDF.

Appendix

Nederlandse samenvatting

DNA is een complex molecuul dat zich in elke cel van een levend organisme bevindt. Een mens bevat per cel ongeveer 2 meter aan DNA. Alle cellen van een mens bij elkaar opgeteld levert zelfs 74 miljoen kilometer aan DNA op. Dit DNA bevat de benodigde bouwinstructies voor de cellen om te ontwikkelen, groeien en te reproduceren. Het wordt daarom ook wel de blauwdruk van het leven genoemd.

Kanker is een complexe ziekte die in veel gevallen ontstaat door een opeenstapeling van afwijkingen in het DNA tijdens het leven. Deze afwijkingen veranderen de bouwinstructies, waardoor cellen ongecontroleerd gaan groeien en delen. Als gevolg hiervan vormt zich een gezwel van kankercellen: een tumor.

Dat er DNA-afwijkingen zijn, is een karakteristieke eigenschap van alle kankers. Verschillende soorten kankers hebben echter wel hun eigen, typische patroon van afwijkingen (DNA-profielen); de DNA-afwijkingen van een borstkankercel zijn anders dan de DNA-afwijkingen van een huidkankercel. Ook tussen patiënten met hetzelfde soort kanker zijn er verschillen; de ene borstkanker is de andere niet. Om elk soort kanker te begrijpen en de variatie (*heterogeniteit*) tussen patiënten te bevatten, is het daarom van belang om zoveel mogelijk gedetailleerde data te verzamelen.

Met behulp van moderne laboratoriumtechnieken ('*DNA sequencing*') en computeranalyses (het veld van de '*bioinformatica*') zijn er de laatste decennia tienduizenden DNA-profielen van patiënten gedetailleerd in kaart gebracht en bestudeerd. We bevinden ons nu in een fase waarin de opgedane kennis kan worden vertaald naar klinische toepassingen, zoals diagnose (bepaling van kanker soort of subgroep), prognose (voorspelling van ziektebeloop), stratificatie (bepaling van behandelplan), predictie (voorspelling of de behandeling aanslaat) en monitoring (meting van reactie op behandeling). Deze waardevolle informatie vormt de basis voor 'therapie op maat'; een gerichte behandeling gebaseerd op het individuele DNA-profiel van een patiënt.

In dit proefschrift worden verschillende klinische toepassingen van DNA-profilering onderzocht voor patiënten met een non-Hodgkin lymfoom. Deze groep van hematologische kwaadaardige tumoren ontstaat door ongeremde deling van witte bloedcellen, genaamd lymfocyten, die onderdeel vormen van het afweersysteem. Non-Hodgkin lymfoom ontwikkelt zich meestal in de lymfeklieren, het beenmerg of andere lymfeorganen (zoals de thymus en de milt), waar het een gezwel vormt. Aangezien lymfocyten zich van nature door het hele lichaam verspreiden wordt non-Hodgkin lymfoom ook vaak aangetroffen in andere organen, zoals in de arm, long of huid. Dit

worden *extranodale* localisaties genoemd. Volgens de Wereldgezondheidsorganisatie zijn er meer dan 30 soorten non-Hodgkin lymfoom. Deze soorten onderscheiden zich van elkaar op basis van morfologie (cel- en weefselstructuur), immunofenotype (eiwitten in de cel en op het celoppervlak) en genetica (DNA-afwijkingen). Ook het ziektebeloop van verschillende lymfoomsoorten varieert in agressiviteit. Dit verschil in klinische uitkomst komt tot uiting in de twee meest voorkomende soorten lymfomen: diffuus grootcellig B-cellymfoom (DLBCL) en folliculair lymfoom (FL). Dit proefschrift richt zich voornamelijk op deze twee soorten lymfomen.

Hoofdstuk 1 beschrijft, na de algemene introductie, de twee doelstellingen van dit proefschrift:

1. Het ontwikkelen van een uitgebreide DNA-test, van laboratoriumtechniek tot en met de bijbehorende geautomatiseerde computeranalyse. Deze test heeft als doel om relevante DNA-afwijkingen voor non-Hodgkin lymfomen te karakteriseren, en dient toepasbaar te zijn op tumorweefsel materiaal dat standaard in de kliniek wordt verzameld.
2. Het in kaart brengen van de variatie aan DNA-afwijkingen (DNA-profilering) dat voorkomt in non-Hodgkin lymfoom, met als doel om het ziektebeloop beter te kunnen voorspellen vanaf het moment van diagnose.

Dit wordt in **Hoofdstuk 2** gevolgd door een wetenschappelijke literatuurstudie (overzichtsartikel) die de meest recente ontwikkelingen beschrijft omtrent de onderverdeling (*classificatie*) van diffuus grootcellig B-cel lymfoom (DLBCL) in subgroepen, op basis van DNA-afwijkingen. **Hoofdstuk 3** sluit hierop aan met een opiniestuk, waarin wordt beargumenteerd wat de benodigde stappen zijn alvorens deze nieuwe kennis toegepast kan worden in de kliniek. Hierin benadrukken wij de urgentie om de verschillende classificatiesystemen die ontwikkeld zijn terug te brengen tot één systeem middels een consensusbenadering. Hierdoor wordt het mogelijk om nieuwe behandelmogelijkheden gestructureerd te evalueren, in het belang van de patiënt.

In **Hoofdstuk 4** voeren we de uitgebreide DNA-test (doelstelling 1) en classificaties (volgens Hoofdstuk 2 en 3) uit op twee grote groepen van DLBCL-patiënten. Het doel van deze retrospectieve studie is om te onderzoeken of classificaties op basis van DNA-afwijkingen toegevoegde waarde hebben voor het voorspellen van het ziektebeloop van DLBCL-patiënten na standaardbehandeling (immuno-chemotherapie). Daarbij onderzoeken we ook hoe beeldvorming van actief tumorweefsel door middel van PET/CT-scans tijdens en na beëindiging van de standaardbehandeling kan bijdragen aan de prognose.

We identificeren een subgroep van hoog-risico patiënten, op basis van specifieke DNA-afwijkingen. De patiënten in deze groep hebben een kortere overlevingsverwachting dan de overige patiënten, ondanks dat ze dezelfde behandeling ondergaan. Een opmerkelijke bevinding is dat deze groep patiënten aanvankelijk goed lijkt te reageren op de therapie: op de PET/CT-scan is geen actief tumorweefsel meer zichtbaar al vroeg tijdens en direct na afloop van de standaardbehandeling die direct volgt op de diagnose. Echter, bij deze groep patiënten komt de tumor uiteindelijk toch vaak terug (of is nooit helemaal weggeweest). Deze bevindingen, die we bekrachtigen in twee onafhankelijke groepen DLBCL-patiënten, tonen aan dat het voorspellen van het ziektebeloop wordt verbeterd door de combinatie van voorafgaande DNA-profilering en PET/CT-beeldvorming tijdens en na behandeling. Bovendien ondersteunen deze gegevens het idee dat de huidige behandelprotocollen ontoereikend zijn voor de geïdentificeerde groep hoog-risico patiënten en dat deze patiënten daarom mogelijk in aanmerking komen voor aanvullende behandeling, zelfs nadat ze ogenschijnlijk goed hebben gereageerd op de standaardtherapie.

Om de diagnose lymfoom te kunnen stellen wordt er middels een biopsie een lymfeklier of andere tumorlocalisatie (deels) verwijderd uit het lichaam van een patiënt. Dit biopt bevat naast kwaadaardige kankercellen ook gezonde lichaamscellen. Hoe lager het aantal kankercellen, hoe lastiger het wordt om een succesvolle DNA-test uit te voeren. Het is daarom van belang om de fractie aan kankercellen uit het biopt accuraat te kunnen meten ter ondersteuning van de interpretatie van de DNA-test of ter kwaliteitscontrole. Voor deze doeleinden hebben we een softwarepakket ontwikkeld genaamd “ACE”, wat wordt beschreven in **Hoofdstuk 5**. “ACE” kan door iedere onderzoeker worden gebruikt doordat we het vrij toegankelijk hebben gemaakt.

Hoofdstuk 6 is een studie met als doel om het ziektebeloop te kunnen voorspellen aan de hand van DNA-afwijkingen in tumoren van patiënten met folliculair lymfoom (FL). FL is een ongeneeslijke maar niet-agressieve vorm van non-Hodgkin lymfoom die wordt gekenmerkt door meerdere recidieven (terugkomen) met variabele perioden van remissie (afwezigheid van ziekte). In dit onderzoek identificeren we twee DNA-afwijkingen die verband houden met het ziektebeloop bij FL-patiënten behandeld met standaard immuno-chemotherapie. (1) Een extra kopie van chromosoom 18 is sterk geassocieerd met een slechte prognose (d.w.z. ziekteprogressie of sterfte door ziekte binnen 2 jaar). (2) Een mutatie in het gen *EZH2* is sterk geassocieerd met een gunstige prognose (d.w.z. afwezigheid van ziekte langer dan 5 jaar vanaf begin van behandeling).

Hoofdstuk 7 richt zich op de DNA-profilering van een weinig voorkomende soort lymfeklierkanker met een exotische naam: humaan herpesvirus 8-negatief effusie-gerelateerd lymfoom (HHV8-negatief EBL).

De interesse werd gewekt doordat de tumorcellen van dit lymfoom onder de microscoop sterk op DLBCL lijken, maar het ziektebeloop en de verschijningsvorm duidelijk anders is. Waar DLBCL een agressieve vorm van kanker is, lijkt deze soort minder agressief te zijn. Daarnaast wordt dit type lymfeklierkanker niet zoals gebruikelijk gevonden in lymfklieren of organen, maar alleen in het vocht van lichaamsholtes, zoals rondom het hart of rondom de longen. Vanwege de vaak (heel) hoge leeftijd van de patiënten en een vaak onderliggende hart- of leveraandoening willen artsen deze patiëntengroep liever geen zware chemotherapie geven. Het in kaart gebrachte DNA-profiel heeft bijgedragen aan een verfijnde definitie van dit type kanker en heeft daarmee bijgedragen aan de recent gepubliceerde laatste editie van de Classificatie van Hematolymfoïde Tumoren van de Wereldgezondheidsorganisatie.

Hoofdstuk 8 bevat een samenvatting van de hoofdstukken uit dit proefschrift en een discussie. Daarnaast wordt beschreven in welke mate de doelstellingen zijn behaald. Allereerst is er op succesvolle wijze een test ontwikkeld waarmee wetenschappers DNA-afwijkingen in kaart kunnen brengen, met gebruik van tumorweefsel dat standaard in de kliniek wordt verzameld. Ten tweede is deze test succesvol toegepast binnen de studies uit dit proefschrift en andere studies van collega's uit onze onderzoeksgroep. Dit heeft geleid tot een kennistoename over de DNA-afwijkingen van lymfekliertumoren en een betere voorspelling van het ziekteverloop bij patiënten.

De discussie plaatst het onderwerp van dit proefschrift in een bredere context van het onderzoek naar lymfekliertumoren en de behandeling ervan. Door DNA-profilering kunnen we mede dankzij de resultaten beschreven in dit proefschrift beter onderscheid maken tussen DLBCL- en FL-patiënten met een goede en slechte prognose. De DNA-profielen bieden mogelijkheden voor therapie op maat. In de toekomst kunnen er nieuwe medicijnen of behandelmethodes worden getest bij patiënten op basis van deze nieuwe inzichten. Dit biedt hoop voor patiënten, specifiek voor hen die nu in een hoog risicogroep vallen. Momenteel wordt er in de wetenschap niet alleen naar DNA-afwijkingen gekeken, maar worden er ook studies gedaan naar de cellen van het afweersysteem rondom de tumor. Bij immuuntherapie worden de afweercellen geïnstrueerd om de kankercellen aan te vallen. Er zijn stappen gezet, maar er is ook vervolgonderzoek nodig om het ontstaan en de ontwikkeling van het lymfoom volledig te begrijpen en daar therapie op maat voor te kunnen ontwikkelen.

List of publications

Under review

1. **Mendeville**, **M.**, Los-de Vries, G. T.*, Janssen J.*, Richter J., van Dijk E., Nijland M., Roemer, M. G. M., Stathi P., Hijmering N. J., Bladergroen R., Pelaz D. A., Diepstra A., Eertink J. J., Burggraaff C. N., Kim Y., Lugtenburg P. J., van den Berg A., Tzankov A., Dirnhofer S., Duhrsen U., Huttmann A., Klapper W., Zijlstra J. M., Ylstra B.*, de Jong D.*. (2022). Molecular Subtyping Significantly Improves Outcome Prediction in Diffuse Large B-Cell Lymphoma.

   *Authors contributed equally

Published

2. **Mendeville**, **M.**, Roemer, M. G. M., Los-de Vries, G. T., Chamuleau M. E. D., de Jong D., Ylstra B. (2022). The path towards consensus genome classification of diffuse large B-cell lymphoma for use in clinical practice. *Frontiers in Oncology*. https://doi.org/10.3389/fonc.2022.970063
3. **Mendeville, M.**, Janssen, J., Kim, Y., van Dijk, E., de Jong, D., & Ylstra, B. (2022). A bioinformatics perspective on molecular classification of diffuse large B-cell lymphoma. *Leukemia*, *36*(9), 2177–2179. https://doi.org/10.1038/s41375-022-01670-6
4. Los-de Vries, G. T., Stevens, W. B. C., van Dijk, E. van, Langois-Jacques, C., Clear, A. J., Stathi, P., Roemer, M. G. M., **Mendeville, M.**, Hijmering, N. J., Sander, B., Rosenwald, A., Calaminici, M., Hoster, E., Hiddemann, W., Gaulard, P., Salles, G. A., Horn, H., Klapper, W., Xerri, L., … de Jong, D. (2022). Genomic and microenvironmental landscape of stage I follicular lymphoma, compared with stage III/IV. *Blood Advances*, *6*(18). https://doi.org/10.1182/bloodadvances.2022008355
5. Plaça, J. R., Diepstra, A., Los, T., **Mendeville, M.**, Seitz, A., Lugtenburg, P. J., Zijlstra, J., Lam, K., da Silva, W. A., Ylstra, B., de Jong, D., van den Berg, A., & Nijland, M. (2022). Reproducibility of Gene Expression Signatures in Diffuse Large B-Cell Lymphoma. *Cancers*, *14*(5). https://doi.org/10.3390/cancers14051346

6. Los-de Vries, G. T., de Boer, M., van Dijk, E., Stathi, P., Hijmering, N. J., Roemer, M. G. M., **Mendeville, M.**, Miedema, D. M., de Boer, J. P., Rakhorst, H. A., van Leeuwen, F. E., van der Hulst, R. R. W. J., Ylstra, B., & de Jong, D. (2020). Chromosome 20 loss is characteristic of breast implant-associated anaplastic large cell lymphoma. *Blood*, *136*(25), 2927–2932. https://doi.org/10.1182/blood.2020005372
7. Poell, J. B., **Mendeville, M.**, Sie, D., Brink, A., Brakenhoff, R. H., & Ylstra, B. (2019). ACE: Absolute copy number estimation from low-coverage whole-genome sequencing data. *Bioinformatics*, *35*(16). https://doi.org/10.1093/bioinformatics/bty1055
8. **Mendeville, M.**, Roemer, M. G. M., Van Den Hout, M. F. C. M., Los-De Vries, G. T., Bladergroen, R., Stathi, P., Hijmering, N. J., Rosenwald, A., Ylstra, B., & De Jong, D. (2019). Aggressive genomic features in clinically indolent primary HHV8-negative effusion-based lymphoma. In *Blood* (Vol. 133, Issue 4, pp. 377–380). American Society of Hematology. https://doi.org/10.1182/blood-2017-12-822171
9. Boot, M. V, van Belzen, M. J., Overbeek, L. I., Hijmering, N., **Mendeville, M.**, Waisfisz, Q., Wesseling, P., Hennekam, R. C., & de Jong, D. (2018). Benign and malignant tumors in Rubinstein–Taybi syndrome. *American Journal of Medical Genetics, Part A*, *176*(3), 597–608. https://doi.org/10.1002/ajmg.a.38603
10. Stevens, W. B. C.*, **Mendeville, M.***, Redd, R., Clear, A. J., Bladergroen, R., Calaminici, M., Rosenwald, A., Hoster, E., Hiddemann, W., Gaulard, P., Xerri, L., Salles, G., Klapper, W., Pfreundschuh, M., Jack, A., Gascoyne, R. D., Natkunam, Y., Advani, R., Kimby, E., … De Jong, D. (2017). Prognostic relevance of CD163 and CD8 combined with EZH2 and gain of chromosome 18 in follicular lymphoma: A study by the Lunenburg Lymphoma Biomarker Consortium. *Haematologica*, *102*(8), 1413–1423. https://doi.org/10.3324/haematol.2017.165415

    *Authors contributed equally

About the author

Matías Sebastiaan Mendeville was born on February 12, 1987 in Amsterdam. In 2005 he passed his final exam at the Barlaeus Gymnasium in Amsterdam. After a gap year in Chile, the country where his father was born, he started studying Biomedical Sciences at VU University (VU) in Amsterdam in 2007. After he passed his bachelor's degree in 2011, he opted for the master's program in Bioinformatics and Systems Biology at the VU University in Amsterdam. His curiosity about the biology of the human body came together in this study with his interest in technology and mathematics.

During his first internship, he participated in the International Genetically Engineered Machine Competition 2012 (https://igem.org/). In this competition, multidisciplinary student teams from all over the world compete by designing and building projects using cutting edge synthetic biology. As part of the student team of VU Amsterdam representatives, he developed a bacterial memory module by repurposing the existing phenomenon of DNA methylation. This project was concluded with an exhibition of synthetic biology in the NEMO Science Museum.

Matías performed his second internship under supervision of prof.dr. Bauke Ylstra at the Tumor Genome Analysis Core (TGAC) at the department of Pathology of Amsterdam UMC, location VUmc. Under the guidance of his day-to-day supervisor, dr. Oscar Krijgsman, Matías investigated the transition from microarrays to Next Generation Sequencing for the detection of copy number aberrations in DNA of tumour tissue. In 2014 he graduated, with the master thesis entitled: "*Next-Generation Sequencing (NGS) as a robust and low-cost alternative for aCGH*". This internship sparked his interest in the application of bioinformatics to study cancer biology. When he was offered the opportunity to start a PhD project within the same lab, he therefore did not have to think twice. This PhD project, which was funded by the Dutch Cancer Society (KWF) and granted to prof.dr. Daphne de Jong, was the kick-off of the lymphoma-oriented research group within the TGAC under supervision of prof.dr. Bauke Ylstra. The aim of this project was to characterize the genomic landscape of patients with B-cell non-Hodgkin lymphoma in the Netherlands. To this end, the required laboratory and bioinformatics procedures had to be designed and implemented. This thesis, entitled *"Computational solutions in genomic pathology of non-Hodgkin Lymphomas"* is the result of this PhD project. Matías' position in the lab was extended as a post-doc fellow from 2018 to 2021.

In 2021 he decided to take on a special challenge at Hartwig Medical Foundation as a bioinformatician. This position ties in well with his previous research into cancer genome

analyses, and he is honoured to be able to further his knowledge and experience. In his current function at Hartwig, he makes a valuable contribution to society by making an impact on the treatment processes and thus the lives of patients with cancer.

Dankwoord

Met deze woorden sluit ik een bijzondere fase in mijn leven af, waarin ik veel heb geleerd over de inhoud van mijn onderzoek, over het leven en niet in de laatste plaats over mezelf. Voor deze ervaring ben ik heel dankbaar. Alle mensen die betrokken zijn geweest wil ik bedanken voor de steun die ik heb gevoeld, alsmede de kennis en ervaring die zij hebben overgebracht.

Allereerst natuurlijk mijn promotoren **Daphne** en **Bauke**. Ik wil jullie oprecht bedanken voor het krijgen van deze kans en het vertrouwen in mij. Zonder jullie enthousiasme, drive en passie voor de wetenschap zou ik nu niet op dit punt hebben gestaan. En natuurlijk ook de gezelligheid tijdens onze werkoverleggen. Jullie hebben mij laten zien dat wetenschap en humor heel goed hand in hand gaan.

Daphne, bedankt voor het delen van al je mooie verhalen en levendige anekdotes over uiteenlopende onderwerpen, vaak gevolgd door prachtige uiteenzettingen over jouw expertise, die onze experimenten in context plaatsten. Je opbeurende en motiverende woorden op momenten dat het even tegenzat, zal ik niet snel vergeten. Ook herinner ik me ons allereerste gesprek. Je vroeg me abrupt: 'kan je goed koken?' Ik antwoordde in de strekking dat ik niet de snelste kok ben, maar dat ik door een precieze afweging van smaken en handelingen ik uiteindelijk zeker iets kwalitatiefs kan presenteren. Ik zie een verband met de totstandkoming van dit proefschrift. Ik ben benieuwd of je deze vraag vaker stelt bij sollicitatiegesprekken om te weten wat voor vlees je in de kuip hebt.

Bauke, wat was het fijn dat ik na een succesvolle stageperiode definitief aan de slag kon gaan als PhD-student in jouw lab. Zonder jouw aanbeveling bij Daphne was mijn pad anders gelopen. Het samen opzetten van het DNA-onderzoek voor lymfomen was een hele waardevolle ervaring. Door jou heb ik kritisch naar resultaten leren kijken. Van het opzetten van valide experimenten tot aan het verwoorden van de kernboodschap; jij was voor mij een inspirerende mentor. Ik bewonder je visie en doorzettingsvermogen. Op momenten dat ik twijfels had over de ingeslagen weg, zette jij door. Dit heeft ons uiteindelijk een aantal prachtige publicaties opgeleverd. Ik heb altijd het gevoel gehad dat je deur open stond. Deze toegankelijkheid en behulpzaamheid hebben mij er tot in deze laatste fase van mijn promotietraject doorheen gesleept.

En dan mijn paranimfen. **Marit**, vanaf het moment dat je bij de TGAC kwam werken merkte ik gelijk wat voor een geweldig waardevolle toevoeging jij was voor ons team. Wat een kennis bracht jij mee uit Boston! Een echt wetenschappelijk talent. Maar bovenal een superfijn en gezellig mens. Geen wonder dat je de populairste collega was, waar

iedereen het liefst een kantoor mee deelde. Zelf heb ik helaas nooit dat privilege gehad ;) Jouw aanwezigheid is altijd zeer motiverend geweest en ik voel me dan ook vereerd dat je naast me staat tijdens dit laatste deel van mijn promotietraject.

Tim, waar moet ik beginnen? Bij het begin natuurlijk: op de 14e in de Jordaan, gevolgd door het Barlaeus, daarna allebei een PhD, sinds kind af aan al samen op voetbal en still going strong. Bijzonder hoe onze levens met elkaar verbonden zijn. En dan nu zelfs allebei een zoon op komst, bijna gelijk uitgerekend! Wel loop ik altijd iets op je achter: vanaf een eerste vriendinnetje tot aan het vaderschap, en idem met het afronden van onze PhD's. Het maakt je tot mijn ideale raadgever.

Aan de leden van de promotiecommissie**: Jacqueline Cloos**, **Bjoern Chapuy**, **Laura Van't Veer**, **Martine Chamuleau**, **Edwin Cuppen**, **Oscar Krijgsman**, bedankt voor het nemen van de tijd en moeite om mijn proefschrift te beoordelen. Ik kijk ernaar uit om tijdens mijn verdediging van gedachte te wisselen over het proefschrift. **Bjoern**, as first author of your Nature Medicine paper, which laid the foundation of the new molecular classification of DLBCL that played a fundamental role in about half of my chapters, your (last) name was probably the most heard name in our lab throughout the last years of my tenure. Quite a remarkable impact. Thank you for reading and approving my thesis. I'm looking forward to our discussions.

Oscar, als mijn stagebegeleider heb je mij geïntroduceerd in de TGAC. Met jouw aanstekelijke enthousiasme heb je een cruciale rol gespeeld in het begin van mijn wetenschappelijke carrière. Het was een eer dat ik destijds jouw paranimf mocht zijn. Mooi dat jij nu een rol speelt in de afronding van mijn promotieproject als lid van de leescommissie.

Aan al mijn eerste collega's van de TGAC: voor mij was het een eyeopener om vanuit de studiebanken op een dagelijkse basis met collega's over de wetenschap te kunnen praten. En dan ook nog met zulke leuke collega's! Ik voelde me vanaf het begin zeer welkom door jullie positieve energie.

Om te beginnen, **Daoud**, jij hebt mij wegwijs gemaakt in de wereld van de bioinformatica. Jij was voor mij, als beginnend bioinformaticus, de fakkel in de duisternis van mijn terminalscherm; je had altijd een antwoord voor alle issues waar ik tegenaan liep. Bedankt voor het vertrouwen dat je me in een vroeg stadium al gaf m.b.t. toegangsrechten voor grote datasets. Ik weet dat dit niet jouw woorden zijn, maar jij hebt ze me wel geleerd: '*with great power comes great responsibility*'.

Paul, als pater familias van de TGAC heb jij je altijd bekommerd om het welzijn van ons team. Dat siert je. Van mentale ondersteuning tot later zelfs fysieke ontspanning in de vorm van (sport)massages. Ik heb er nog steeds één van je tegoed ;)

Dirk, het optimaliseren van de DNA-kwaliteit uit FFPE-samples was voer voor eindeloze discussies, die soms uitzichtloos bleken (want garbage in = garbage out). Ik heb genoten van je R-skills (maak je nog steeds zulke kunstwerken?). We hebben tot tranen aan toe gelachen bij de koffieautomaat, wat we tegenwoordig weer kunnen voorzetten als buren op het Science Park.

Ilari, thanks for all your knowledge and patience with me, especially in R-related topics. I enjoyed our time as colleagues and conversations about ice-hockey and sailing. **Hinke**, jij was de enige waar ik mee kon praten over mijn andere grote liefde naast de wetenschap: voetbal. Ook je betrokkenheid in periodes dat het iets minder ging waren bijzonder fijn. **Martijn**, mijn buddy aan het begin van de PhD. Het was altijd gezellig, onder andere op congressen, en we hadden grootse plannen voor onze TGAC-band; helaas is het bij ideeën gebleven. **Stef**, gelukkig is het niet nodig om afscheid van je te nemen nu we weer samenwerken bij Hartwig. Onze squash wedstrijdjes boden een fijne afwisseling tijdens het afronden van mijn proefschrift. Ik hoop dat ik over een jaartje eindelijk een keer een game van je kan winnen! **Christian**, bedankt voor het delen van jouw ervaring en kunde op verschillende vlakken, zoals de bioinformatica (de implementatie van onze pipeline in het NCA-cluster), als ook de huizenmarkt. **Jos**, ik heb genoten van onze brainstormsessies en ben dankbaar dat ik kon meeliften op jouw kennis en bevlogenheid bij de totstandkoming van ACE. Je enthousiasme is erg aanstekelijk en motiverend en weet je zélfs over te brengen op de door jouw geschreven software-documentatie!

En dan het lymfoom team. **Reno**, gelukkig kwam jij ons team al vrij snel na de start van mijn promotie versterken, want het werd al gauw duidelijk dat ik onmogelijk in mijn eentje het *drylab*- én het *wetlab*-werk voor ons project kon uitvoeren. Met jouw bijdrage is de basis gelegd voor onderzoeksprojecten waaruit inmiddels meerdere publicaties zijn verschenen. **Phylicia**, ik heb veel bewondering voor de manier waarop jij in een mum van tijd overzicht en orde hebt geschept rondom al onze experimenten. Je was onze rots in de branding! En daarnaast een supergezellige en attente collega. **Nathalie**, zonder jouw onuitputtelijke doorzettingsvermogen voor het verzamelen van alle benodigde samples en patiëntengegevens zou dit boekje er heel anders uit hebben gezien (of er überhaupt niet zijn geweest). Bedankt, ook voor alle gezellige praatjes tussendoor! **Wendy**, bedankt voor de fijne samenwerking op de LLBC-projecten (waaronder mijn eerste wetenschappelijke publicatie) en veel succes met de laatste loodjes van jouw proefschrift!

Tjitske, met de door jouw ontwikkelde SV-calling hadden we tegen het einde van je stage een essentiële nieuwe toepassing aan onze genoomanalyses toegevoegd; een prachtige opstap naar een welverdiende promotieplek in de lymfoomgroep van de TGAC. Zonder jouw doortastendheid zou ik hoogstwaarschijnlijk zijn verdwaald in het doolhof van sample verwisselingen. Hiervoor, en voor onze aangename en productieve samenwerking in het algemeen, ben ik je erg dankbaar. Inmiddels heb je ook een prachtig boekje af en rest voor jou ook nog slechts de verdediging. Ik heb er al het vertrouwen in dat dit helemaal goed komt! **Jurriaan**, wat mochten wij in ons handjes knijpen dat jij bij de TGAC terecht kwam voor jouw stage. Met een verbluffende snelheid heb jij je ingewerkt in ons onderzoek. Met behulp van jouw skills en toewijding is het 'DLBCL-radiogenomics' artikel tot de huidige staat gebracht, waar we allemaal heel trots op zijn. Ik wens je veel succes met het vervolg van je PhD. En hoop dat ik je DJ-skills binnenkort ook een keer kan bewonderen. **Yongsoo**, I thank you for your private machine learning lectures, your contribution to the DLBCL-radiogenomics project, for always being so cheerful and positive and for your homemade kimchi! **Erik**, bedankt voor je bereidheid om altijd te helpen, de gezellige en goed getimede koffiepauzes en je humor. Echt leuk dat we weer collega's zijn!

Aan alle overige (ex-)collega's van de TGAC: **Thomas**, **Tanya**, **Jamie**, **Barbara**, **Jacqueline**, **Hedde**, **Irene**, **Daniëlla**, **Jeroen**, **Liping**, **Francois**. Bedankt voor alle gezelligheid op het werk, tijdens de lunch, bij borrels en teamuitjes. Het was een genoegen om met jullie in dezelfde groep te werken! Aan de groep van **Renske**: **Lise**, **Barbara**, **Wina**, **Iris**, **Sander**, **Ramon**, **Birgit**, **Lisanne.** Het was fijn om de ups en downs van het promotietraject met jullie te kunnen delen. Alle betrokkenen bij de VUmc-lymfoom groep: **Michiel**, **Esther**, **Monique**, **Nils**, **Chantal**, **Danijela**, **Vera**, **Martine**, **Hilma**, **Yvonne**, **Josée**, **Corine**, **Coreline**. Bedankt voor alle interessante presentaties en multidisciplinaire overleggen. **Josée**, **Corine** en **Coreline**, bedankt voor de fijne samenwerking op het radiogenomics project. **Saskia**, bedankt voor je positieve feedback op mijn onderwijswerkzaamheden, en voor de gezelligheid op kantoor. **Marcel**, jouw getoonde betrokkenheid en motiverende woorden waardeer ik enorm!

To all members of the **Lunenburg Lymphoma Biomarker Consortium**: thank you for the great cooperation. I really enjoyed our annual meetings, including the memorable Boston duck tour (quack! quack!).

I would like to thank all not yet mentioned co-authors who contributed to chapters in this thesis: **Julia**, **Wolfram**, **Diego**, **Arjan**, **Elly**, **Anke**, **Alexander**, **Stefan**, **Ulrich**, **Andreas**, **Arjen**, **Ruud** and **Mari.**

Ik wil **Hartwig Medical Foundation** bedanken voor het genereren en beschikbaar maken van de hoogkwalitatieve data die voor een deel van dit proefschrift gebruikt is. Ook wil ik mijn huidige collega's bij **Hartwig** bedanken voor het warme welkom en de getoonde interesse in mijn promotie én uiteraard het bijbehorende feestje.

Tot slot, mijn vrienden en familie, die de laatste jaren van onschatbare waarde zijn geweest. Bedankt voor alle gezelligheid en support op de momenten dat ik het nodig had om even los te komen van het harde werk en weer op te laden. Ik prijs me heel gelukkig met een grote groep vrienden waarop ik op een "aardig niveautje" (lees: nét geen kelderklasse) nog regelmatig een balletje kan trappen: **Etkin**, **Philipp**, **Hendrik**, **Marius**, **Quirijn**, **Thomas**, **Wessel** (2x), **Killian**, **Julian**, **Arne**, **Josse**, **Jaco**, **Jorrit**, **Daan**, **Sjoerd**, **Tonnie**, **Jules**, **Koen**, **Wout**, **Frans**. Ik hoop dat we deze sociale en sportieve uitlaatklep ondanks onze leeftijd en de bijkomende issues nog lang volhouden. Ook al pieken we vooral tijdens de derde helft en de epische teamuitjes!

Berno, onze gymsessies waren de ideale manier om elkaar geregeld te zien in onze krappe schema's en vormden een bron van broodnodige afleiding en motivatie. Bedankt voor de reps, biri's en adviserende en opbeurende woorden. Hetzelfde (ogenschijnlijke) gemak waarmee jij door je PhD bent gevlogen als waarop jij pull-ups doet is verbluffend. Ik ben heel benieuwd wat een man met even brede skills als armen nog meer in zijn mars heeft! **Jim** en **Youri**, mede door jullie aanmoedigingen bij het programmeren van Mastermind ben ik op het spoor gekomen van de (bio)informatica. **Stefan** en **Ali**, de Hollandsnieuwe posse! Ik verheug me op nog vele borrels, etentjes en concerten. **Rafaella**, met jouw artistieke ontwerp voor de vormgeving van mijn boekje heb je geholpen om mijn promotie letterlijk tot een "mooi" einde te brengen. Ik ben heel erg blij met het resultaat!

Familie Kemp, ik heb bergen aan werk verzet tijdens mijn schrijfretraite in de Rembrandthoeve. Een jaar eerder was ik ook in jullie warme nest toen ik het nieuws kreeg te zijn aangenomen voor mijn huidige baan. Zo vormen jullie een onmisbare schakel binnen deze reis.

Annefie, jouw creatieve ingevingen en verrassende verbanden daagde mij altijd uit om mijn onderzoek vanuit een andere invalshoek te bekijken en uit te leggen. **Jan** en **Jos**, bedankt voor jullie steun en interesse in mijn promotietraject en alle heerlijke diners waarmee jullie ons hebben verwend!

Mi querida familia Chilena, aunque vivimos al otro lado de esta tierra y no nos vemos a menudo, siempre se sienten cerca. Estoy orgulloso de que pronto tendré el mismo título que Tata. Espero con ansias nuestra próxima reunión familiar, donde con suerte estarán representadas las cuatro generaciones.

Pablo, in de periode tijdens mijn promotieonderzoek waarin ik mijzelf beter heb leren kennen, heb ik jou ook beter leren kennen. Ik vind het krachtig en inspirerend om te zien hoe jij jezelf ontwikkelt, vasthoudend aan je eigen kompas.

Ramón, wat ben ik trots op jou als ik je op het podium zie en jij onze muzikale opvoeding recht aandoet. Jouw muziek motiveert en helpt me er op moeilijke momenten doorheen. Ook de momenten met Luna geven me veel energie. Ik verheug me enorm op alles wat nog gaat komen als Luna er straks een neefje bij heeft!

Pap en **mam**, jullie hebben mij altijd gestimuleerd om naast muziek en sport te blijven studeren. Jullie onvoorwaardelijke steun, liefde en vertrouwen zijn altijd heel belangrijk voor me geweest. Ook jullie perfectionistische aard heeft een belangrijke bijdrage geleverd aan de totstandkoming van dit proefschrift. Het tot vervelens aan toe repeteren van toonladders en akkoordenschema's op de piano hebben mijn oog (en oor) voor detail enorm gestimuleerd. Ik heb het maar getroffen met jullie!

Lieve **Roos**, eindelijk is het dan zover! Al die jaren heb je mij moeten delen met mijn PhD, waarin je mij zo vaak hebt horen zeggen dat het schrijven bijna klaar was, terwijl er in werkelijkheid nog stapels werk te verzetten waren. Dat was niet altijd even makkelijk, maar je bleef gelukkig in me geloven. Dank voor al je geduld en onvoorwaardelijke liefde. Ons volgende avontuur staat inmiddels al voor de deur. Ik kan niet wachten om dat samen met jou te beleven! Fuiste, eres y serás, el amor de mi vida.